On the circulation of the North Atlantic shadow zone

Jesús Peña-Izquierdo

Tesis dirigida por Dr. Josep Lluís Pelegrí Llopart

Institut de Ciències del Mar, CSIC

Tesis presentada para obtar al título de doctor por la Universitat Politécnica de Catalunya
Barcelona 20 de Enero de 2015

A mi padres

Some of us think holding on makes us strong;
but sometimes it is letting go

Hermamn Hesse

Contents

Preface

This dissertation, entitled ON THE CIRCULATION OF THE NORTH ATLANTIC SHADOW ZONE, is presented as a partial requirement to obtain the Doctoral degree from the Universitat Politècnica de Catalunya. This investigation is the compilation of three studies aimed at describing the circulation within the North Atlantic shadow zone an its role on the ventilation of the North Atlantic Oxygen Minimum Zone. This thesis investigation was conducted between 2009 and 2014 under the guidance of Dr. José Luís Pelegrí Llopart, who is an investigator from the Institut de Ciències del Mar - Consejo Superior de Investigaciones Científicas, supported through an FPI predoctoral grant (BES-2009-021691) in the frame of the research project entitled "Ocean Climate Memory: mechanisms and paths of surface water formation in the Equatorial Atlantic" (MOC2-Ecuatorial, ref. CTM2008-06438-C02-01/MAR).

This doctoral dissertation is structured with an introductory chapter which describes the main dynamic systems that interplay in the circulation of the shadow zone. The following three chapters constitute the core of the dissertation, each of them is presented as a scientific article. While writing this thesis, the first of these articles has been published in Scientia Marina. The second and third chapters have been submitted to Journal of Geophysical Research as one sole article and it is currently under revision. The thesis concludes with a discussion of the main results from this work. Asides the above-mentioned articles, along this period of research the author of this thesis has engaged in two collaborative research stays abroad (USA and Australia), has participated in seven symposia, has coauthored two other published peer-review papers, has been the coauthor of two chapter of a book, has attended two international training schools and has participated in three research cruises.

Summary

Regions isolated from the wind-driven circulation are found in the eastern margins of the world's tropical oceans. The weak and stagnant circulation of these so-called 'shadow zones', in combination with the intense respiration of organic matter provided by the overlying highly productive waters, promotes the existence of large oceanic volumes with very low dissolved oxygen. These volumes are known as oxygen minimum zones (OMZs). The last decades of observations have revealed that OMZs are in general expanding, and thus potentially threatening the surrounding rich marine ecosystems. However, it is not clear whether this change is based on natural variability or it has an anthropogenic origin. Furthermore, under a global warming scenario, the future evolution of the OMZs is uncertain due to the complex interaction between the physical and biochemical processes that interplay in the OMZs dynamics.

This dissertation seeks to unravel the key elements of the circulation in the North Atlantic shadow zone, aiming to provide a deeper understanding of the physical components that rule the dynamics of the North Atlantic OMZ (naOMZ) – this being the less intense OMZ of the world ocean but the one that has experienced the largest expansion. A comprehensive description of the North Atlantic shadow zone circulation is presented from novel (CANOA08 cruise) and historic observations, including numerical outputs from the assimilative ECCO2 circulation model.

The main outcome of our work is that two markedly distinct regimes of circulation exist in the thermocline layers of the naOMZ, above and below σ_θ=26.8 kg m^{-3}. In the upper layer, within the upper Central Water (uCW), the circulation is governed by the cyclonic regime of the subtropical cell. This stratum is characterized by relatively high oxygenation, with a predominance of South Atlantic Central Water (SACW). The lower layer, within the lower Central Water (lCW), presents a drastic decrease in the oxygen content due to its sluggish circulation; in contrast with the uCW, a mean anticyclonic circulation leads to a marked increase of North Atlantic Central Water (NACW). This result implies an equatorward

transfer of mass from the subtropical gyre to the shadow zone, providing a previously unaccounted supply of oxygen from the well-ventilated subtropical thermocline. In fact, at the core of the naOMZ, the contribution of NACW is 50%. Such a mixture of SACW and NACW, with very low oxygen levels, is defined as the regional water mass of the naOMZ, the Cape Verde SACW (SACWcv).

A broad band of eastward flows is located between 10ºN and 20ºN, just south of the westward flowing North Equatorial Current. These flows, here referred as the Cape Verde Current system, emerge as the major contributor in the water mass supply to the naOMZ. Lagrangian simulation reveals that while in the uCW, most of the water supply occurs south of 10ºN, in the lCW, more than two thirds of the total water supply takes place north of 10ºN, through the Cape Verde Current system with a high contribution of water directly recirculated from the subtropical gyre. The accurate numerical reproduction of the water mass composition within the naOMZ thermocline, as directly deduced from particle-track Lagrangian simulations, supports the goodness of the ECCO2 velocity field.

The uCW and lCW strata not only exhibit opposite circulation patterns, they also present opposite large-scale vertical motions with predominant upwelling in the uCW as part of the subtropical cell regime while the lCW presents a broad downwelling pattern. We propose the existence of an inverse subtropical cell within the lCW dynamically coupled to the uCW regime. The major role these cells play in the circulation of the North Atlantic shadow zone, together with their substantial natural interannual and decadal variability, makes them major players on the oxygen anomalies observed during the last decades in the world OMZs.

Chapter I

Introduction

1.1 Background

The discovery in 1751 by captain Henry Ellis that deep water in the subtropical Atlantic was cold despite the warm temperature at the surface may seem obvious to us today but it was a great surprise at that time and the first known evidence of the permanent thermocline. The explanation for the permanent thermocline did not appear, however, until much later with the classical scheme of the water mass formation proposed by *Iselin* [1939]. Iselin's idea is based on the remarkable similarity of the temperature and salinity of the surface waters along a meridional section with the ones observed in a vertical profile at lower latitudes [Figure 1]. Thermocline water, also called Central Water, originates at the sea surface by subduction through Ekman pumping along the subtropical convergence. Once isolated from the atmosphere after the spring time restratification, the water mass propagates with the prevailing current at depth, along the corresponding surface of constant density (isopycnal), to finally compose the observed vertical hydrographic profile at lower latitudes, the permanent thermocline.

Iselin's conceptual model, however, only considers meridional motions, thus neglecting the zonal movement related with the gyre-scale circulation within a basin. It was four decades later when *Stommel* [1979] and *Luyten et al.* [1983] combined Iselin's meridional water mass formation scheme with the wind-driven theory of circulation [*Sverdrup*, 1947], originally proposed for a homogeneous ocean, in the first three-dimensional analytical model of the thermocline ventilation. The existence of the permanent thermocline is therefore a direct consequence of the Sverdrup circulation, thereby also referred as the thermocline circulation.

A major outcome from the *Luyten et al.* [1983] model is the distinction of two main dynamics regions: the "ventilated thermocline" (the subtropical gyre itself), where subsurface layers are continuously renewed through the wind-driven circulation, and the "shadow zone", a thermocline region in the eastern tropical ocean isolated from this ventilation. This shadow zone appears from the condition that subducted water

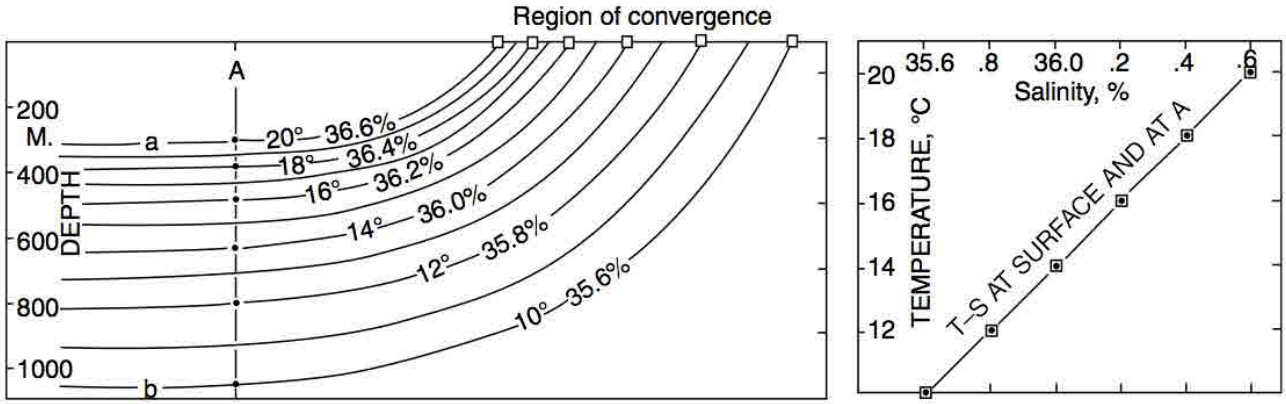

Figure 1. Schemtaic representation of water mass formation due to water sinking along isopycnal surfaces (*Iselin* [1939], reproduced from *Huang* [2010])

parcels have to conserve their potential vorticity (PV) along their trajectories [Figure 2]. The PV is quite uniform in the subtropical gyre thermocline [*Rhines and Young*, 1982], thus meridional and zonal motions are allowed within this region. The marked gradient of PV along the boundary with the tropical ocean [Figure 2] implies a strong restriction for subsurface trajectories from the subtropics towards the tropics. Below the surface layer, the shadow zone presents a stagnant circulation and an extremely poorly ventilated thermocline.

The existence of these two large-scale circulation domains can also be clearly distinguished by the presence of large contrasts in the subsurface fields of dissolved oxygen and other properties such as inorganic nutrients and tracers [*Sarmiento et al.*, 1982; *Kawase et al.*, 1985] [Figure 2]. In particular, the oxygen content of a water parcel is set up when it is formed at the ocean surface, thus in contact with the atmosphere. Once the water parcel subducts, its oxygen content decreases continuously due to biological activity. This implies that the isolated thermocline shadow zones should present extremely low oxygen content and thus they are also identified as Oxygen Minimum Zones (OMZ) [*Karstensen et al.*, 2008].

All OMZs present hypoxic conditions under which most marine species cannot survive [*Vaquer-Sunyer and Duarte*, 2008]. Moreover, oxygen also plays a major role in biogeochemical processes, such as in the nitrogen and carbon cycles [*Bopp et al.*, 2002; *Lam and Kuypers*, 2011; *Paulmier et al.*, 2011], with a direct impact on climate dynamics. Several decades of observations have revealed that the world ocean OMZs are, on average, growing and reducing their oxygen content [*Garcia et al.*, 1998; *Joos et al.*, 2003; *Stramma et al.*, 2008a, 2009]. However, the exact way the OMZs deoxygenize is yet to be deciphered, with some studies relating the observed trends to global warming [*Matear and Hirst*, 2003; *Oschlies et al.*, 2008] while others point at natural decadal variability [*Gnanadesikan et al.*, 2007; *Deutsch et al.*, 2011]. The key role of the oxygen content for the marine ecosystem endorses the crucial need for further research on the OMZs dynamics.

In this thesis we study the circulation and the main processes involved in the water mass renewal of the

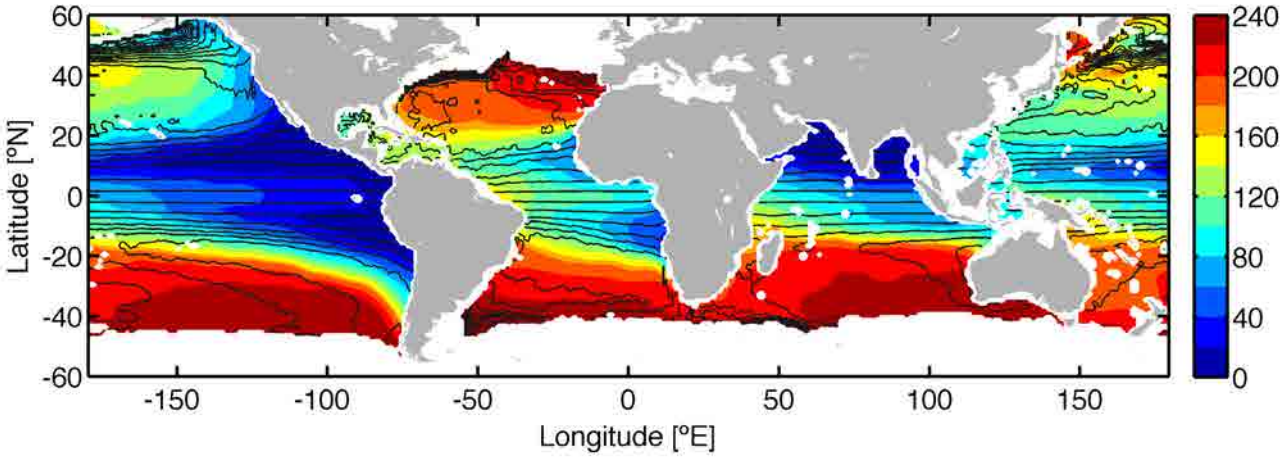

Figure 2. Mean oxygen content (color, umol kg^{-1}) and contours of Potential Vorticity (black lines, PV~=f/H) for the thermocline layer defined between density levels σθ=26.3 and σθ=27.15 kg m^{-3}. Note how the strong PV gradient delimits the minimal oxygen values. Climatological data from [Gouretski and Kolterman, 2004]

North Atlantic shadow zone thermocline, and thus of the North Atlantic OMZ (naOMZ). Using new and historic hydrographic and velocity datasets, together with numerical simulations, a novel description of the water mass pathways to the shadow zone is presented. Our results reveal a substantial water exchange between the shadow zone and the subtropical region, with important implications for the understanding of the OMZs dynamics.

1.2. Circulation

Although the simplified model of *Luyten et al.* [1983] captures the main features of the thermocline circulation, the circulation in the eastern tropical North Atlantic is made up by the interplay of different dynamic systems presented below.

1.2.1. The subtropical gyre

The wind-driven circulation of the ocean is a mirror of the atmospheric circulation. In the subtropical Atlantic region, the wind pattern depicts an anticyclonic circulation around the Azores High pressure system with easterly/westerly winds along the southern/northern boundary. Wind starts to drag surface water downwind but, due to the Coriolis force, the movement is deflected to the right in the northern hemisphere. As a net result, surface water is forced to converge, pile up and sink in the center of the subtropical region [Figure 3a]. This creates an oceanic high-pressure system equivalent to the atmospheric Azores High, which deforms the whole thermocline and leads to the deepening of the isopycnals in the subtropical region. Below the sea surface, away from the direct effect of the wind stress, the predominant low-period forces are the pressure gradient and the Coriolis force: any water movement in the direction of down-pressure gradients is deflected by the Coriolis force until the geostrophic balance is finally

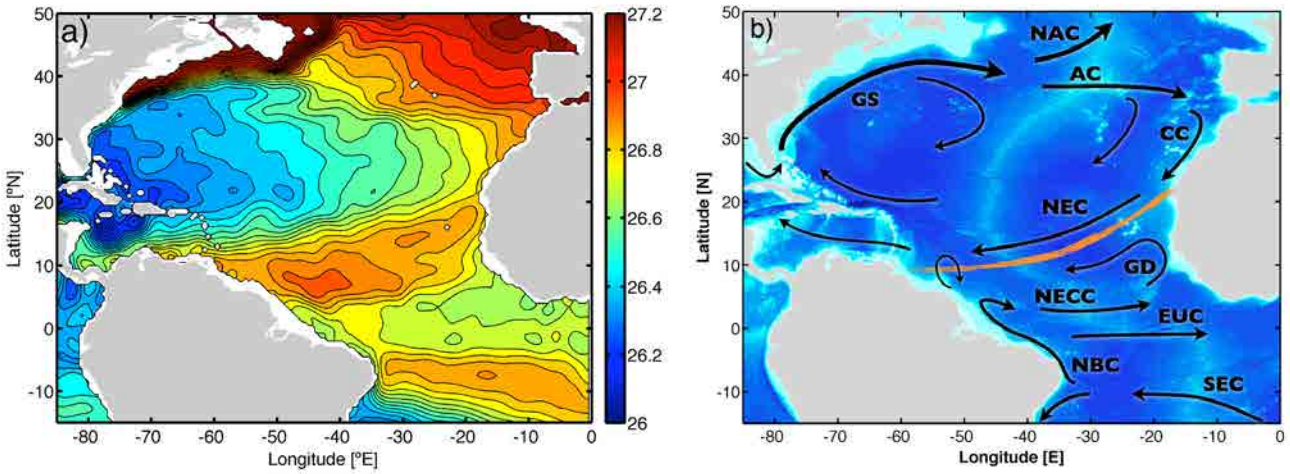

Figure 3. (a) Climatological density field at 250m depth [Gouretski and Kolterman, 2004]. The subtropical (tropical) gyre is depicted by the deepening (outcroping) of the isopycnals, i.e. lower (higher) values. (b) Scheme of the North Atlantic thermocline circulation. Orange line depicts the frontal zone between the subtropical and the tropical gyres. The main currents are: Gulf Stream (GS), North Atlantic Current (NAC), Azores Current (AC), Canary Current (CC), North Equatorial Current (NEC), Guidean Dome (GD), North Equatorial CounterCurrent (NECC), Equatorial UnderCurrent (EUC), North Brazil Current (NBC) and South Equatorial Current (SEC).

achieved; the outcome is the anticyclonic circulation in the upper 1000 m of the ocean, the North Atlantic subtropical gyre [Figure 3b].

In the North Atlantic Subtropical Gyre, the Canary Current (CC) is the eastern boundary current [Figure3b]. The CC, fed by the Azores Current (at 35ºN), flows southwards in a broad band along the North West African margin and through the Canary Islands [*Machín et al.*, 2006]. When the CC reaches Cape Blanc (at 20ºN), it encounters the so-called Cape Verde Frontal Zone (CVFZ) [*Zenk et al.*, 1991] and flows offshore. Hence, the CVFZ acts as the effective barrier to the large-scale subtropical flow, restraining the direct supply of recently subducted northern subtropical waters to the southeastern stagnant shadow zone [*Luyten et al.*, 1983]. The CC then becomes the North Equatorial Current (NEC), which crosses the Atlantic basin westward to feed the Gulf Stream (GS), the western boundary current of the subtropical gyre. The Gulf Stream flows northwestward along the American margin to ultimately flow into the Azores Current, closing the subtropical gyre circulation.

1.2.2. The tropical gyre

The NEC is therefore considered to flow along the southern boundary of the subtropical gyre, and also along the northern boundary of the tropical gyre. Easterly winds weaken south of the NEC flow, implying a meridional divergence in the surface northward Ekman transport that is balanced by the upward pumping of subsurface waters [Figure 3a]. Therefore, contrary to what happens in the subtropical gyre, in the tropical region the wind field leads to the development of an oceanic low-pressure system that drives a broad cyclonic gyre [Figure 3b]. The tropical gyre presents notable differences with the subtropical gyre, exhibiting a much shallower and zonal circulation with strong seasonality [*Stramma and Schott*, 1999; *Lázaro et al.*, 2005; *Rosell-Fieschi et al.*, 2015].

The southern boundary of the tropical gyre is the North Equatorial CounterCurrent (NECC), a broad band of eastward flow between 5ºN and 10ºN [*Sverdrup*, 1947; *Stramma and Schott*, 1999]. In contrast with the permanent flow of the NEC, the NECC is a surface current (top 100m) with a marked seasonality linked to the meridional migration of the easterly winds [*Rosell-Fieschi et al.*, 2015]. In winter, with the arrival of the northeasterly winds, the NECC disappears or even reverses. In summer, the absence of wind favours the development of the NECC. At subsurface levels, the eastward flow is weaker and presents a reduced seasonality. The main two contributors are the North Equatorial UnderCurrent (NEUC) at 5ºN, reaching 300 m, and the deeper NECC, usually referred as the northern NECC (nNECC), centred at 9ºN and flowing in the top 800 m of the water column [*Stramma et al.*, 2005, 2008b; *Brandt et al.*, 2010].

A fraction of these eastward flows (NECC, NEUC and nNECC) recirculates northward near the eastern margin, particularly clear in late summer and fall. Near the surface, induced by the enhanced positive Ekman pumping [*Siedler et al.*, 1992], a localized cyclonic structure develops centred at 10ºN and 22ºW, the so-called Guinea Dome. At the subsurface levels, this northward recirculation is much broader, extending between 30ºW and the African continent and covering the top 300 m [*Elmoussaoui et al.*, 2005]. The northward flow is especially enhanced at surface and subsurface layers along the African continent, by the development of the Mauritanian Current (MC) at the surface [*Mittelstaedt*, 1991; *Lázaro et al.*, 2005] and the Poleward UnderCurrent at the subsurface, linked to the coastal upwelling system [*Barton*, 1989; *Mittelstaedt*, 1991]. At Cape Blanc, these northward flows meet the southward CC and most of the flow is forced to retroflect westward into the NEC.

While the tropical gyre is reduced to the seasonal Guinea Dome near the sea surface, in subsurface layers the cyclonic circulation comprises the whole Atlantic basin, with a southward branch at the western margin that is usually referred as the Guyana UnderCurrent [*Schott and Böning*, 1991]. Moreover, in addition to the horizontal scheme of circulation, the tropical gyre also includes a complex and shallow overturning circulation: The continuous upwelling of subsurface waters near the equator and the later poleward Ekman transport along the surface tropical branch is compensated by the southward flow of subtropical waters subducted along the NEC path [*Liu and Philander*, 1994; *Zhang et al.*, 2003; *Schott et al.*, 2004]. This three dimensional description of the tropical gyre is also referred as the Subtropical Cell (STC) [*Liu and Philander*, 1994], establishing a connection between the tropics and the subtropics [Figure 4]. However, this circulation cell is quite shallow, typically below the density level sigma0 26.8 (roughly 300 m) [*Elmoussaoui et al.*, 2005]. Below the tropical gyre, the mean flow is extremely weak, dominated by mesoscale eddy diffusion [*Stramma et al.*, 2008b].

South of the tropical gyre (south of 5ºN) another important dynamic system appears: the equatorial system of zonal jets. Its proximity to the equator causes the Coriolis force to be very small, so the primary forces are the pressure gradients, the wind stress and the subsurface friction. This system is primary governed by the Equatorial Undercurrent (EUC), an eastward jet at the equator with its core found at depths of

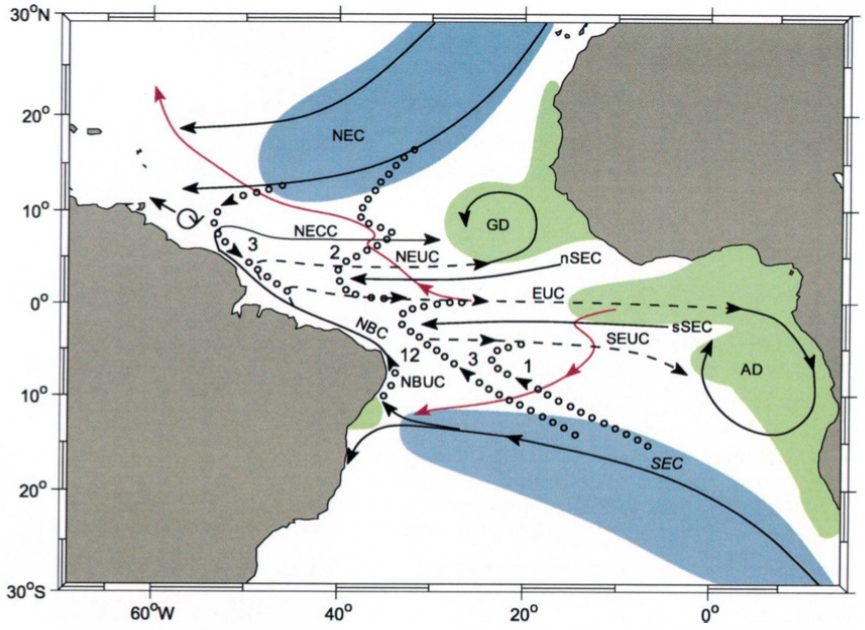

Figure 4. Circulation scheme of the two subtropical cell circulation in the tropical Atlantic. Predominant upwelling takes place in the eastern margins (highlighted in green) around the Guinea and the Angola Domes (GD and AD respectively). Subduction occurs along the subtropical branch; the North and South Equatorial Currents (highlighted in blue). *Schott et al.,* [2004]

50-100 m, driven by the zonal pressure gradient created by the easterly winds [*Brandt et al.*, 2014]. The EUC is surrounded by two slightly deeper jets, with their core found near 200 m, the North and South Equatorial Undercurrents. At intermediate depths we find other subsurface eastward jets: the Equatorial Intermediate Current (EIC) just at the equator and the South and North Intermediate Countercurrents (SICC and NICC) as close as 2º from the equator [*Brandt et al.*, 2008; *Rosell-Fieschi et al.*, 2015].

The final component of the complex tropical North Atlantic circulation is the upper limb of the meridional overturning circulation [*Broecker*, 1991]. As part of the global conveyor belt, about 15 Sv of southern hemisphere thermocline waters are transported to the northern hemisphere to compensate the formation and southward export of North Atlantic Deep Water. This interhemispheric northward transfer of southern waters occurs via the North Brazil Current (NBC) along the American continent [*Johns et al.*, 1998]. North of the equator, typically at 2ºN and 7ºN, the NBC retroflects east to feed both the EUC, and its northern and southern branches, and the NECC. About half of the northward 15 Sv retroflects into the tropics to finally flow in to the subtropical North Atlantic through the ocean interior via Ekman dynamics [*Fratantoni et al.*, 2000]; the other half reaches the subtropics along the American margin via huge mesoscale eddies shed by the NBC [*Garzoli et al.*, 2004]. As a result of this meridional transfer, the thermocline of the tropical North Atlantic is predominantly made up with southern origin waters [*Poole and Tomczak*, 1999] with a weak import of northern subtropical waters via the STC [*Fratantoni et al.*, 2000].

1.2.3. The eastern boundary coastal upwelling system

The other major dynamic element in the northeastern tropical Atlantic is the North West Africa coastal

upwelling system. The along-shore component of the large-scale winds encircling the Azores High induces offshore Ekman transport along the African coastline, leading to upwelling over the continental shelf that is compensated through subsurface shoreward flow [Figure 5]. The outcropping into the photic zone of subsurface nutrient-rich waters fuels an intense primary productivity along the coast sustaining very rich pelagic fisheries [*Arístegui et al.*, 2009]. The seasonal migration of the Azores High leads to the distinction of two different upwelling domains. Seasonal upwelling develops between Cape Verde (15ºN) and Cape Blanc (20ºN) in winter/spring and north of the Canary Islands (25ºN) in summer [*Nykjaer and Camp*, 1994]. Permanent upwelling occurs all year long between Cape Blanc (20ºN) and the Canary Islands (25ºN),

In addition to this cross-shore (zonal) circulation cell, an along-shore (meridional) system of currents is also associated to the coastal upwelling [Figure 5]. This system comprises the Canary Upwelling Current (CUC) near the sea surface [*Pelegrí et al.*, 2005] and the Poleward Undercurrent (PUC) at subsurface layers [*Barton*, 1989; *Mittelstaedt*, 1991]. The CUC is a narrow (50 km) geostrophic southward flow, highly linked to the blowing wind, appearing when the upwelling is strong enough to cause the cross-shore uplift of the density levels outside the shelf. The PUC instead is typically found between 100 and 300 m of depth, leaning on the continental slope. The PUC is driven by the along-shore pressure gradient, established by the equatorward component of the wind [*Tomczak and Godfrey*, 1994], being decoupled from the direct wind forcing. North of Cape Blanc the northward flow of the PUC has to overcome the southward CC; hence, the PUC tends to become weaker and deeper, even reaching intermediate depths [*Barton*, 1989].

The coastal upwelling system also plays the role of an important along-shore conveyor, capable of occasionally breaking the large-scale barrier of the CVFZ [*Pelegrí et al.*, 2005]. The southward CUC, in

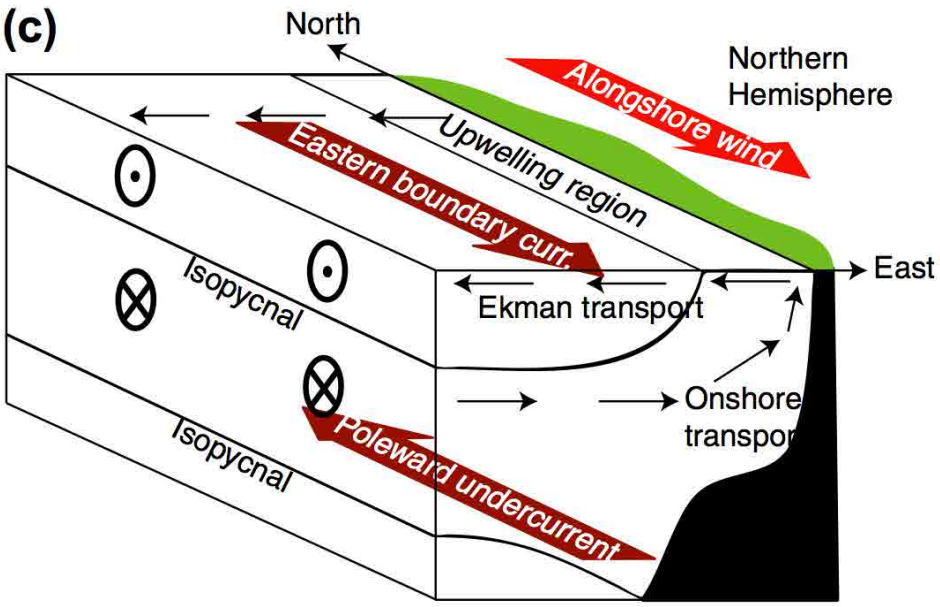

Figure 5. Scheme of the coastal upwelling system. Offshore Ekman transport at the surface drives on-shore transport below. The outcroping of the isopycnals along the coast sustained an equatorward baroclinic jet, the CUC. The along-shore pressure gradiente gradient promote the development of the PUC typically at 200m depth. [Talley, 2011].

addition to assure the along-shore coherence of the coastal upwelling [*Benazzouz et al.*, 2014], advects northern subtropical waters beyond Cape Blanc into the tropical domain in winter and spring [*Lázaro et al.*, 2005]. In contrast, the northward PUC injects tropical waters into the subtropical domain as north as 25ºN, typically during the fall season.

1.3. Thermocline water masses

A water mass is defined as a large volume of water with a common formation history [*Tomczak*, 1999]. The formation of a water mass typically refers to the moment when part of the surface waters becomes isolated from direct atmospheric forcing through wind-driven subduction or deep convection. After that moment, the physical properties (temperature and salinity, thus density) of the water mass are preserved and they only slowly change through mixing with other subsurface water masses. Non-conservative properties, mainly biochemical properties like inorganic nutrients and oxygen, are subject to change in time due to biological activity. These "preformed" properties, set under the specific atmospheric and biochemical conditions at the formation region, are the fingerprint of each water mass.

Hence, the identification of the different water masses from hydrographic observations allows the analysis of how they spread within the ocean interior, thus providing a complementary description of the mean large-scale circulation especially under the scarcity of direct velocity observations. In this sense, the water mass analysis can be specifically useful in regions with stagnant circulation like the abyssal ocean [*Warren*, 1983] or in the subtropical shadow zones (chapters II and III). For these sluggish regions, the detailed description provided by numerical circulation models can also be validated through the comparison between the observational water mass composition and the content deduced from the modelled water mass pathways (chapter IV).

As discussed before, the permanent thermocline of the ocean is formed as a consequence of the three-dimensional circulation of the subtropical gyres [*Luyten et al.*, 1983]. Only waters subducting during late winter and early spring are able to escape from the surface mixed layer and join the thermocline circulation [*Stommel*, 1979]. These waters are formed in the central and high latitude regions of the subtropical gyre, being called Central Waters. They form the permanent thermocline of the subtropical gyre, extending vertically between the lowest and highest winter density values observed within the subtropical gyre, typically between σ_θ 26.3 and 27.15.

In the North Atlantic basin, both the North Atlantic and South Atlantic Central Water (NACW and SACW, respectively) are located along the returning path of the meridional overturning circulation, with the SACW forming most of the tropical Atlantic thermocline [*Poole and Tomczak*, 1999]. However, despite the identical formation process, the hydrographic properties of the NACW and SACW are quite different. NACW is warmer and saltier than SACW as a result of the distinct supply of fresh water (evaporation/

precipitation, rivers, Mediterranean Outflow) within each basin. Moreover, the long pathway SACW has to follow a long path to reach the tropical North Atlantic from its formation regions in the southern hemisphere, leading to a marked decrease/increase on its oxygen/inorganic nutrient content due to the along-path organic matter decomposition. The SACW that fills the tropical thermocline is therefore much older than the recently ventilated NACW, the latter presenting much higher oxygen lower inorganic nutrient contents. As a result, the frontal zone between SACW and NACW depicts a drastic change in hydrographic properties especially in eastern margin where the dynamic barrier between the tropics and subtropics is stronger, the CVFZ [Figure 6] [*Kawase et al.*, 1985].

At intermediate depths, between 700 and 1500 m, two other water masses of northern and southern origin meet in the subtropical/tropical front, although in a much more diffuse pattern: the Antarctic Intermediate Water (AAIW) and the Mediterranean Water (MW). A salinity minimum clearly identifies the AAIW, centered at about 800 m depth slightly above the MW. The AAIW is formed in the Subantarctic Front and transported with the South Atlantic subtropical gyre towards the tropics [*Suga and Talley*, 1995]. Most of the AAIW reaches the subtropics along the western margin via the NBC [*Kawase et al.*, 1985; *Kirchner et al.*, 2009]. However, the northward penetration of AAIW has also been described to occur along the African coastline, reaching the Canary Islands with a maximum flow in the fall season [*Machín et al.*, 2010]. MW, on the other hand, is the outcome of the Mediterranean waters entering the Atlantic through the Strait of Gibraltar. These waters are very salty and, therefore, dense, but undergo intense mixing shortly after they leave the Strait [*Gasser et al.,* 2011]. Contrary to the AAIW, the MW is very a salty water mass with salinities above 37 in the Gulf of Cadiz. This supply of salt plays a major role in the salinification of the North Atlantic and thus in the formation of deep water mass, with a direct impact on the strength of the meridional overturning circulation and on the global climate. There are two main spread pathways of the MW [*Bozec et al.*, 2011; *Burkholder and Lozier*, 2011]: a northward route along the continental slope of the Iberian Peninsula, reaching as far as the northern North Atlantic, and a

Figure 6. Distribution of water masses aong the North West Africa coast [Pastor et al., 2012]. The water masses are South Atlantic Central Water (SACW), North Atlantic Central Water (NACW), Mediterranean Water (MW), Antarctic Intermediate Water (AAIW) and North Atlantic Deep Water (NADW).

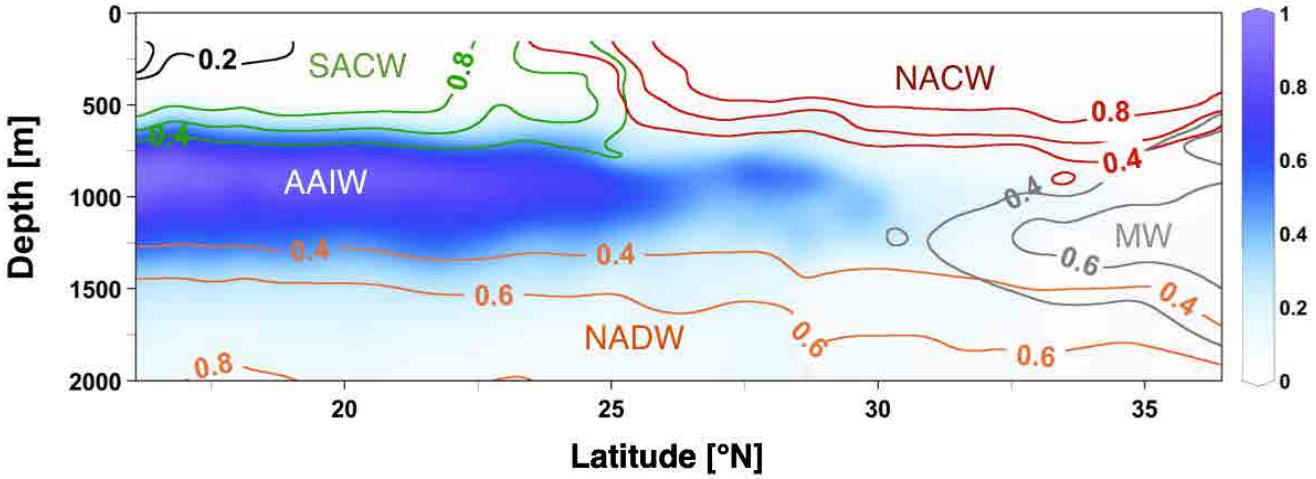

southward route taking place in the form of lateral advection and mixing into the intermediate layers (600 to 1200 m) found under the subtropical gyre.

1.4 The North Atlantic Oxygen Minimum Zone

The best evidence of the poor ventilation of the shadow zone thermocline is the development of Oxygen Minimum Zones (OMZs) in the eastern margin of all tropical oceans, at depths between about 200 and 700 m [*Karstensen et al.*, 2008][Figure 7a]. OMZs have recently gain especial attention due to the potentially major consequence that global warming may have on the evolution of the oxygen content in the world's ocean [*Matear and Hirst*, 2003; *Stramma et al.*, 2011].

Oxygen is a key component of the marine ecosystem. Asides being essential for the sustainability of marine life, oxygen plays a direct role in the biogeochemical cycling of carbon, nitrogen and many other elements (P, Fe, Mn, etc.) with a clear impact on the climate system [*Bopp et al.*, 2002; *Keeling et al.*, 2010]. Atmospheric oxygen dissolves on the ocean surface waters depending mostly on their temperature – the colder the water the more oxygen is dissolved. Hence, the deoxigenation of the global ocean has been diagnosed as a likely direct impact of the global warming [*Sarmiento et al.*, 1998]. Moreover, the predicted enhancement of the stratification may additionally reduce the supply of oxygen to the deep ocean, and increased temperatures may also enhance the microbial respiration rate, thus further reducing the oxygen dissolved in the subsurface ocean.

Decades of observations are revealing that such a deoxygenation trend is especially consistent at higher latitudes, like the North Pacific [*Whitney et al.*, 2007] or the southern ocean [*Helm et al.*, 2011]. However, the low temperature of these regions ensures the maintenance of relatively high concentration of dissolved oxygen, so the observed deoxygenation implies a minor impact on the marine ecosystem. At low latitudes, the expansion of the OMZs has also been observed during last decades [*Stramma et al.*, 2008a], although exhibiting a weaker and patchier pattern [Figure 7] [*Stramma et al.*, 2010]. However, since the hypoxic conditions of the present OMZs (oxygen concentration below 60umol/kg) are already detrimental for most organisms [*Vaquer-Sunyer and Duarte*, 2008], the expansion of the OMZs would have a clear impact on the surrounding highly productive tropical waters [*Stramma et al.*, 2010, 2011].

Besides the expected changes in the physical supply of oxygen, the changes in the biological consumption of oxygen are expected to be equally important for the evolution of the OMZs. For example, under a global warming scenario, the supply of oxygen to the OMZs is expected to get reduced as a result of both an enhanced stratification and a weakened tropical circulation [*Matear and Hirst*, 2003]. However, the same scenario also leads to a reduction in the oxygen consumption at subsurface layers due to the decline in primary productivity via reduced upwelling, even counteracting the effect of the former physical decrease in the oxygen supply [*Ridder and England*, 2014]. A deep understanding of both physical and

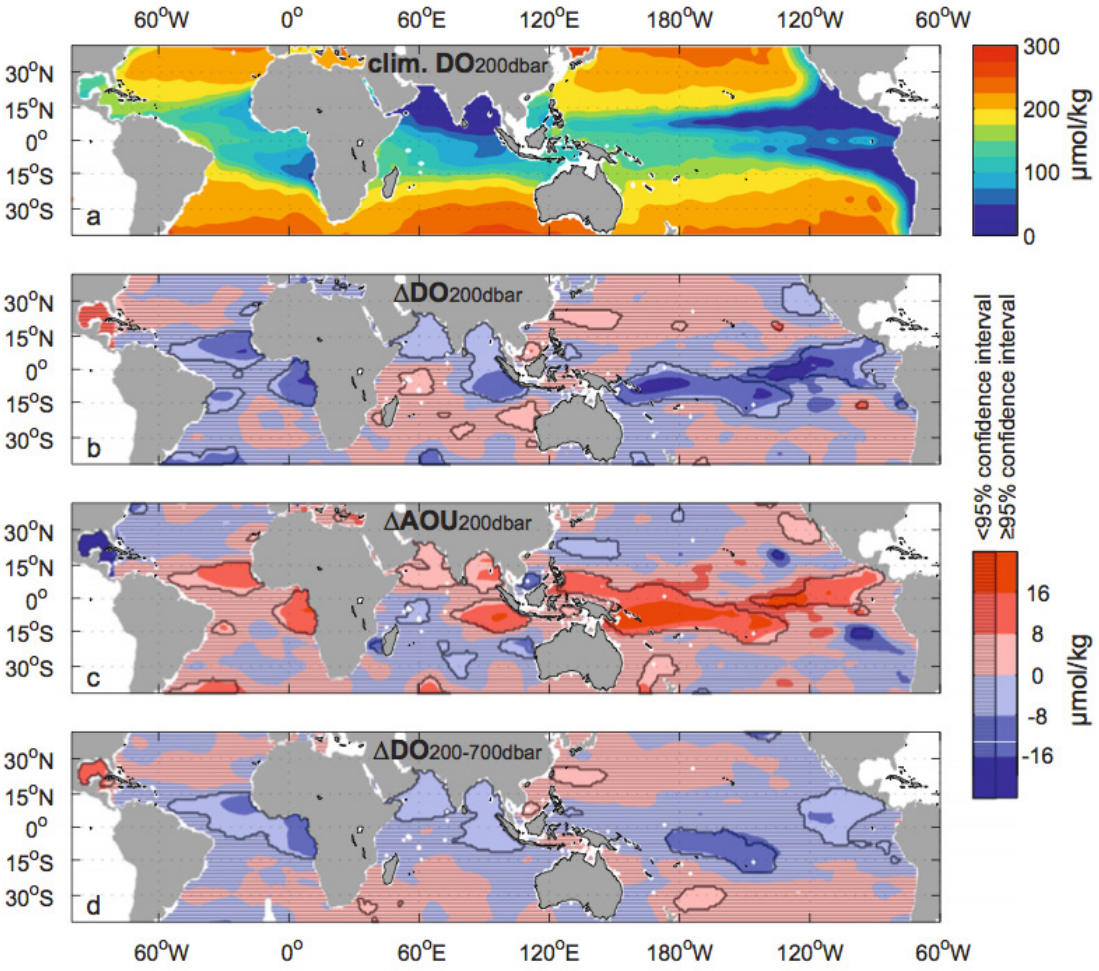

Figure 7. Climatological dissolved oxygen (DO) mean at 200dbar, as well as changes between 1960–1974 and 1990–2008 of (b) dissolved oxygen (DDO) at 200 dbar, (c) apparent oxygen utilization (DAOU) at 200 dbar and (d) DDO vertically- averaged over 200–700dbar. In (b)–(d) increases are red and decreases blue, and areas with differences below the 95% confidence interval are shaded by black horizontal lines. [Stramma et al., 2010]

biochemical systems is required to correctly assess the future evolution of the OMZs

The North Atlantic OMZ (naOMZ) is located east of 25ºW, between 10ºN and 15ºN of latitude, with minimal oxygen values found between 400 and 500 m [*Karstensen et al.*, 2008]. The ventilation of the (naOMZ) is traditionally attributed to the eastward flowing jets, which advect oxygen-rich water from the western margin while westward flows tend to drain the oxygen-poor water from the naOMZs [*Stramma et al.*, 2008] [Figure 8]. The main oxygen suppliers to the naOMZ are therefore the NEUC and the nNECC through northward branching in the eastern margin. However, this tropical cyclonic circulation

Ocean areas (Fig. 1)	Oxygen trend (μmol kg^{-1} year^{-1})	Temperature trend (°C year^{-1})
North Atlantic	−0.34 ± 0.13	+0.009 ± 0.008
Equatorial Atlantic	−0.19 ± 0.12	+0.005 ± 0.008
Southern Atlantic	−0.17 ± 0.11	+0.002 ± 0.011
Eastern Pacific	−0.13 ± 0.32	−0.001 ± 0.009
Central Pacific	−0.19 ± 0.20	−0.010 ± 0.008
Eastern Indian	−0.09 ± 0.21	+0.005 ± 0.007
N. Pacific, 100 to 400 m depth (*11*)	−0.39 to −0.70	+0.005 to +0.012

Table 1. Linear trends of temperature and oxygen with 95% confidence intervals since 1960 in a 300m to 700m layer for select ocean areas, and integrated oxygen loss, assuming a nominal density of 1027.2 kg m−3. [*Stramma et al.* 2008a]

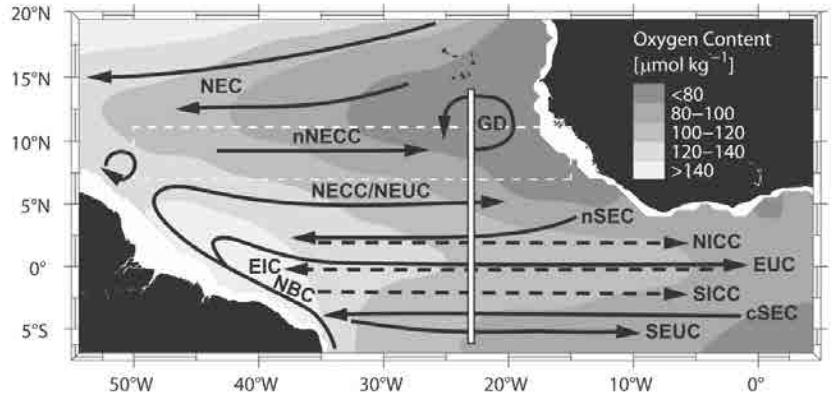

Figure 8. Scheme of the main currents in the tropical North Atlantic. The climatological oxygen mean for the layer between 300m to 500m is grey shaded. [*Brandt et al.* 2010]

only covers the top 300 m [*Elmoussaoui et al.*, 2005]; further below, at the core of the naOMZ, the pathways to the naOMZ are much more diffuse and the ventilation is supposed to be mainly carried out by eddy and diapycnal diffusion [*Fischer et al.*, 2013; *Hahn et al.*, 2014].

The naOMZ is the smallest in extension and presents the highest oxygen content of the world OMZs [*Karstensen et al.*, 2008]. While the minimal oxygen content in the North Pacific OMZ is around 0.1 umol/kg, the smallest values within the naOMZ are about 40 umol/kg. Even in the South Atlantic OMZ the minimal oxygen content is half that in the naOMZ, also occupying a volume twice larger. The better oxygenation of the naOMZ has been explained both by the shorter zonal extension of the tropical north Atlantic basin and by the enhanced supply of thermocline waters into the tropics due to the meridional overturning circulation [*Karstensen et al.*, 2008]. However the naOMZ is shoaling and reducing its oxygen content at least twice as fast as the other OMZs [*Stramma et al.*, 2008a][Table 1.]. The loss of habitat for pelagic fish in the tropical eastern North Atlantic during the 1960-2010 period has been recently estimated at 15% [*Stramma et al.*, 2011], threatening the sustainability of the valuable pelagic fisheries and marine ecosystems.

1.5. Objetives and thesis outline

With this thesis we aim at investigating the predominant patterns of circulation in the shadow zone of the North Atlantic permanent thermocline. We will do so using historical and novel hydrographic data, both from cruises and the Argo program, and by examining numerical outputs from ocean circulation models. In chapter II we will focus on the along-slope current system, emphasizing the transfer of properties across the CVFZ by the poleward undercurrent. In chapters III and IV we will explore the patterns of ventilation associated to the system of equatorial zonal jets and the possible contribution of cross-frontal exchange. We close in chapter V with the conclusions and a description of undergoing and proposed future research.

Chapter II

The continental slope current system between Cape Verde and the Canary Islands

This chapter has been published as Peña-Izquierdo, J., J.L. Pelegrí, M.V. Pastor, P. Castellanos, M. Emelianov, M. Gasser, J. Salvador, and E. Vazquez-Dominguez (2012), The continental slope current system between Cape Verde and the Canary Islands, Sci. Mar., 76, 65–78

Abstract

We use hydrographic, velocity and drifter data from a cruise carried out in November 2008, to describe the continental slope current system in the upper thermocline (down to 600 m) between Cape Verde and the Canary Islands. The major feature in the region is the Cape Verde Frontal Zone (CVFZ), separating waters from tropical (southern) and subtropical (northern) origin. The CVFZ is found to intersect the slope north of Cape Blanc, between 22 and 23ºN, but we find that southern waters are predominant over the slope as far north as 24ºN. South of Cape Blanc (21.25ºN) the Poleward Undercurrent (PUC) is a prominent northward jet (50 km wide), reaching down to 300 m and indistinguishable from the surface Mauritanian Current. North of Cape Blanc the upwelling front is found far offshore which opens a near-slope northward path to the PUC; nevertheless, the northward PUC transport decreases from 2.8 Sv at 18ºN to 1.7 Sv at 24ºN. South of the CVFZ there is an abrupt thermohaline transition at s_q=26.85 kg m^{-3}, which points at the lower limit of the relatively pure (low salt and high oxygen content) South Atlantic Central Water (SACW) variety that coexists with the dominant locally-diluted (salinity increased through mixing with NACW but oxygen diminishes because of enhanced remineralization) Cape Verde (SACWcv) variety; at 16ºN about 70% of the PUC transport corresponds to the SACW variety but over 1 Sv recirculate offshore just south of Cape Blanc, in agreement with the trajectory of subsurface drifters. However, between Cape Verde and Cape Blanc and in the $26.85<s_q<27.1$ layer, we measure up to 0.8 Sv of SACWcv being transported south. The results strongly endorse the idea that the slope current system plays a remarkable role in tropical-subtropical water mass exchange.

2.1. Introduction

The principal physical oceanographic importance of continental slopes is due to the fact that many major ocean currents, known as boundary currents, flow over them. The continental slopes underlie a relatively minor fraction of the world's oceans but yet they are the actual boundaries of the permanent upper-thermocline waters. The East and West slopes of all continents break the dominant zonal circulation in this upper ocean, forcing the flow to recirculate meridionally, often along isobaths as relatively narrow jets.

The upper thermocline along the continental slope off NW Africa is particularly complex as it runs from subtropical to tropical regions. It spans the top 600 m of the water column, occupied by waters formed in central regions of subtropical gyres, or central waters. The major water contrast takes place at the Cape Verde Frontal Zone (CVFZ) which approximately stretches from the Cape Verde Islands to about Cape Blanc [Kawase et al., 1985; Zenk et al., 1991; Pastor et al., 2012]. North of the CVFZ there is a dominance of North Atlantic Central Water (NACW), of northern subtropical origin; south of the front the waters have a much farther origin, originally coming from the subtropical South Atlantic but becoming largely modified after a long journey in the tropical regions (Fig. 1a). [Pastor et al., 2012] have recently emphasized that the top 300 m south of the CVFZ have characteristics close to equatorial waters, therefore being even more distinct from NACW.

The NACW flows southwards as the Canary Current (CC) until reaching the CVFZ where it departs offshore as the North Equatorial Current (NEC). South of the CVFZ the upper thermocline is meteorologically driven by seasonal changes in the Intertropical Convergence Zone (ITCZ). The cyclonic winds cause positive Ekman pumping which drives offshore upwelling, the outcome being the Guinea Dome (GD) and the associated cyclonic circulation [Siedler et al., 1992]. In idealized classical thermocline theories the region south of the CVFZ has been named shadow zone [Luyten et al., 1983; Kawase et al., 1985], as sudbucting waters in the subtropical gyre cannot reach this region; the CVFZ, therefore, has been thought to be an effective barrier to the large scale flow, between NACW and southern waters, although several studies have shown the presence of substantial interleaving and intermittent eddy mixing [Barton, 1987; Zenk et al., 1991].

During summer the ITZC moves north and the wind regime follows it. Two transatlantic eastward zonal jets, the North Equatorial Undercurrent (NEUC) at about 4ºN and the North Equatorial Counter Current (NECC) approximately along 8ºN, intensify and feed the southern portion of a relatively large summer GD [Siedler et al., 1992; Lázaro et al., 2005; Stramma et al., 2005]. During winter the ITZC moves south and the NECC weakens [Stramma and Schott, 1999; Lankhorst et al., 2009]. South of the CVFZ, the cyclonic winds remain intense but move southeast, its centre being located near-shore [Nykjaer and Camp, 1994]. Since the GD is forced by the wind field it follows the seasonal ITCZ displacements, hence moving southeast from summer to winter [Nykjaer and Camp, 1994]. As a result the northward

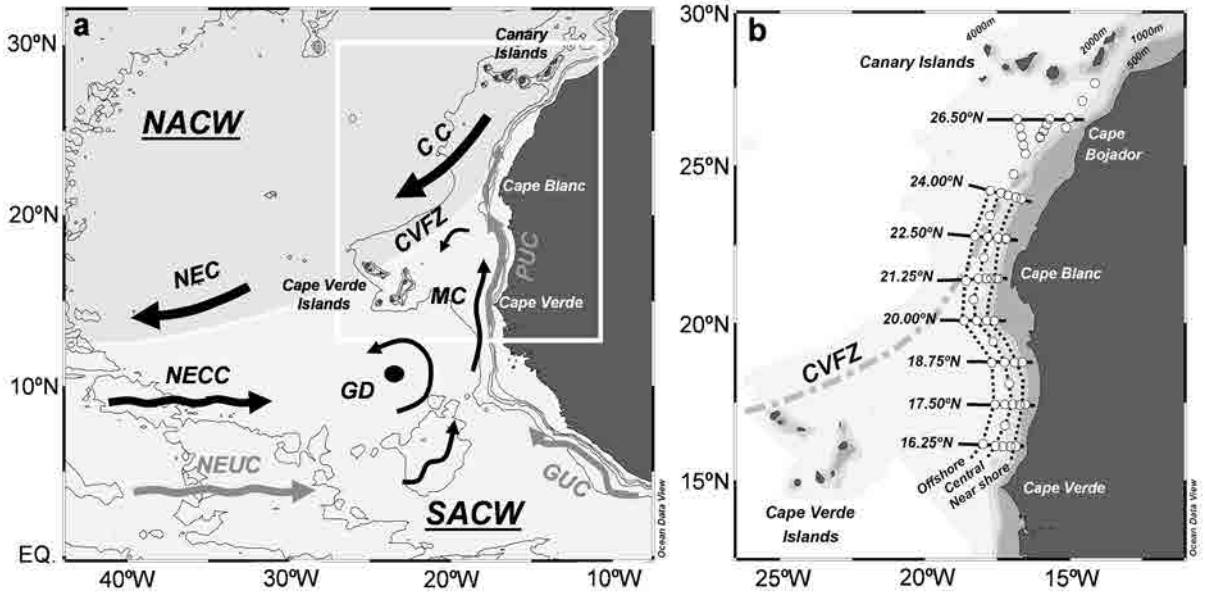

Figure 1. Left panel: Schematic pattern of the circulation showing the main currents and dynamic features: Canary Current (CC), North Equatorial Current (NEC), North Equatorial Counter Current (NECC), North Equatorial Under Current (NEUC), Poleward Undercurrent (PUC), Mauritania Current (MC), Guinea Undercurrent (GUC), Guinea Dome (GD) and Cape Verde Frontal Zone (CVFZ). Right panel: Map of the study area showing the hydrographic stations and the cross and along slope sections used in this work. Contours of 500, 1000, 2000 and 4000 m isobaths are grey coloured. The nearshore and central meridional sections approximately follow the 1000 and 2000 m isobaths

along-slope flow between Cape Verde and Cape Blanc, some times named the Mauritania Current (MC) [Mittelstaedt, 1991; Lázaro et al., 2005], intensifies in summer and weakens in winter [Mittelstaedt, 1991].

Over the continental African slope there is yet another frontal system, the wind-induced coastal upwelling system. This is a relatively shallow system which occupies the depth of direct wind influence, typically no more than 200 or 250 m depth. The region between Cape Blanc and the Canary Islands, dominated by NACW, is characterized by year-long intense upwelling [Van Camp et al., 1991] and the associated near-slope southward Canary Upwelling Current (CUC) [Pelegrí et al., 2005, 2006; Mason et al., 2011]. South of the CVFZ, upwelling is present only in winter, when the ITCZ migrates south. The essential elements of the upwelling system are (i) westward (offshore) Ekman transport of the surface mixed-layer waters, (ii) subsurface compensating eastward (onshore) flow which upwells over the slope due to the coastal constraint, and (iii) southward (along-slope) baroclinic flow linked to the frontal system. The southward winds are also responsible for (iv) building a large-scale pressure gradient which induces an along-slope subsurface current, known as the poleward undercurrent (PUC) [Barton, 1989]. In winter the southward winds intensify the PUC south of Cape Verde, effectively becoming the winter counterpart of the near-surface MC.

Along-slope poleward undercurrents are ubiquitous features in all major eastern boundary current system. The Northeastern Atlantic PUC was studied mostly during the 70's and 80's when an intense international research effort took place to understand the NW Africa upwelling system (for a review see [Machín et

al., 2006]). The PUC is normally observed as a narrow jet (about 50 km wide) leaning on the continental slope and centered between 100 and 300 m; the poleward flow is sometimes observed to extend much deeper, to intermediate waters [Barton, 1989; Machín et al., 2006; Machín and Pelegrí, 2009]. The PUC appears as a natural extension of the westward Guinea Undercurrent (GUC) and the summer MC, but it also incorporates water recirculating around the GD. The PUC has been traditionally linked to the advection of pure SACW, even beyond Cape Blanc where it encounters the CC and is usually found deeper, centred at some 500 m depth [Mittelstaedt, 1983, 1991; Hagen, 2000].

In this study we aim at providing a detailed description of the complex system of currents over the continental slope in the eastern margin of the North Atlantic Ocean, from Cape Verde to the Canary Islands (about 16 to 27ºN). We will do so through a set of measurements taken during November 2008, with eight high-resolution cross-slope transects and several along-slope sections. First, we present the collected data set and the sea-surface wind fields during the cruise. This is followed by a brief review of a recent water-mass composition analysis carried out by [Pastor et al., 2012], to be used in this work. The subsequent sections are the heart of this paper, where we explore the velocity field and the distribution of water properties over the continental slope. The purpose is to draw a picture of the circulation patterns over the continental slope and their role on the propagation of water masses of southern and northern origin.

2.2. Data and methods

2.2.1 Data set

The CANOA08 cruise was carried out in November 2008 onboard R/V Sarmiento de Gamboa. A total of 55 stations were occupied along the NW Africa coast from Cape Verde to the Canary Islands (Fig. 1b). Except for the first nine northeastern-most stations, which were done between 9 and 12th November, all stations were carried out between 20 and 29th November with the vessel travelling from South to North. A total of eight cross-slope sections were completed, typically with five stations each, separated by about 1.25º of latitude; an additional station was taken between sections approximately over the 2000 m isobath. The resolution in the cross-slope direction increased from 30 km offshore to 5 km near-shore while the resolution in the along-slope direction was about 60 km over the 2000 m isobath; two additional along-slope sections, with half this resolution, may be constructed offshore and over the 1000 m isobath as far north as 24ºN, as shown in Figure 1. Additionally to the hydrographic measurements, several subsurface buoys, dragged at 100 m depth, were launched.

The stations were sampled using SeaBird 911plus Conductivity-Temperature-Depth (CTD) sensors and a SBE-43 dissolved oxygen (O_2) sensor. The CTD-O_2 probe was mounted on a 24 Niskin bottles rosette that collected water samples at standard depths. These waters were analysed for dissolved oxygen onboard and samples were frozen for a posterior analysis of inorganic nutrients. Oxygen from the bottle samples

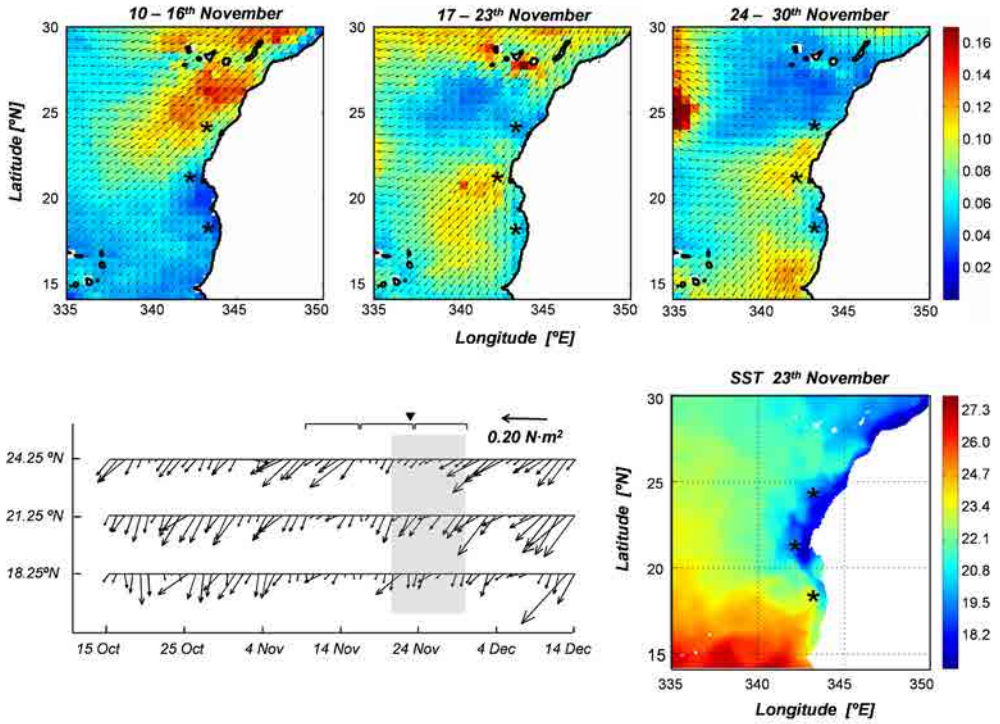

Figure 2. Top panels: Weekly-averaged wind stress fields [N m-2] for three consecutive weeks, starting on 10, 17 and 24th November 2008. Bottom left panel: Temporal series of the surface wind stress vector at three different latitudes over the slope (asterisks in top panels). The shaded area, the top brackets and the tick mark respectively indicate the duration of the cruise, the average intervals for the wind stress field, and the day of the SST image (source: QuikSCAT). Bottom right panel: SST [ºC] on 23th November 2008, as obtained from OSTIA.

was determined by the Winkler titration method. The relation between the oxygen determined by the electrode in the CTD and the Winkler method was signifficant (r^2>0.96, p<0.01, n>12), and the average difference between the oxygen from the CTD and the Winkler method was -0.63 ml l^{-1}.

The velocity of the upper ocean currents was measured with a 75 kHz shipboard Ocean Surveyor Acoustic Doppler Current Profiler (OS-ADCP) which samples the top 600 m of the water column with a good signal-to-noise ratio. The OS-ADCP was configured to produce five-minute average velocity profiles and collected single-ping data with a vertical resolution of 8 m at 75 kHz. The ADCP was initially calibrated over the continental shelf through bottom tracking so that the alignment angle and scale factor were determined; later, from the comparison of consecutive repeated sections in a region of high horizontal shear, a meridional velocity offset of 0.02 m s^{-1} was detected and the velocity field was corrected. A Lowered ADCP (LADCP) system, consisting of two RDI 300 kHz Workhorse Monitor used in synchronized master-slave mode, was also mounted on the rosette but it did not work properly on all stations. Nevertheless, a comparison between the available LADCP profiles and the corrected on-station ADCP data shows good agreement (not shown) and gives us confidence on the good quality of this ADCP data set. Therefore, in this study a velocity profile is calculated at each station through averaging all ADCP data collected while the vessel was on that position.

The surface wind field, prior and during the execution of the experiment, has been extracted from the QuikSCAT data set (Fig. 2). We may appreciate a predominance of north-easterly winds during the cruise over the whole study area. During the first week of measurements the wind was quite intense north of Cape Blanc; during the second and third weeks it respectively weakened and intensified north and south

of Cape Blanc. For the time period of the cruise the Sea Surface Temperature (SST) field was available on near-real time through the Operational SST and Sea Ice Analysis (OSTIA) product 3 [Stark et al., 2007].

2.2.2. Optimum Multi-Parameter analysis

An Optimum Multi-Parameter (OMP) method aims at finding the contribution of different predefined source water types in a water sample. These contributions are determined as a linear mixing combination in a multi-parameter space [Mackas et al., 1987; Tomczak and Large, 1989]. Each parameter is given a different weight according to its accuracy and natural variability. In this study we follow the application of the OMP for the NW Africa region as presented in [Pastor et al., 2012] and explained in the appendix. Five independent variables (potential temperature, salinity, oxygen, phosphate and silicate) are combined with mass conservation, and a total of six water types are specified. The analysis is applied to data in the density range $26.46<s_q<27.82$, specifically excluding near-surface data (down to about 100 or 150 m) in order to avoid atmospheric and biogeochemical processes (hereafter we use sigma-theta or potential density anomaly, equal to potential density less 1000, in units of kg m^{-3}).

One relevant contribution of [Pastor et al., 2012] has been the distinction of two different varieties of southern waters, predominantly found in the region south of CVFZ. While the regional central water mass of southern origin was defined by [Tomczak, 1981], a fresher and colder variety, therefore with purer South Atlantic characteristics, may also be detected from historical observations in the southeastern North Atlantic [Voituriez and Chuchla, 1978]. The distinction between the two varieties allows us to discern the different contribution of both water masses on the slope undercurrent. Therefore, hereafter we refer to the regional variety as Cape Verde South Atlantic Central Water (SACWcv), defined in the OMP analysis by the contribution of two water types (upper and lower Cape Verde South Atlantic Central Water, SACWcv-u and SACWcv-l respectively); in contrast, the purer variety is simply named South Atlantic Central Water (SACW), being solely represented by one point in the multi-parameter space (one water type) due to its shallowness, as we discuss in next sections. The contribution of North Atlantic Central Water (NACW) is assessed again through the combination of two points, the upper and lower North Atlantic Central Water (NACWu, $NACW_l$). Figure 3a shows the location of these northern and southern central waters in a temperature-salinity diagram. Additionally, the presence of Antarctic Intermediate Water (AAIW) was also introduced in the analysis to properly describe the water masses distribution at the bottom of the thermocline, however we will not use it in this work.

2.3. Results

2.3.1 Penetration of SACW characteristics

In this section we examine the latitudinal dependence of mean water properties with the help of scattered plots, where the spatial variability is smoothed out through a reduced Data Interpolating Variational Analysis (DIVA, http://modb.oce.ulg.ac.be/viewsvn/) technique (Figs. 3b, c). These plots do not aim at examining the detailed distribution of water properties but are rather used to view the gross latitudinal property patterns.

The most remarkable feature of the hydrographic field is the clear distinction between northern and southern central waters (Fig. 3a). At the southernmost part of the region, for σ_q <26.85, we may distinguish the presence of the fresher and more oxygenated SACW, the further south the more oxygen we find at these upper levels. In contrast, on the northern end we find only NACW; on a same isopycnal surface, NACW is a much saltier, colder and oxygen richer water mass than the southern water masses. However, the most common water in the shadow zone is the regional SACWcv variety, substantially saltier than SACW. Further, the SACWcv presents the minimum oxygen concentrations of the three central water masses (Fig. 3b). This suggests that the SACWcv water mass represents an old SACW variety that has lost most of its oxygen content while also mixing slowly with the nearby salty NACW. The SACW variety thus represents a relatively young water mass that renovates the upper layers of the shadow zone through direct advection of the tropical eastward zonal jets, the NEUC and NECC [Elmoussaoui et al., 2005].

Another prominent characteristic is the vertical salinity minimum observed at σ_q = 26.8 kg m^{-3}, an abrupt salinity, and even temperature, inversion at depth. This salinity minimum matches with the point of SACW definition and it is also found just a little deeper than the subsurface oxygen maximum (Fig.

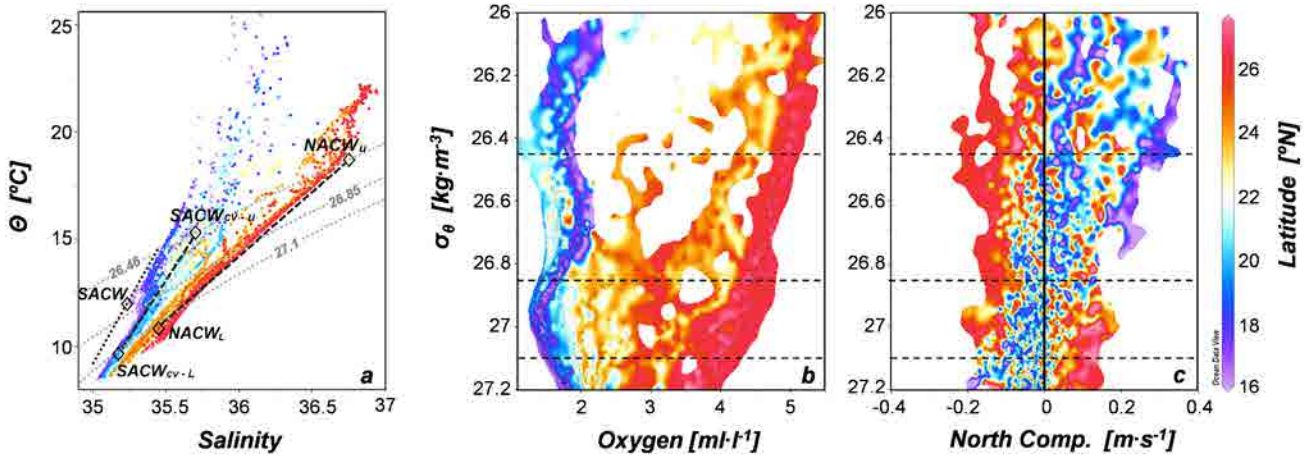

Figure 3. Left panel. Potential temperature - salinity diagram as obtained using the whole data set. Void diamonds indicates the water types used in the OMP analysis of Pastor et al. (2011). Central and right panels: Smoothed scatter plots, again obtained using the whole data set, of dissolved oxygen and meridional velocity (in [m s-1], positive northwards) as a function of potential density. In all plots the latitude [ºN] is colour-coded according to the right-hand-side colour bar.

3). These features may be detected in salinity distributions presented by several authors for the region south of the CVFZ [Tomczak, 1972; Fraga F., 1974; Hughes and Barton, 1974] but yet few studies have explored its significance [Voituriez and Chuchla, 1978] early proposed that this salinity minimum represents a boundary between northward flow of SACW in upper layers and a southward flow of NACW deeper. More recently, [Elmoussaoui et al., 2005] have used a high-resolution model to highlight the existence of a thermohaline transition (smoothed in their numerical solution) at σ_θ = 26.8 kg m^{-3}. The numerical output suggests that the NEUC and NECC merge southwest of the GD from where they reach towards the African slope and recirculate north towards the CVFZ. However, these relatively shallow jets may only ventilate the shadow zone down to some 300 m, i.e. the lower portion of the upper thermocline is not renewed so that its waters have long residence time which leads to high remineralization rates and low oxygen concentrations [Stramma et al., 2005, 2008; Karstensen et al., 2008].

A scattered plot of the meridional velocity interpolated as a function of density illustrates the predominant propagating directions of southern and northern waters (Fig. 3c); the interpolation smoothes out the velocity fields so that, despite the existence of high spatial variability, we may identify mean flow patterns. The meridional velocity component presents a similar depth transition, in agreement with Voituriez and Chuchla 1978. All the way until 22.5ºN, those layers with σ_θ<26.85 kg m^{-3} move predominantly northwards, with speeds up to 0.3 m s^{-1}, carrying oxygen with SACW characteristics. This northward flow reaches significantly north of Cape Blanc, i.e. past the traditional interjection of the CVFZ with the continental slope. At 24ºN the flow is approximately null and further north it appears to reverse but obscured because of the mesoscalar variability south of the Canary Islands. Contrarily, at latitudes less than Cape Blanc the deeper layers ($26.85 \leq \sigma_\theta < 27.1$) predominantly move southwards, carrying SACWcv characteristics. North of Cape Blanc, these deep layers do not display a predominant propagation pattern. Hence, near the CVFZ there is substantial convergence on layers shallower than σ_θ = 26.85 kg m^{-3} and weak divergence below.

According to the above observations, and following [Elmoussaoui et al., 2005], we may distinguish between Surface Waters (SW; σ_θ<26.46, down to about 100 m), upper Central Waters (uCW; $26.46 \leq \sigma_\theta < 26.85$, between some 100 and 300 m) and lower Central Waters (lCW; $26.85 \leq \sigma_\theta < 27.1$, between about 300 and 500 m). We set the interface between uCW and lCW slightly deeper than in [Elmoussaoui et al., 2005], i.e. σ_θ=26.85 rather than 26.8, in order to better match the observed abrupt vertical transition in southern water characteristics and to include the full low-salinity SACW signal within the uCW.

2.3.2 Cross-slope sections

Despite the general smoothed picture arising from Figure 3c, the slope current system does present high spatial variability. In order to appreciate this variability and to identify the propagating paths we examine the distributions of salinity, oxygen, meridional velocity and water-mass composition in eight cross-slope

sections at nominal latitudes of 16.25, 17.5 18.75, 20.0, 21.25, 22.5, 24.0 and 26.5ºN (Figs. 4 and 5). Trade winds were present during the whole cruise, leading to intense upwelling off NW Africa region as illustrated by the SST image in Figure 2. South of Cape Blanc upwelling is the result of the predominant local winds, but yet the uCW and SW layers display a remarkable northward along-slope flow which may be interpreted as a late expression of the summer MC on top of the PUC. North of Cape Blanc upwelling is very intense and located far offshore, probably arising from the build up of wind impulses during the summer-long upwelling season [Csanady, 1977]. The combination of both features should allow the propagation of the PUC, manifested as a northward flow within SW and uCW layers, well beyond Cape Blanc. Figure 4 indeed shows a well-defined northward flow attached to the continental slope, with maximum values in all sections above 0.2 m s^{-1}, extending from the surface down to 300 m in the southern sections and shoaling towards the north. In this figure it is difficult to distinguish the near-surface MC from the subsurface PUC; therefore, our measurements reflect the late summer and autumn conditions south of Cape Blanc, when the MC is strengthened [Mittelstaedt, 1991] and northward transport is maximum [Elmoussaoui et al., 2005].

The SW layer is highly influenced by the upwelling system. Within this layer the contours of all properties uplift towards the slope, except for the presence of relatively low oxygen content as a sign of high productivity (Fig. 5). A marked change in properties is observed just north of Cape Blanc (Fig. 5f), denoting the location of the CVFZ. The surface flow has a predominant northward direction in all cross-slope sections (Fig. 4), typically wider than about 50 km; in the southern sections this could be interpreted as the MC while beyond Cape Blanc it would be the surface manifestation of the PUC. North of Cape Blanc, the offshore extreme of these 100-km wide sections flows south (Fig. 4), likely related with the far offshore location of the coastal upwelling jet during the intense upwelling season (Fig. 3). At 26.5ºN, south of the Canary Islands, the flow is dominated by intense mesoscalar activity. The near-slope high salinity and oxygen values at 22.5ºN, north of Cape Blanc, suggest that the flow direction at the CVFZ is intermittent, being northward during the cruise but having possibly changed direction at previous times. It is therefore possible that the 22.5ºN latitude corresponds to a mean northern limit of the MC, in agreement with the results of [Lázaro et al., 2005].

The uCW layer is characterized by the presence of the PUC in all sections except 26.5ºN (Fig. 4). In this layer and south of the CVFZ, the slope current appears as a northward jet with a width of several tens of kilometres, which reaches down to over 200 m and is hardly distinguishable from a slightly wider surface MC. South of about 20ºN the uCW layer appears as an oxygen maximum stratum, with values as large as 2.12 ml l^{-1} (Fig. 5). This relative high content of oxygen is related to the predominance of SACW which is present only in this layer. The presence of SACW is progressively reduced as we move north along the slope, with decreasing oxygen content. Mixing with salty NACW is responsible for the significant salinity increase near Cape Blanc but, despite NACW is higher in oxygen than SACWcv, the near-slope oxygen content is notably reduced. Near the Cape Blanc filament the near-slope subsurface oxygen level is further exhausted, with values as low as 1.14 ml l^{-1} (Fig. 5e), and the offshore waters appear slightly

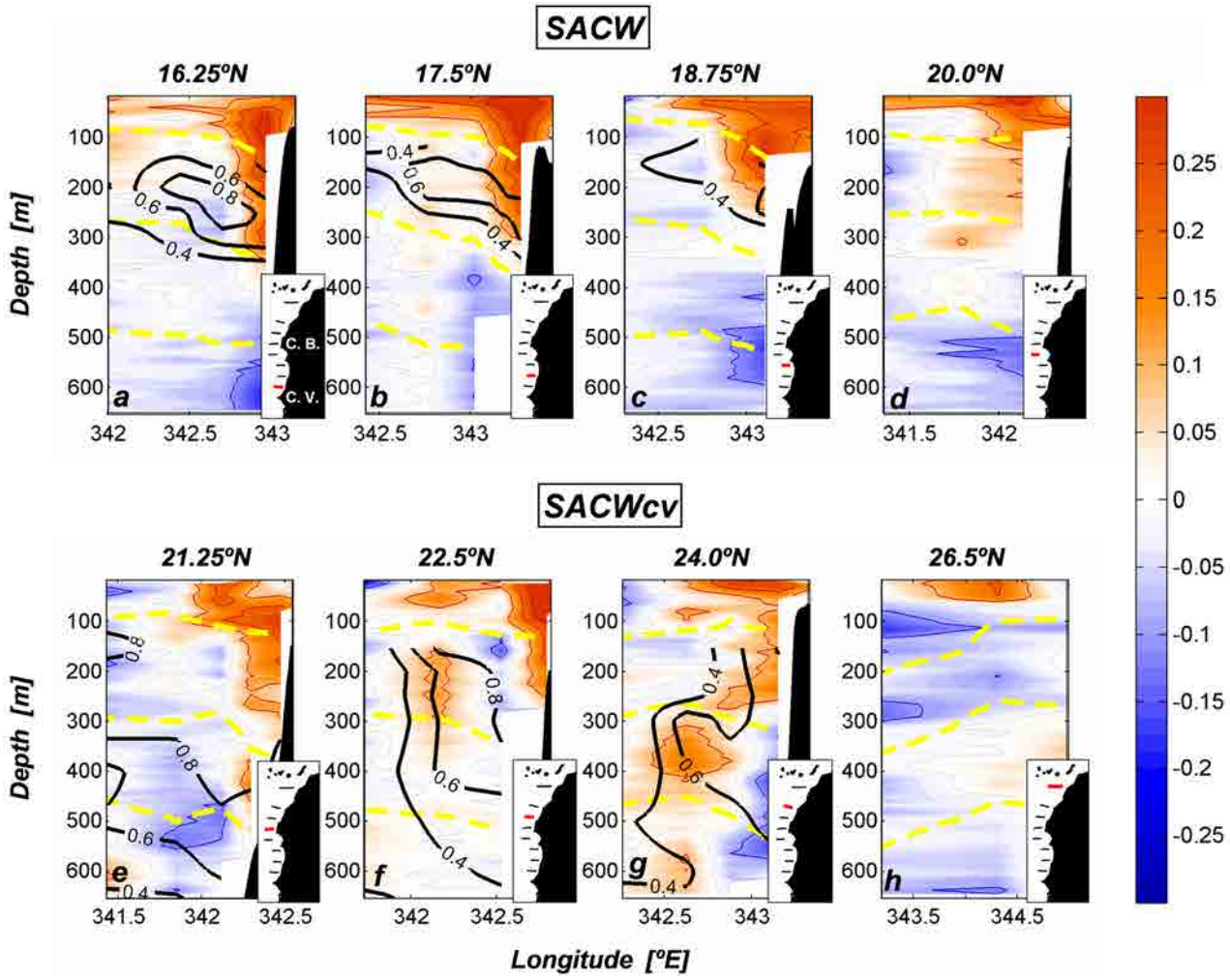

Figure 4. Distribution of water properties on eight different cross-shore sections (Fig. 1). The meridional velocity (in [m s-1]) is colour-coded according to the right-hand-side colour bar, with positive values denoting northward flow; contours are drawn every 0.1 m s-1 intervals. The black lines show either the fraction of SACW south of Cape Blanc (top panels) or the fraction of SACWcv north of Cape Blanc (bottom panels); in the upper panels the remaining water mass contribution is only SACWcv while in the lower panels it is NACW. Three selected isopycnals (26.46, 26.85 and 27.1 kg m-3) are drawn in yellow. The map insets indicate the location of the corresponding section.

more oxygenated. This suggests that the CVFZ prevents some of the southern waters to flow north of Cape Blanc, this becoming an area where SACWcv is formed through mixing of SACW with NACW and enhanced oxygen consumption of SACW (because of remineralization taking place under the highly productive upwelled waters). Despite the blockage of the CVFZ, some of this oxygen-poor and relatively salty SACWcv is transported along the slope by the PUC (Figs. 4f and 5f) and released as far north as Cape Bojador (Fig. 4g).

The northeastward extension of the NEUC slowly advects SACW to the northern part of the GD during summer, but only a fraction of this relatively pure SACW is eventually incorporated by the relatively shallow PUC (which occupies the uCW). The core of SACW is located seawards from the PUC core, in agreement with observations by [Hughes and Barton, 1974], in some cross-slope sections coinciding with the presence of a weak southward flow (Figs. 4a, b). Therefore, it appears that most of the SACW inflow may recirculate meridionally between the continent and the Cape verde Islands and that the PUC

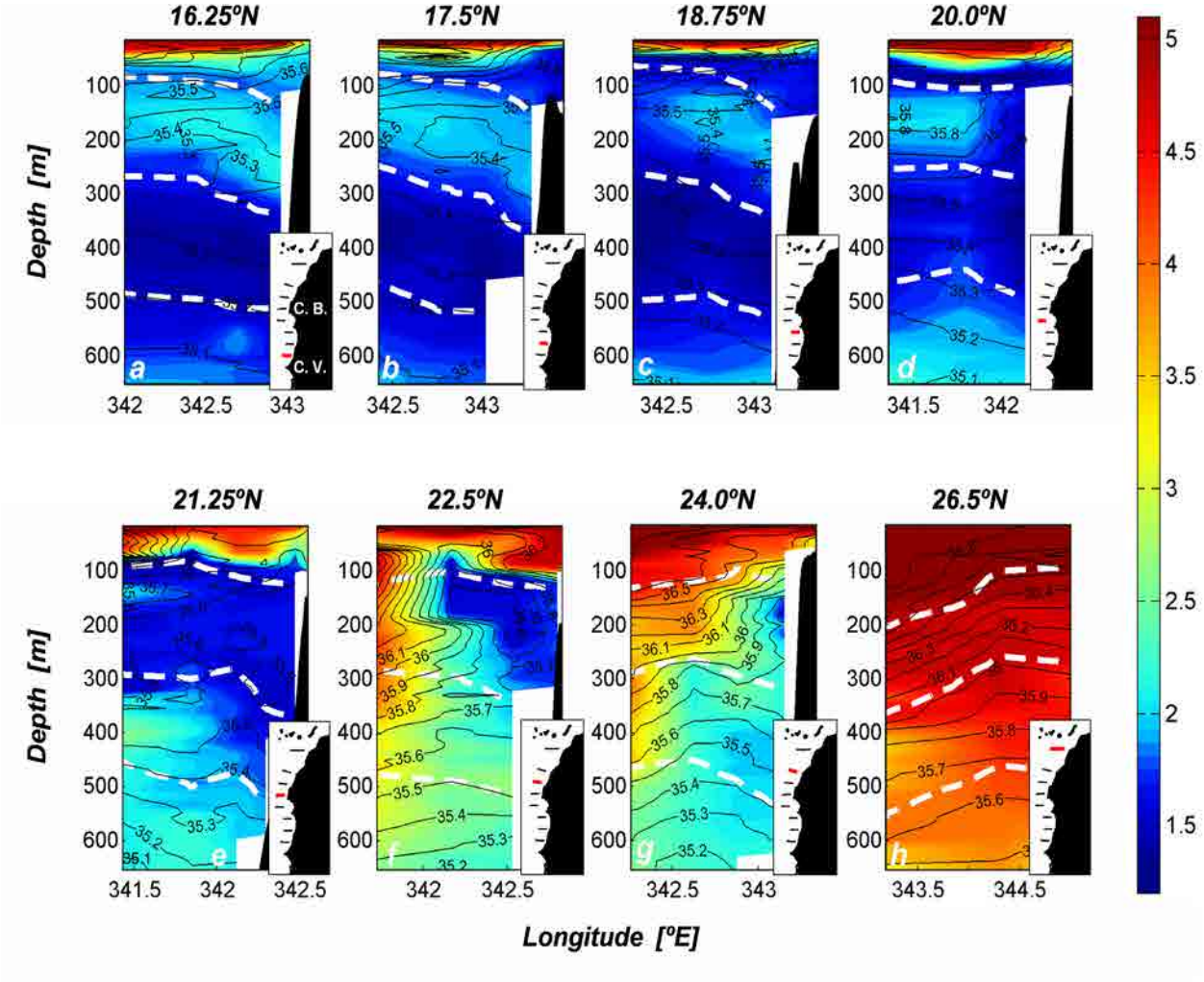

Figure 5. Distributions of oxygen content ([ml l-1], coloured) and salinity (black contours) on eight cross-shore sections. Three selected isopycnals (26.46, 26.85 and 27.1 kg m-3) are shown as dashed white lines. The map insets indicate the location of the corresponding section.

is not always directly fed by SACW, hence validating [Elmoussaoui et al., 2005] numerical results. In most sections the dominant water mass advected by the PUC is the recirculating SACWcv (Figs. 4 and 5), although it has an important SACW contribution that arises from the extension of the tropical zonal jets and, possibly, also from the low-latitude along-slope Guinea Undercurrent [Mittelstaedt, 1991]. North of Cape Blanc the southern central waters, already fully transformed into SACWcv, penetrate northwards through the along-slope PUC [Fraga F., 1974; Hughes and Barton, 1974; Hagen, 2000]. The salinity distributions for the cross-shore sections between 21.25 and 24.0ºN show that this intrusion occupies a 50-100 km wide near-slope meridional band. Such a PUC penetration is likely favoured by the high intensity of upwelling during the previous weeks or months (Fig. 3), so that the distant offshore position of the upwelling front is coupled to the propagation of relatively fresh and cold SACWcv (Figs. 5e, f, g). The lCW and uCW layers display quite opposite distributions south of Cape Blanc. In the lower layer the oxygen content reaches minimum values in the southern sections (1.27 ml l^{-1}, Fig. 5), similar to those found in the GD oxygen minimum zone [Stramma et al., 2005], and increases towards the north under the influence of NACW. North of Cape Blanc the minimum oxygen values are found near the slope,

indicative of the presence of SACWcv (Figs. 5 and 6c, g). However, a divergent flow is observed along the continental slope, with moderate (maximum 0.15 m s^{-1}) southward flow at latitudes less than 22ºN and the presence of substantial variability further north. The existence of southward flow is counter-intuitive with the presence of waters of southern origin (SACWcv) and raises the possibility that the direction of the flow may seasonally reverse, we will come back to this issue in next section.

2.3.3 Along-slope sections

The high cross-shore variability in the distribution of water properties is accompanied by substantial along-slope coherence (Fig. 6). This coherence is the result of the system of meridional along-slope currents, although it breaks at the PUC-CC convergence region north of Cape Blanc, as well as off Cape Bojador because of intense mesoscalar activity [Rodríguez-Marroyo et al., 2011]. The minimum oxygen distribution depicts a vertically-tilted CVFZ which separates northern from southern central waters, with the transformation of SACW into SACWcv near the slope and interleaving of SACWcv and NACW further offshore (Fig. 6).

The velocity field along the African slope shows that SW and uCW, composed by the surface MC and a relatively shallow PUC down to 300 m depth, converge towards about 22ºN. The underlying lCW layers flow towards the equator at latitudes less than 20ºN and do not have a clear predominant direction at northern latitudes (Figs. 4 and 6). As already pointed out, the southern sections only have limited NACW

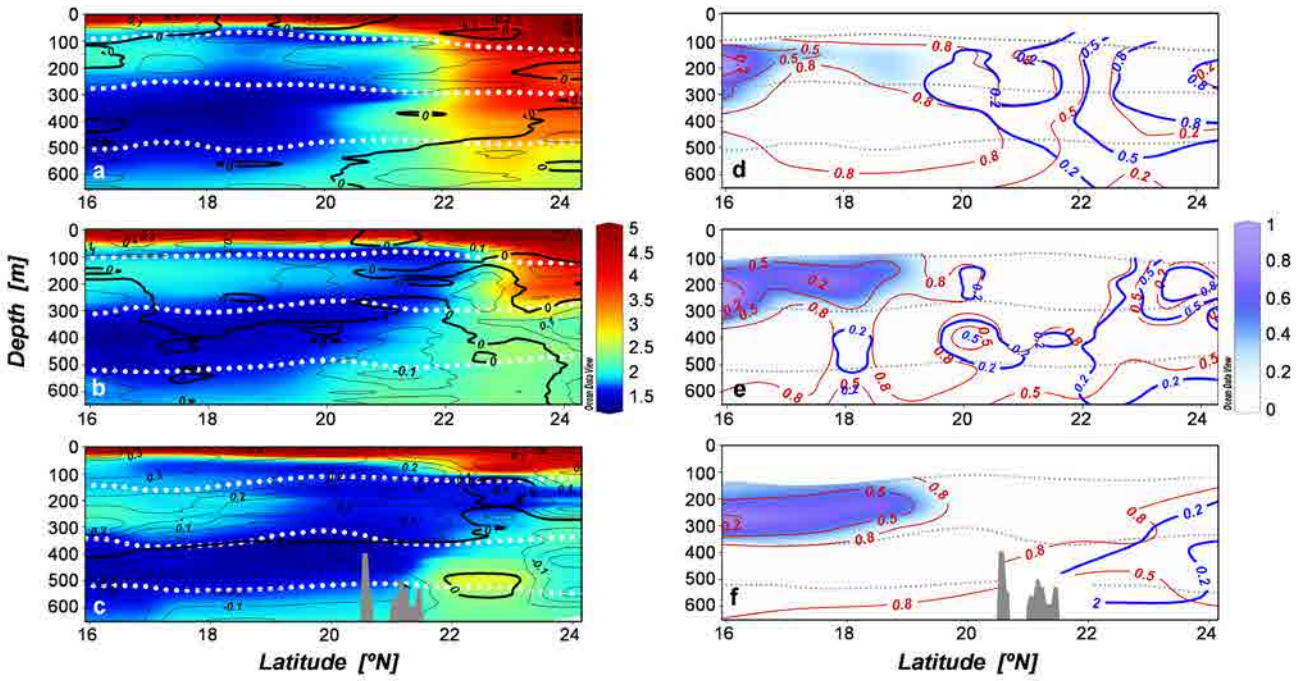

Figure 6. Left panels: distributions of oxygen content ([ml l-1], colour-coded according to the right-hand-side colour bar) and meridional velocity ([m s-1], black lines, positive northward). Right panels: contribution of three different water masses along the same sections; SACW (blue colours following the right-hand-side colour bar), SACWcv (red contours) and NACW (blue contours). Three selected isopycnals (26.46, 26.85 and 27.1 kg m-3) are indicated with white (grey) dotted lines in the left (right) panel. The top, central and bottom panels respectively correspond to the along-slope sections located offshore and over the 2000 and 1000 m isobaths (Fig. 1).

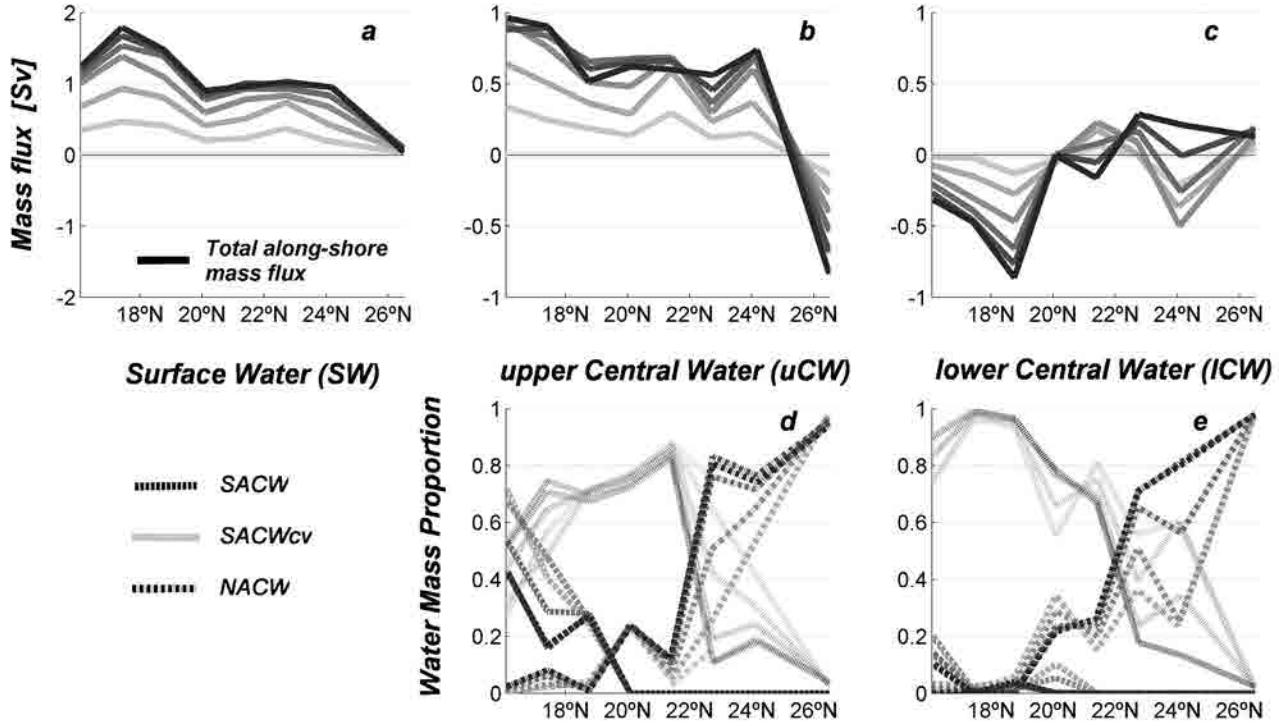

h Figure 7. Top panels: Latitudinal change in meridional mass transport (positive northward [Sv]) for three different layers. The transports are calculated through the eight cross-shore sections, with the accumulated transports (increasing seawards from the shelf break) represented by curves of increased darkness. Bottom panels: Average SACW, SACWcv and NACW fractions in each cross-shore section interpolated every 10 km; the increased darkness again represents the increasing seaward distance from the shelf break. Notice that no OMP solution is available for SW, also note the different vertical scale for the left panel.

influence within the lCW layers, mostly in the form of water patches (Fig. 6f), while there is much more significant SACWcv presence beyond 24ºN (Fig. 6e, f, g). This suggests that an enhanced and deep PUC could have developed before our observations, resembling the characteristic winter flow conditions proposed by [Mittelstaedt, 1991].

The presence of lCW areas with NACW influence south of Cape Blanc may be related to meanders detaching from the CVFZ but its ubiquity along the slope suggests that they are caused by the deep flow reversals, in instances such as proposed by [Voituriez and Chuchla, 1978]. The existence of an along-slope southward flow within lCW, bringing NACW south of Cape Blanc, would help explain our observations of NACW in this region, as well as related observation of slong-slope high-salinity waters in [Elmoussaoui et al., 2005] simulations. Such a flow, however, is not endorsed by our observations, therefore it would have an intermittent, probably seasonal, character.

The abrupt vertical transition between the uCW, dominated by the low-salinity SACW, and the underlying lCW, consisting almost exclusively of SACWcv, is located at about 300 m depth. This is also the depth reached by the summer-autumn PUC and by the eastward tropical jets (recall the NECC only develops in summer-autumn), therefore suggesting that the enhanced ventilation of the uCW is related to the seasonal atmospheric forcing and the consequent regional circulation pattern. The location of the high SACW core, slightly offshore from the PUC (Figs. 4a, b), suggests that the connection between the zonal tropical jets and the PUC may not be direct, taking place through some recirculation loops. During winter

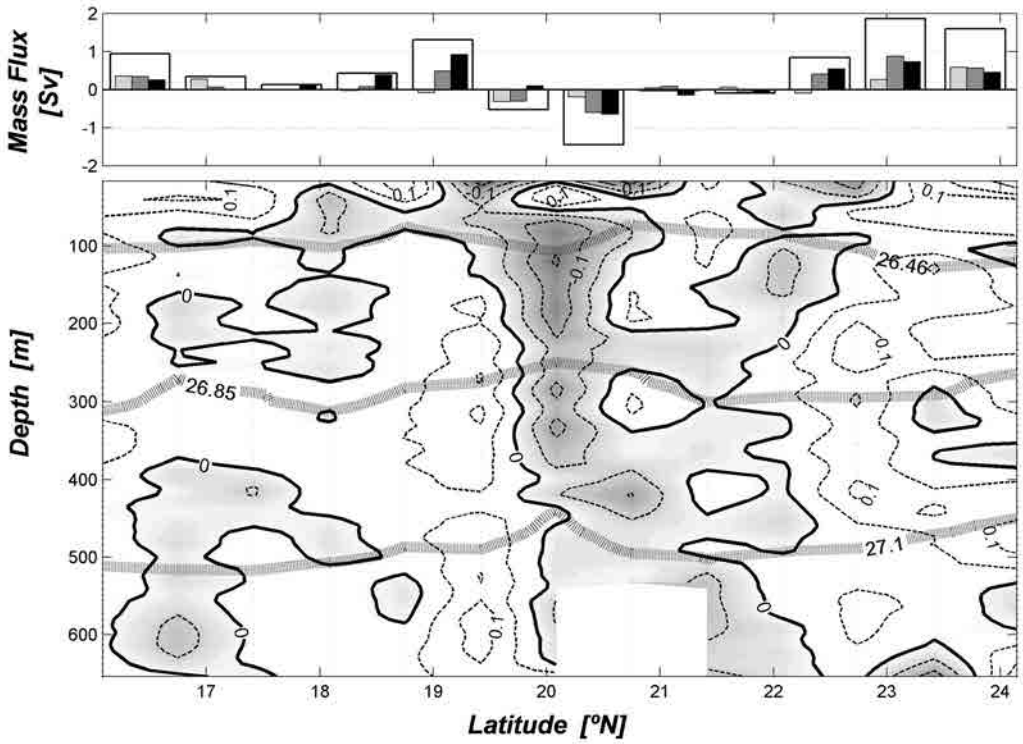

Figure 8. Bottom panel: Distribution of zonal velocity on the 2000-m isobath along-slope section (Fig. 1) (in [m s-1], contours are drawn every 0.05 m s-1; positive values denote eastward flow, westward velocities are shaded in grey). The grey thick lines show the three selected isopycnals (26.46, 26.85 and 27.1 kg m-3). Top panel: Corresponding zonal transports per water stratum as calculated between each pair of stations located along the 2000-m isobath section; SW (dotted line), uCW (solid black line), lCW (dashed black line) and the total (gray line); positive values denote eastward transport.

the PUC deepens and the connection with the zonal jets probably weakens; at this time the PUC would transport both regional southern water varieties.

The meridional mass fluxes, integrated through the cross-shore sections, are shown in Figure 7. The SW follow north through all sections, reaching up to 1.8 Sv south of the CVFZ (Fig. 7a). The uCW also move north through all sections, as a narrow jet along the continental slope, except at the northernmost section where the flow is controlled by mesoscale variability (Fig. 7b). In the southernmost section this jet transports 1 Sv with a 70% average contribution of SACW (30% of SACWcv). This transport, and the pure SACW contribution, decreases steadily northwards, turning into the SACWcv variety as it approaches the CVFZ (Fig. 7d). The maximum presence of this oxygen-poor variety is reached near Cape Blanc (80% in average). North of Cape Blanc (22ºN) this southern water mass turns into the predominant NACW, although as far as 24ºN there still is a northward flow of 0.7 Sv as a mixed water mass which includes 40% of SACWcv. Taking into account both SW and uCW layers, the maximum poleward flow reaches 2.7 Sv at 18ºN and decreases to 1.7 Sv at 24ºN, north of the CVFZ.

In the lCW the integrated along-slope mass transport is rather variable. South of Cape Blanc, there is a southward transport of SACWcv, its contribution reaching more than 90% and up to a maximum of 0.8 Sv (Figs. 7c, e); this water must come from the interior as near-zero along-slope transport takes place at the frontal zone. It is north of Cape Blanc (beyond 22ºN) where NACW becomes the dominating water mass, particularly in the offshore stations where there is only a weak northward flow (Figs. 6a, e and 7c, e); the situation is different in the nearshore stations, where substantial SACWcv is found despite the

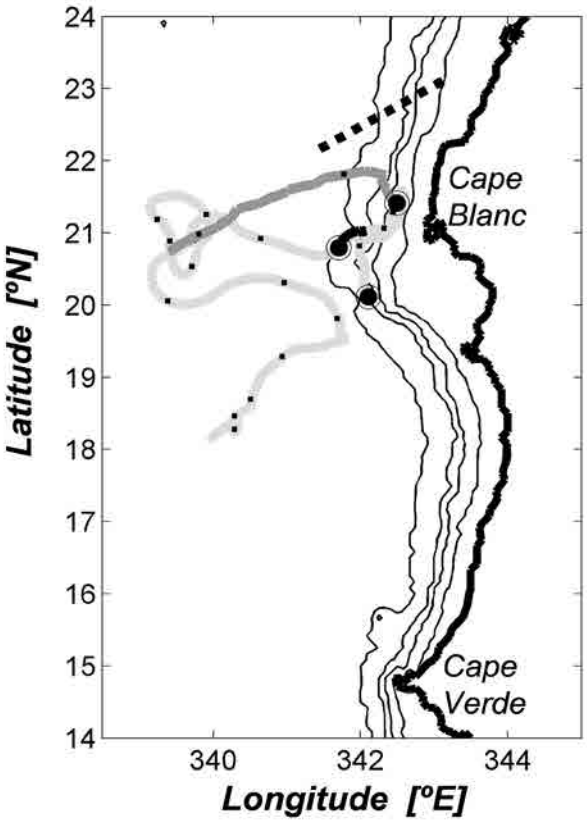

Figure 9. Trajectories of three buoys dragged at 100 m and deployed near Cape Blanc during the cruise. The black circles indicate the deployment positions; the black trajectory corresponds to 9 days, the dark-gray trajectory to 22 days and the light-gray trajectory to 170 days. The tick marks in the light-gray and dark-gray trajectories indicate the position every week. The thick dotted line indicates the approximate position of the CVFZ as inferred from the location of the 36.0 isohaline at 100 m (Zenk el at., 1991).

predominance of a southward flow (Figs. 6c, g and 7c, e). This reinforces the idea of seasonal reversals in the deep along-slope current, as found in numerical simulations by [Elmoussaoui et al., 2005] and reported by [Machín et al., 2010] for the underlying intermediate waters.

Within an upwelling region we are used to think of the cross-shore flow as resembling an idealized vertical cell, with offshore Ekman flow in the surface layers and a compensating onshore subsurface flow. However, the previous results illustrate the existence of substantial along-slope water convergence within both SW and uCW (Fig. 6), in our case this being the main responsible for the cross-shore circulation patterns. This is confirmed by the presence of substantial offshore flow in these two water strata, between about 19 and 21ºN (Fig. 8). The existence of water export is confirmed by the trajectories of three drifters dragged at 100 m (Fig. 9). All three drifters initially followed north along the slope and at least two of them (the third one stopped transmission) departed offshore south of the position of the CVFZ, which at the time was located as far north as 22 to 23ºN (Fig. 9). Within SW the flow pattern is more complex, probably as the result of coastal filaments and the associated recirculation patterns (Fig. 8). Finally, within the lCW layer, we find that waters south of 20ºN recirculate onshore between 19 and 20ºN and find their way south along the slope (Figs. 7c, e) . In this lower stratum there appears to be a good connection between the slope current and the interior GD ocean which gives rise to the observed southward flow of the SACWcv variety. North of 20ºN another recirculation may be occurring, with onshore flow between 22.5 and 23.5ºN and offshore export between 20 and 21ºN.

2.4. Discussion and conclusions

The comprehensive data set acquired during the CANOA08 cruise provides a good picture of what probably is the characteristic late-summer and autumn circulation of surface and central waters along the continental slope between Cape Verde and the Canary Islands (Fig. 10). Two quite different dynamic regions may be distinguished, separated by the Cape Verde Frontal Zone (CVFZ) which crossed the slope at a position north of Cape Blanc (22-23ºN). North of this frontal zone, the circulation pattern is highly variable as a result of the interaction between coastal upwelling, the Poleward Undercurrent (PUC) and the intense mesoscalar activity in the region south of the Canary Islands. South of Cape Blanc the dynamics is dominated by the along-slope PUC and the surface northward branch of the cyclonic circulation around the Guinea Dome (GD), the Mauritanian Current (MC). Our dataset corresponds to a situation when maximum northward flow takes place [Mittelstaedt, 1991; Elmoussaoui et al., 2005], thanks to an enhanced MC (up to 1.8 Sv) within Surface Waters (SW; σ_q <26.46, down to about 100 m) and through a well-defined but relatively shallow along-slope PUC (1 Sv) within upper Central Waters (uCW; 26.46 $\leq \sigma_q <$ 26.85, between some 100 and 300 m). Poleward along-slope transport reaches until at least 24ºN, where we still find 1.7 Sv of SW and uCW, favoured by the far offshore position of the coastal upwelling front.

The upper-thermocline circulation in the GD region has been traditionally thought as having long residence times [Kawase et al., 1985; Zenk et al., 1991]. Tropical water feeds the GD through the North Equatorial Undercurrent (NEUC) at about 4ºN and seasonally also by the North Equatorial Counter Current (NECC) at about 7-8ºN, but this only occurs in the relatively shallow uCW layers [Elmoussaoui et al., 2005; Stramma et al., 2008]. Further deep, within the lower Central Waters (lCW; 26.85 $\leq \sigma_q <$ 27.1, between about 300 and 500 m), the GD waters have much longer residence times [Kawase et al., 1985; Zenk et al., 1991].

How much of the NEUC and NECC connects with the PUC and how much crosses the CVFZ? The distinction of two varieties of southern central waters (relatively pure SACW and the more diluted, regional, SACWcv) has allowed us to better understand the complex processes that characterize the CVFZ. The SACW variety, characterized by a salinity minimum and relatively high oxygen content, is found only within uCW. This water type fits well the characteristics of the upper thermocline waters at 7.5ºN [Arhan et al., 1998], therefore confirming that they represent tropical waters advected eastwards by the shallow NEUC and NECC jets. These jets do not appear to feed the continental slope currents through some specific location, as the core with highest SACW content appears offshore from the PUC and the proportion of SACW increases progressively equatorwards, but rather the connection spreads all the way between Cape Blanc and Cape Verde and even further south. Similarly, the lCW layers appear as connected to the interior ocean through an anticyclonic gyre, possibly the eastern limb of a more closed-like system that would favour perpetuate the old SACWcv as the regnant water variety in the shadow

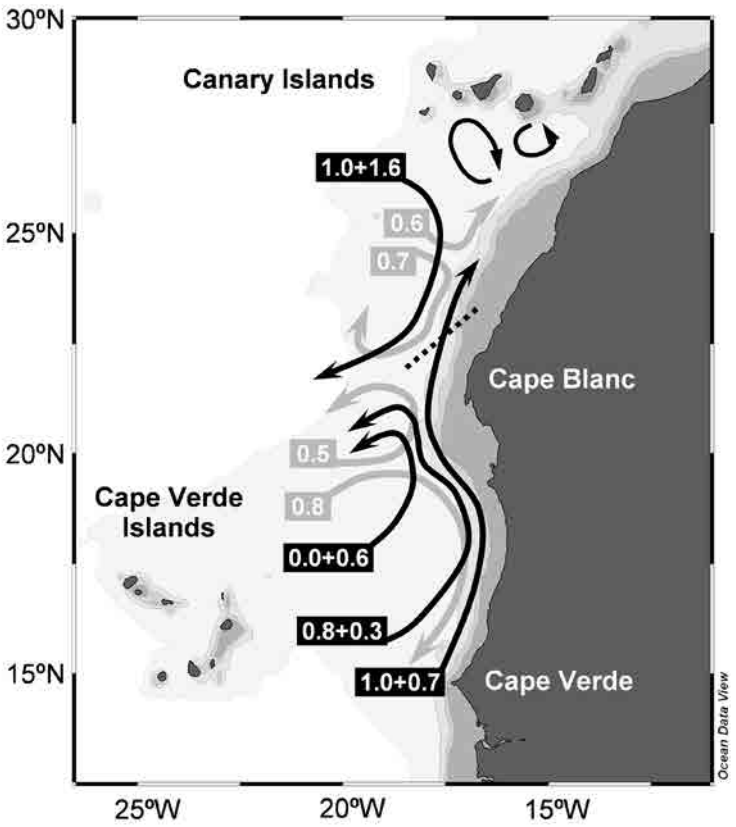

Figure 10. Circulation patterns and mass fluxes [Sv] of SW+uCW (black line) and lCW (gray line) during CANOA08. The thick dashed line illustrates the position of the CVFZ.

zone.

Just north of Cape Verde, at 16ºN, about 70% of the water transported by the PUC is pure SACW. On one hand, incorporation of NACW across the CVFZ results in a salinity increase; on the other hand, high productivity in the along-slope upwelling region and the Cape Blanc giant filament [Gabric et al., 1993] leads to sinking of organic particles and enhanced oxygen consumption. Both processes cause the full transformation of SACW into the SACWcv variety. Some SACW is exported offshore near Cape Blanc (between about 20 and 21ºN) and likely recirculate south; however, an important fraction of southern waters, already transformed as SACWcv, follows north along-slope, with as much as 0.7 Sv reaching at least 24ºN. The waters located off Cape Blanc, during our cruise found just south of the CVFZ, appear to be the site of substantial mesoscale recirculations which would enhance the exchange of southern and northern waters (Fig. 10).

Our observations at the lCW level also show that, at latitudes higher than Cape Blanc, there is a substantial amount of SACWcv which flows south. This raises the possibility of seasonal current reversals in this deep water stratum, in agreement with numerical simulations by [Elmoussaoui et al., 2005]. These reversals would occur between a deep PUC phase, which would take SACWcv north along the slope, and a shallow summer-fall phase as observed during our cruise. During this shallow phase the reversal would not necessarily bring SACWcv back south, our results rather suggest that a significant fraction of the southward flow feeds from the interior ocean, possibly in some sort of basin-wide anticyclonic gyre, so

that this process would lead to the permanent transfer of southern waters into the subtropical gyre. This agrees with the predominant one-way entrainment of southern waters into the subtropical gyre found by [Klein and Tomczak, 1994].

In this study we have presented a rather novel perspective of the current system over the continental slope off NW Africa. Many previous studies have emphasized the importance of the equatorward and offshore transport of properties by the subtropical eastern boundary system [Mittelstaedt, 1983, 1991; Barton, 1989; Van Camp et al., 1991; Pelegrí et al., 2005, 2006]. Other works stressed the importance of the CVFZ as a barrier between waters of northern and southern origin and a region of water convergence and export [Barton, 1987; Zenk et al., 1991; Gabric et al., 1993]. However, here we have shown that the continental slope current system, between the sea surface and least 500 m, may indeed break most of these major constraints. The slope system does play a significant role both in cross-CVFZ transfer and in the ventilation of the GD region, therefore being a significant pathway of water mass exchange between tropical and subtropical gyres.

Chapter III

The circulation of the North Atlantic OMZ

This chapter is the first part of the work Peña-Izquierdo J., E. van Sebille, J.L. Pelegrí, J. Sprintall, E. Mason, P.J. Llanillo and F. Machín. Water mass pathways to the North Atlantic OMZ. Under review, JGR

Abstract

The circulation in the North Atlantic Oxygen Minimum Zone (naOMZ) is traditionally sketched as being isolated from the northern subtropical gyre and embedded within the cyclonic tropical gyre, predominantly made up with South Atlantic Central Water (SACW). However, historical hydrographic observations in the northeastern tropical Atlantic usually show an abrupt thermohaline transition at the potential density level of $\sigma_\theta = 26.8$ kg m^{-3} (σ26.8, approximately 300 m depth), within the Central Water stratum. Saltier and warmer water is found below σ26.8, suggesting the presence of North Atlantic Central Water (NACW) and thus pointing out a connection with the northern subtropical gyre. We perform a water mass analysis of all available temperature and salinity observations to discern the exact contribution of NACW and SACW within the naOMZ. Our results show that above σ26.8 the SACW predominates but below this level the proportion of NACW increases abruptly, contributing with up to 50% at the core of the naOMZ and thus representing a major previously unaccounted supply of oxygen. In agreement with this contrasting water mass distribution, the velocity field from the ECCO2 numerical model also depicts marked different dynamic regimes above and below σ26.8. In the upper layer, a prevailing cyclonic circulation assures the supply of SACW through the northward branching from the eastward flow of the northern North Equatorial CounterCurrent (nNECC). In contrast, this northward supply is reduced in the lower layer though a mean anticyclonic pattern that instead enhances the contribution of NACW from a previously unreported band of eastward flow near the Cape Verde Islands.

3.1. Introduction

The classical theory on thermocline ventilation [*Luyten et al.*, 1983] postulates the existence of ocean regions isolated from the wind-driven subtropical circulation in the eastern margins. A sluggish circulation characterizes these so-called shadow zones, located between the well-ventilated subtropical gyres and the tropical system of zonal jets. The combination of weak ventilation and enhanced microbial respiration of organic matter, from the nearby highly productive coastal upwelling system, leads to the development of Oxygen Minimum Zones (OMZs), located between 200 and 700 m depths, thus within Central and Intermediate Waters strata [*Karstensen et al.*, 2008].

In this study we focus on the characteristics and renewal patterns for the North Atlantic OMZ (naOMZ). Earlier studies have assumed that most of the water supply to the naOMZ comes from the south, through the cyclonic tropical circulation pattern [*Stramma et al.*, 2005, 2008b; *Brandt et al.*, 2010, 2014]; this agrees with the idea that the southeastern corner of the North Atlantic, which geographically belongs to the subtropical gyre, is actually a shadow zone to waters of northern origin [*Luyten et al.*, 1983], with the Cape Verde frontal region acting as the barrier between the subtropical and the tropical gyres [*Zenk et al*., 1991]. The existence of an inter-hemispheric northward transfer of mass linked to the upper limb of the Atlantic Meridional Overturning Circulation, further leads to the predominance of southern origin waters in the whole tropical thermocline [*Kirchner et al.*, 2009]. South Atlantic Central Water (SACW) and Antarctic Intermediate Water (AAIW) cross the equator mostly along the western margin via the North Brazil Current (NBC) and partly retroflect east to feed the tropical system of jets [Figure 1].

The considered major pathways to the naOMZ are subsurface eastward jets located south of 10ºN: the North Equatorial UnderCurrent (NEUC) at 4ºN and the northern branch of the North Equatorial CounterCurrent (nNECC) at 8-9ºN [*Stramma et al.*, 2005; *Karstensen et al.*, 2008; *Brandt et al.*, 2010]. Nevertheless, the core of the naOMZ lies further north. The link between these jets and the naOMZ is therefore explained by the cyclonic circulation around the Guinea Dome, a general uplift of the isopycnals within the surface and subsurface levels driven by the local cyclonic wind-stress [*Siedler et al.*, 1992; *Lázaro et al.*, 2005]. Moreover, this northward branching to the naOMZ is enhanced along the African continent by the seasonal Mauritanian Current at the surface and by the ubiquitous subsurface along-slope Poleward UnderCurrent [*Barton*, 1989; *Mittelstaedt*, 1991; *Peña-Izquierdo et al.*, 2012].

In this sense, while direct velocity observations and Lagrangian drifters show a clear connection between the NEUC/nNECC and the naOMZ at depths above 300 m [*Stramma et al.*, 2005, 2008b; *Brandt et al.*, 2010], neither observations nor numerical simulations [*Elmoussaoui et al.*, 2005] give evidence for such a link at deeper levels. We may, therefore, wonder what is the maximum depth reached by this circulation scheme and what are the responsible dynamics further below.

Some hints to a vertical limit in the connection between the NEUC/nNECC and the naOMZ come

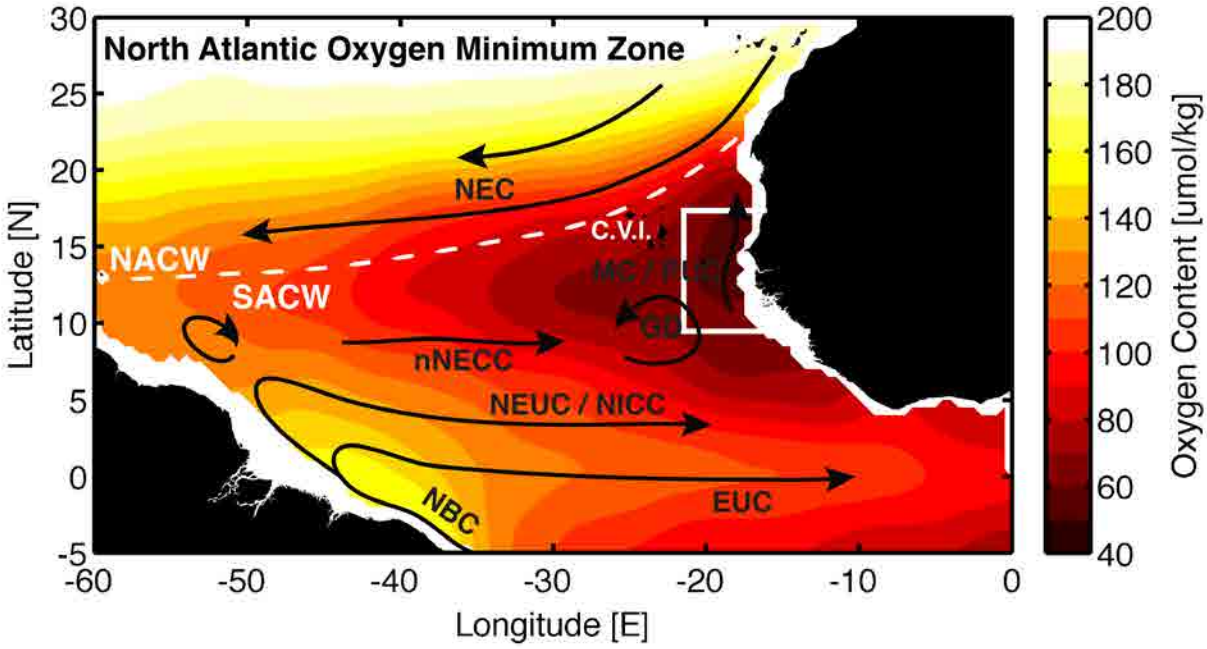

Figure 1. Schematic circulation pattern in the tropical Atlantic Ocean as derived from previous studies, overlying the climatological oxygen content of the 200 to 500 m layer. The frontal zone between SACW and NACW is shown as a white dashed line; C.V.I. refers to the Cape Verde Islands. Main currents: North Brazil Current (NBC), Equatorial UnderCurrent (EUC), North Equatorial UnderCurrent (NEUC), North Intermediate Countercurrent (NICC), northern branch of the North Equatorial CounterCurrent (nNECC), Mauritanian Current (MC), Poleward UnderCurrent (PUC), Guinea Dome (GD) and North Equatorial Current (NEC).

from historical temperature and salinity profiles in the eastern tropical North Atlantic. A salinity and temperature inversion is usually observed at σ_θ = 26.8 kg m^{-3} (σ26.8), located at about 300 m within the Central Water stratum [*Fraga F.*, 1974; *Voituriez and Chuchla*, 1978; *Poole and Tomczak*, 1999; *Pastor et al.*, 2012; *Peña-Izquierdo et al.*, 2012]. Fresher and colder waters are found only above this level, indicative of SACW, while an enhanced influence of saltier and warmer North Atlantic Central Water (NACW) is present below. *Voituriez and Chuchla* [1978] earlier proposed that the σ26.8 thermohaline transition corresponds to a mean northward penetration of SACW in the overlying layer and a southward inflow of NACW in the underlying layer. Nevertheless, the circulation pattern leading to such a transition has not yet been properly addressed.

The numerical simulation of *Elmoussaoui et al.* [2005] shows that σ26.8 roughly matches with the lowest vertical extent of the northward branch of the nNECC towards the naOMZ. Their results suggest there is no direct water supply associated with the NEUC/nNECC below this level – implying a reduction in the proportion of SACW. Indeed, oxygen concentrations decrease rapidly in the naOMZ below σ26.8 [*Fischer et al.*, 2013], pointing to weaker ventilation and longer residence times. The appearance of a signal of NACW in this deep layer is especially relevant because (1) it points to a new pathway and source of oxygen for the naOMZ not previously taken into account and (2) it also reveals a vertical limit to the constraint for mass transfer from the subtropical gyre to the shadow zone [*Luyten et al.*, 1983].

In this study we first characterize the exact contribution of northern and southern origin water masses

within the Central Water stratum of the Tropical Atlantic. To do so we perform a water mass analysis with a high-density temperature and salinity dataset comprising all available historic observations. The calculated water mass distributions are later compared with the circulation patterns as deduced from an assimilative numerical model. The large-scale pattern of the velocity field reveals, in agreement with the hydrographic analysis, a markedly different dynamics within the upper and lower Central Water strata of the naOMZ.

3.2. Data and methods

3.2.1 Dataset of T/S profiles

This work focuses on the naOMZ, here defined by the region located east of 22ºW between 9ºN and 17ºN comprising the lowest oxygen content values [*Fischer et al.* 2013]. However, to gain a broader insight in to the water mass distribution we extend the area of study to the entire North Atlantic tropical Ocean (from 60ºW to 0º) and from the southern hemisphere to beyond the southern edge of the North Atlantic Subtropical Gyre (from 5ºS to 30ºN). A dataset of observed temperature and salinity (*T/S*) profiles has been used, instead of a climatological database, to avoid the loss of variability after climatologic averaging. This dataset has been created with CTD profiles obtained from the National Oceanographic Data Center (http://www.nodc.noaa.gov) together with Argo profiles downloaded from the European Argo Data Center (http://www.coriolis.eu.org). While the set of CTD profiles used here spans a longer period of time (since 1971), their number is smaller than the number of available Argo profiles, which has been growing fast since 2005. Both Argo real time and delayed mode profiles have been examined in this dataset. The initial data set includes 21,242 CTD casts and 39,919 Argo profiles, comprising data from 1971 to 2011.

Although the data centers perform an automatic quality control on the data, an additional procedure has been followed to ensure we have a high quality set of data: (1) For the CTD dataset, only profiles with an "accepted" NODC quality flag are used; (2) for the Argo dataset, only data with a "good" quality flag are selected; (3) profilers included in the grey list provided by the Argo Data Centers are removed; (4) all profiles are required to span the entire depth range between 100 m and 1000 m to ensure the sampling of the upper thermocline, with a minimum vertical resolution of 10 m for the whole profile; (5) all profiles with density inversions greater than 0.01 kg m^{-3} are removed.

After this initial selection, we retain a total of 9,607 CTD's and 30,136 Argo *T/S* profiles. The *T/S* values are then linearly interpolated to selected potential density levels, in average separated by about 10 m. These interpolated profiles are then sorted geographically in bins of 3.5º × 5º degrees of latitude and longitude for a final statistical test. The average *T* and *S* values at each density level are computed for each bin so that any profile with data beyond three standard deviations from the mean is removed. The

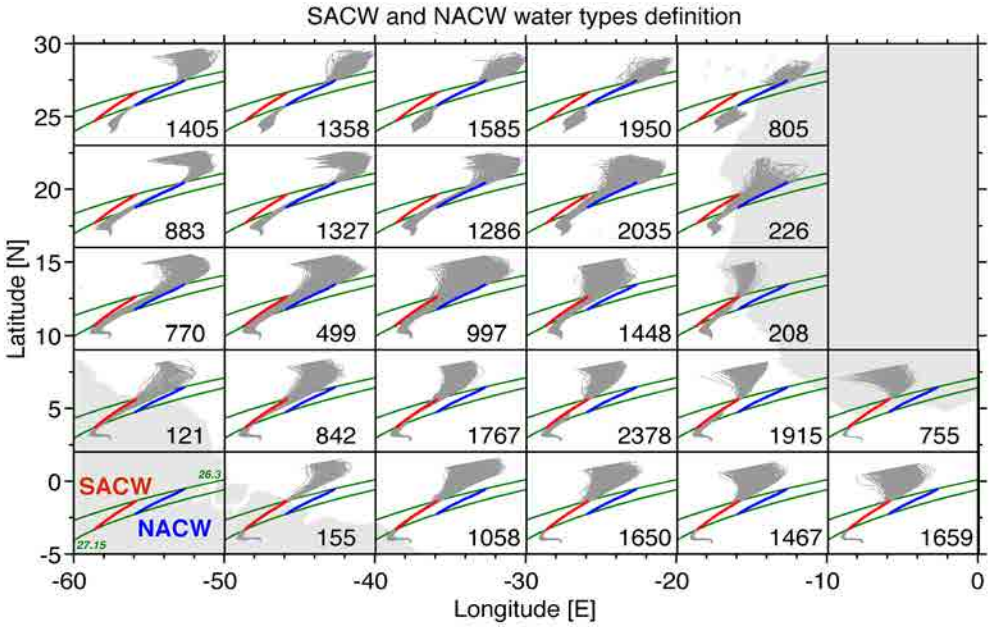

Figure 2. T/S diagrams for all available profiles inside each 10º latitude × 7º longitude bin. Each box shows the definition of SACW/NACW (red/blue lines), the isopycnal limits of the central water stratum (σ26.3 to σ27.15, green lines) and the number of observational profiles.

final (*T/S*) dataset includes 30,485 profiles on σ_θ coordinates.

We also use the ocean oxygen content field from the annual WOCE atlas [*Gouretski, V. and Koltermann*, 2004] with 0.5º horizontal resolution and 45 vertical levels. An advantageous feature of this climatology is the isopycnal data averaging, instead of the more common isobaric computation. This method mimics the preferential along-isopycnal mixing that occurs in the real ocean and therefore preserves the water mass identities. For this same reason, throughout the whole manuscript we will use potential density instead of depth coordinates.

3.2.2. Water mass analysis

A water mass analysis is carried out to distinguish the contribution of water masses with southern and northern origin to the naOMZ thermocline. We focus on the Central Water stratum where the upper part of the naOMZ is found; therefore, only the contributions of Atlantic central waters, NACW and SACW are calculated. We define these two water types as the mean *T/S* profile between latitudes 5ºS and 0ºS for SACW and 25ºN and 30ºN for NACW, after averaging on isopycnal surfaces. The averaged profiles are computed within the Central Water stratum, defined in the tropical Atlantic Ocean for σ_θ between 26.3 and 27.15 kg m^{-3} [*Kirchner et al.*, 2009]. Following previous studies in the tropical Atlantic [Elmoussaoui et al., 2005; Rhein et al., 2005; Kirchner et al., 2009; Peña-Izquierdo et al., 2012] we will refer to waters with σθ between 26.3 and 26.8 kg m^{-3} as the upper Central Water (uCW) and to waters with σθ between 26.8 and 27.15 kg m^{-3} as the lower Central Water (lCW). Figure 2 shows how these definitions of SACW and NACW correctly confine the variability of central waters within the tropical Atlantic.

The analysis implemented here is a simplified isopycnal version of the Optimum Multiparameter Analysis [*Mackas et al.*, 1987; *Tomczak and Large*, 1989]. The method aims at finding the contribution of predefined water types in each data point determined as the best linear mixing combination in a multi-variable space. In our case we only use two hydrographic variables (temperature and salinity) together with the mass conservation constraint.

For every data point, each modeled variable $V_{Mod,i}$ (i.e. *T/S* and mass) is calculated from a combination of SACW and NACW proportions (x_{SACW} and x_{NACW}):

$$V_{Mod,i} = x_{SACW} V_{SACW,i} + x_{NACW} V_{NACW,i}$$

where $V_{SACW,i}$ and $V_{NACW,i}$ denote the values of the normalized variable *i* for the SACW and NACW water types at the density of the observation. For the conservation of mass (*i=mass*), the above equation becomes simply $V_{Mod,mass} = x_{SACW} + x_{NACW}$ . .

The best combination is obtained minimizing, in a non-negative least squares sense, the total residual *R*, defined as

$$R = \sum_{i=T,S,mass} w_i \, r_i \equiv \sum_{i=T,S,mass} w_i \, (V_{Mod,i} - V_{Obs,i})$$
$$= \sum_{i=T,S,mass} w_i \, [(x_{SACW} V_{SACW,i} + x_{NACW} V_{NACW,i}) - V_{Obs,i}]$$

This total residual represents the weighed summation of the residuals of all three variables (r_i), each one calculated as the difference between the modeled $(V_{Mod,i})$ and observed $(V_{Obs,i})$ values. While *T* and *S* residuals are weighted equally $(w_T = w_S = 1)$, mass conservation is enforced through a much a greater weight $(w_{mass} = 10)$ therefore ensuring that the water sample is almost totally made from the combination of the predefined water types. Note that $V_{Obs,mass} = 1$.

3.2.3 The velocity field

The numerical simulation used in this study is the open access product from the ECCO2 project (Estimating the Circulation and Climate of the Ocean, phase II, http://ecco2.jpl.nasa.gov). The ECCO2 project synthesizes data obtained by least-squares fit of a global full-depth-ocean and sea-ice configuration of the Massachusetts Institute of Technology Ocean General Circulation Model [*Marshall et al.*, 1997]. It uses both satellite and in situ available data, including the CTD casts and Argo profiles described above. The simulation is an eddy-permitting solution with a 1/4º horizontal resolution and 50 vertical levels, spanning 20 years from 1992 to 2011. A comparison between satellite altimeter and the ECCO2 velocity fields [*Fu*, 2009] shows good agreement in the latitudinal variation of surface zonal velocities, a

reflection of the tropical system of zonal jets.

3.3. Water mass of the naOMZ

Hydrographic observations in the northeastern tropical Atlantic Ocean show an abrupt thermohaline transition usually centered at σ26.8 [*Voituriez and Chuchla*, 1978]. This transition can be easily detected in a *T/S* diagram within the Central Water stratum as a marked salinity depth inversion, sometimes also presenting temperature and even density inversions, indicative of a change in the water mass composition. A relatively fresh and cold water mass indicates the presence of SACW in the uCW while the salty and warm water suggests a greater influence of NACW in the lCW. Figure 3 shows this transition as characteristic for the whole northeastern tropical Atlantic, being clearly present as far west as 40ºW and as far south as 7ºN. In general, the salinity inversion becomes stronger and shallower moving northeastward in the tropical North Atlantic.

This transition is also found in the model climatological mean, with a similar geographic pattern and at the same levels as in the observations (Figures 3a and b). The main difference is observed near Africa at 20ºN where observations show a region with *T/S* transition profiles at density levels shallower than observed

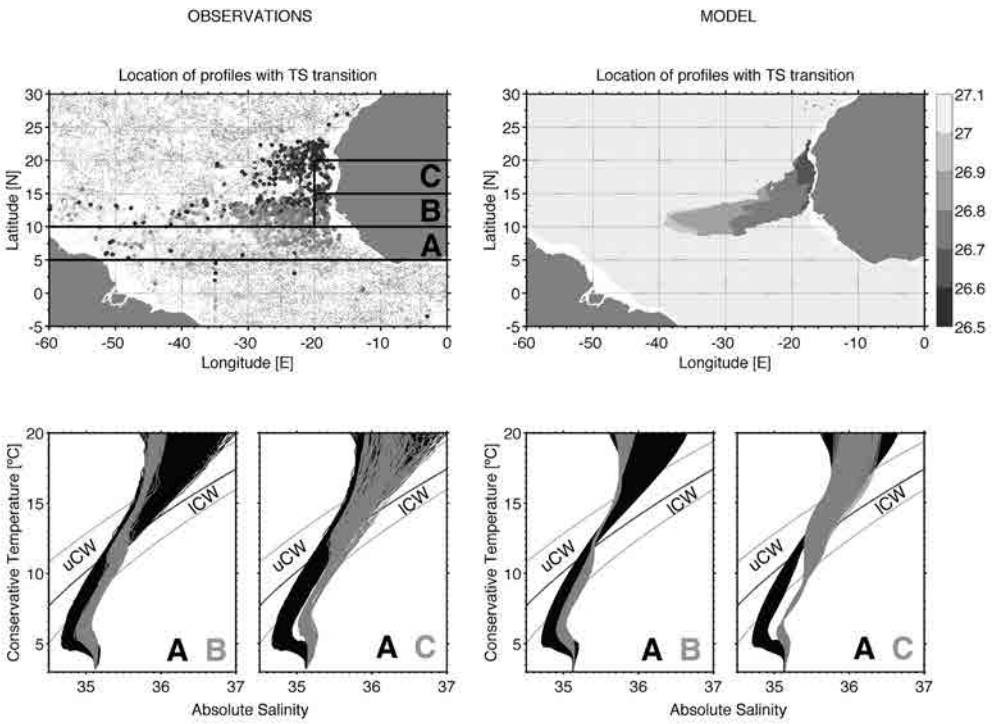

Figure 3. Top panels: Location of the T/S profiles with a marked thermohaline transition, defined as a change in the slope of the T/S profiles greater of 0.1 ºC per salinity unit with respect to the NACW and SACW pre-defined slopes. The density level where the transition is found is plotted in grey colors. Middle panels: T/S diagrams of those profiles located within the regions shown in the top left plot; regions B and C include 135 and 109 profiles, respectively. Bottom panel: Mean profiles of NACW proportion and oxygen content for regions B and C; the dashed lines denote one standard deviation. The left panels are for the observational data set, while the right panels are for the ECCO2 model output. Note that the ECCO2 model does not include the oxygen field.

in the model. This difference is likely due to temporary water mass interleaving in the frontal zone between NACW and SACW [*Tomczak*, 1981], not properly represented by the model climatology which only includes permanent features. Therefore, this ubiquitous hydrographic footprint suggests a distinct and permanent circulation pattern between the uCW and the lCW. Moreover, the vertical distribution of fresher and colder SACW above saltier and warmer NACW avoids the development of salt fingering thus favouring the permanence of this feature in time.

A simple explanation for the formation of the thermohaline transition arises from the spatial distribution of the *T/S* diagrams (Figure 3). Zone A corresponds to the NEUC and nNECC region. The *T/S* diagrams in the naOMZ (zones B and C) indicate the presence within the uCW of pure southern waters advected by these jets, thus revealing a direct connection with zone A. However, the lack of these southern waters suggests this connection disappears below σ26.8 particularly in the northern portion (zone C).

The water mass analysis helps us understand the exact contribution of southern and northern water masses in the renewal of the tropical North Atlantic upper thermocline (Figure 4 and 5). The distributions of NACW and SACW exhibit opposite patterns above and below σ26.8. In the uCW, SACW stretches north

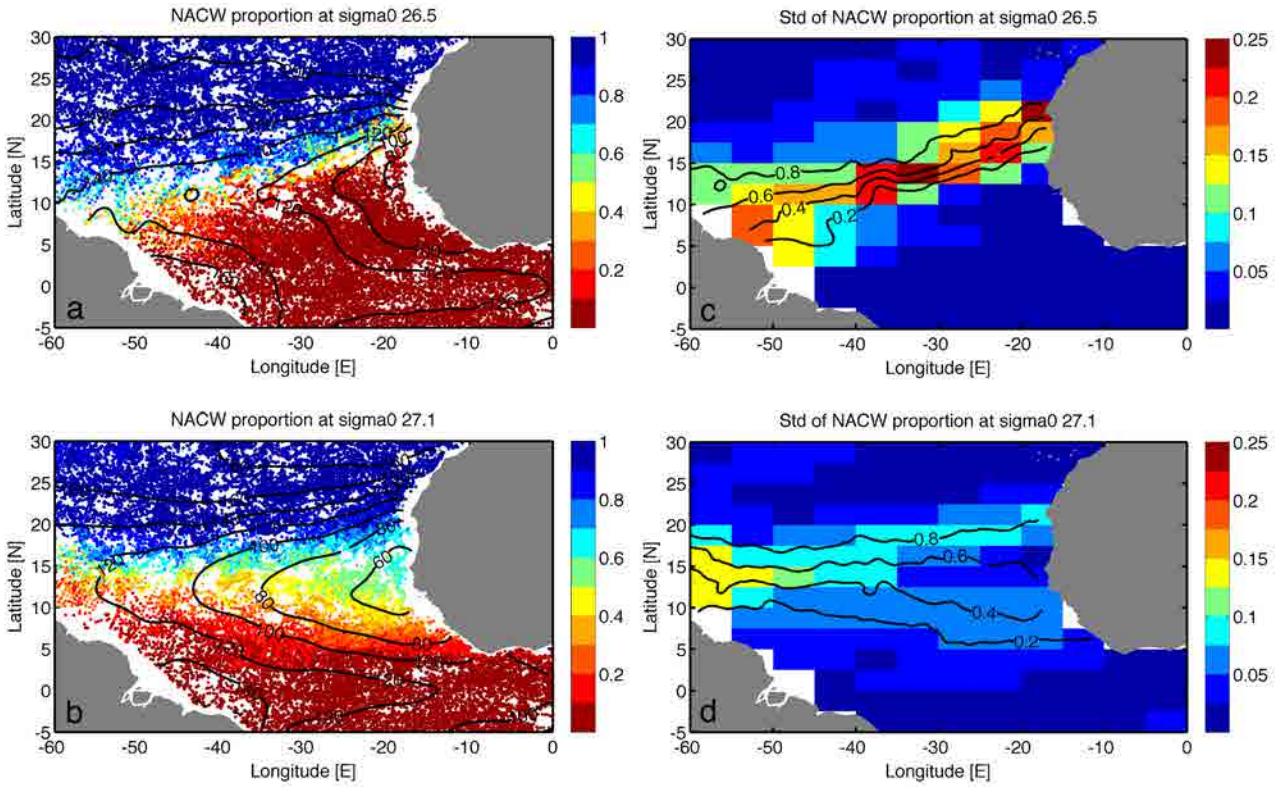

Figure 4. Distribution of central water masses in the tropical Atlantic Ocean. Left panels: Proportion of NACW as deduced from the water mass analysis at (top panel) σ26.5 and (bottom panel) σ27.1. These density levels match with the minimum content of oxygen in the uCW and lCW layers. Black contours show the climatological oxygen field at the respective density levels. Right panels: Standard deviation of the NACW proportion within bins of 2.5° latitude × 5° longitude; all bins include more than 50 observations. Black contours show the smoothed distribution of NACW after a gridding scheme algorithm. Note that SACW proportion always equals the complementary part of the NACW contribution (i.e. SACW + NACW = 1).

along the eastern margin while NACW penetrates into the tropical Atlantic from the western margin. This pattern is in agreement with the Subtropical cell circulation scheme [Schott et al. 2004], with an intense northward flow along the eastern margin *Elmoussaui et al*. [2005], especially in autumn. In the lCW instead, SACW is advected along the American continent towards the Caribbean Sea while NACW spans southwards along the African coast. A similar result was obtained by Poole et al. 1999 before the start of the Argo program thus with a much reduced horizontal resolution. Hence, the naOMZ is dominated by SACW in the uCW while an equally split mixture of NACW and SACW is found in the lCW.

The presence of a large fraction of NACW in the lCW is very relevant for the oxygen supply to the naOMZ since NACW is more recently ventilated than SACW, thus having a higher oxygen content. Nevertheless, the mean profile for the naOMZ (Figure 6) shows that the oxygen concentration decreases just below σ26.8 where the NACW proportion notably increases. Moreover, the absolute oxygen minimum is found at σ27.1, exactly where the NACW fraction is largest (50%). Further, in the lCW the proportion of NACW is quite homogeneous within the naOMZ, as shown by the local minimum in the standard deviation of this fraction (Fig. 4d). The presence in this region of a well-mixed water mass and a notable contribution of NACW but with minimal oxygen content can be explained by a marked reduction in the water supply within this layer. This supply is slow enough to allow, on the one hand, the predominance of biological consumption of oxygen over ventilation, and on the other, mixing over water mass renewal. These results agree with the idea of a regional water mass variety for the naOMZ (the Cape Verde SACW, i.e. SACWcv) proposed by *Peña-Izquierdo et al.* [2012]. The existence of such a regional water mass would explain the presence of the two bands of relatively high standard deviations, south of 10ºN and north of 15ºN in the eastern Atlantic, both suggesting two different mixing fronts: SACW with SACWcv and SACWcv with NACW respectively (Fig. 4d). Therefore, in the lCW, SACW and NACW both reach the naOMZ slowly mixing with SACWcv while reducing its oxygen content.

The mean oxygen profile also shows the existence of two oxygen minima in the CW strata: The absolute minimum is found in the lCW at σ_θ = 27.1 kg m^{-3} and a secondary minimum is located within the uCW at σ_θ = 26.5 kg m^{-3} (Figure 6). This feature also suggests the existence of different regimes in the uCW

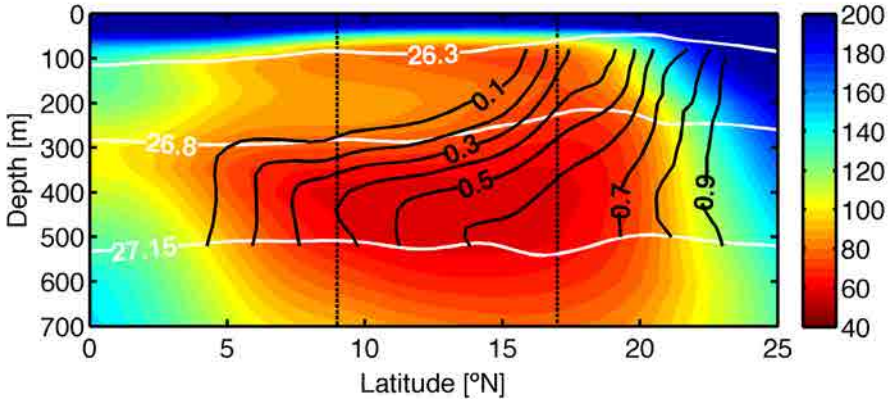

Figure 5. Climatological oxygen content ([umol/kg], in color) along a meridional section (20ºW) across the naOMZ (depicted by the vertical dashed black lines). Black lines represent the smoothed proportion of NACW. Potential density levels are shown with white lines.

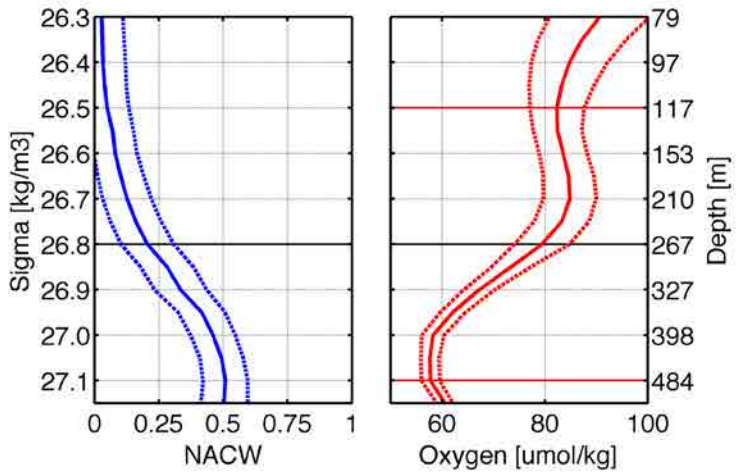

Figure 6. Mean vertical profiles of the NACW proportion and the oxygen content within the naOMZ (defined as the region east of 22ºW and between 9ºN and 17ºN). One standard deviation is shown with dashed lines. The level with minimum oxygen content within the uCW and lCW (σ26.5 and σ27.1) is highlighted with horizontal black lines. The σ26.8 level separating the uCW and lCW is marked with a solid black line.

and lCW layers. In the absence of biological activity, the oxygen content would increase with decreasing temperature, i.e. with increasing depth. Further, biological oxygen consumption is enhanced in the upper levels, where the rain of organic products from the surface is largest, so the oxygen gets reduced toward the sea surface (up to below the mixed layer). These effects may be counteracted by advective and diffusive processes, leading to water mass renewal and oxygen supply; both advection and diffusion are usually most intense at shallow depths so the oxygen minimum is commonly found deeper in the water column.

In steady state respiration and ventilation should balance out. Therefore, a vertical minimum in an oxygen profile will occur as a result of either intense respiration or weak ventilation, or both. In our case the dominance of pure SACW in the uCW suggests there is moderate ventilation linked to the NEUC and nNECC, with the oxygen minimum mainly driven by enhanced respiration. There is possibly some range of oxygen concentrations where the two processes interplay – an increase/decrease in ventilation leads to an increase in oxygen consumption. In the lCW, in contrast, the biological oxygen consumption is reduced and the local minimum in oxygen concentration is likely related to a drastic decrease in the ventilation rate. In this stratum the minimum oxygen concentration is likely set by the activity of advection and, largely, diffusion.

3.4. The thermocline circulation in the ECCO2 model.

3.4.1. The northeastern tropical Atlantic

We may now connect the features that have emerged from the water mass analysis with those that arise from the general circulation of the northeastern Tropical Atlantic as seen in the ECCO2 model. We start by investigating the layer-averaged velocity fields. In the uCW, the model shows a broad cyclonic pattern dominating the annual mean circulation (Fig. 7a). The mean eastward flow south of the Cape

Verde Islands carries SACW from the tropical to the subtropical regions through a marked northward flow between 30ºW and the African continent. This flow is especially enhanced along the continental slope by the PUC, associated with the coastal upwelling system [*Barton*, 1989; *Mittelstaedt*, 1991; *Peña-Izquierdo et al.*, 2012]. Similar results arise from the numerical simulation of *Elmoussaoui et al.* [2005], with a maximum northward transport (including now the uCW and the surface layer) of 4Sv during the Fall season. After joining the westward flow of the subtropical gyre, some of this water recirculates south towards the tropics and then eastwards again via the nNECC and NEUC [*Fratantoni et al.*, 2000].

The cyclonic tropical path forms part of a complex basin-wide recirculation scheme that also includes upwelling along the eastern tropical edge and subduction along the western subtropical boundary, the so called subtropical cell (STC) [*Zhang et al.*, 2003; *Schott et al.*, 2004; *Hazeleger and Drijfhout*, 2006]. Further evidence of this pattern can be found in the mean vertical velocity (Figure 7c). The uCW of the naOMZ is influenced by upwelling, largely enhanced near the continental slope likely due to the coastal upwelling system. North of the Cape Verde Islands, a predominant downward velocity is found related to the subtropical gyre subduction. It is also important to distinguish the Guinea Dome from the STC, the former being a much smaller-scale system acting at shallower levels, located further south and directly driven by the regional cyclonic wind stress [*Siedler et al.*, 1992; *Lázaro et al.*, 2005].

In the lCW, the mean velocity field is relatively weak, with less well-defined circulation patterns than in the uCW (Fig. 7b), yet two main structures can be detected. The first one is an anticyclonic gyre located south of the Cape Verde Islands, made up of a well-defined eastward flow at 14ºN, flowing from at least 35ºW all the way to the African continent, and a southwestward recirculation reaching as far south as 10ºN. This pattern therefore weakens the direct penetration to the naOMZ of water from the south. A similar anticyclonic circulation was proposed, from geostrophic calculations by *Reid* [1994] for the AAIW layer, located below σ27.15. The southward extension of the contour with 20% content of NACW (Fig. 7b) corroborates that this gyre reaches the Central Water stratum. Furthermore, the existence of a relatively closed anticyclonic circulation also agrees with the observed standard deviation minimum in NACW proportion (Fig 4d), indicating the presence of a well mixed water mass, the previously mentioned SACWcv [*Peña-Izquierdo et al.*, 2012].

The second lCW structure is the cyclonic recirculation of part of the subtropical waters (with high proportion of NACW) via a predominant eastward flow centred at 18ºN. Part of the water recirculates northward but some joins the southern anticyclonic gyre through a southward flow along the slope, south of 18ºN. Recent velocity observations during the fall season along the African continental margin [*Peña-Izquierdo et al.*, 2012] have observed a similar circulation pattern for the uCW and lCW layers. They suggest a convergent meridional flow at 22ºN in the uCW and divergent at 18ºN in the lCW. Thus, south of 18ºN the continental slope current system is made up by an intense PUC in the uCW and an enhanced southward flow in the lCW, in agreement with the model velocity field. The mean vertical velocity within the lCW (Fig.7d) also displays a contrasted pattern with respect to the uCW: predominant downwelling/

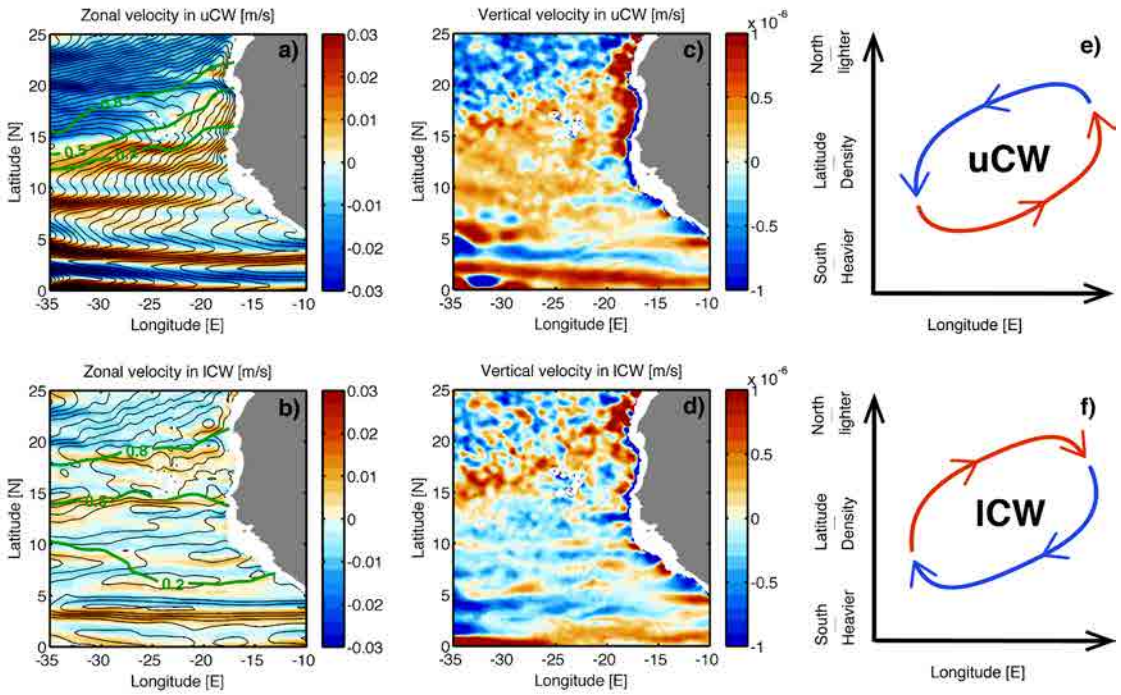

Figure 7. Flow patterns in the northeastern tropical Atlantic Ocean as deduced from the climatological ECCO2 annual-mean flow field. Vertically-averaged zonal velocity (in color) for (a) the uCW and (b) the lCW strata; positive values denote eastward flow. Black contours denote the Eulerian stream function with 0.1 Sv increments. Green contours represent the averaged NACW proportion within the corresponding layer. (c and d) Analogous plots but for the vertical velocity, with the positive values denoting upward flow. (e and f) Simplified schemes of the 3D circulation in both layers.

upwelling taking place south/north of the Cape Verde Islands.

The opposite horizontal and vertical patterns in the uCW and lCW strata resemble the stacked meridional overturning cells scheme proposed by *Wang* [2005] for both sides of the equator. The upper cell, the so called tropical cell [*Lu et al.*, 1998] occupies the upper 100 m and is made up by the equatorial Ekman-driven upwelling, surface poleward flow up to the downwelling band at 3º-4º of latitude, and equatorward flow in the subsurface. The lower cell, named the sub-thermocline tropical cell [*Wang*, 2005], has a weak circulation between 100 and 300m, with a pattern opposite to the tropical cell. Analogously, we propose for the northern part of the tropical Atlantic, and for larger spatial and temporal scales, a very simplified arrangement of stacked meridional overturning cells within the uCW and lCW. The upper cell (Fig. 7e) would correspond to the subtropical cell while the lower one (Fig. 7f) would respond to a lower subtropical cell with reversed flow direction. No direct observations of the whole system are available, yet the simplified layered circulation model discussed by *Fratantoni et al.*, [2000] also appears to capture the opposing vertical velocity fields corresponding to the opposing cells (their Figure 15).

While a detailed understanding of the processes that lead to such a complex three-dimensional circulation is beyond the scope of this work, we may look for some hints in the structure of the thermocline. The distributions of the depth and thickness of the uCW and lCW (Fig. 8) suggest the existence of a baroclinic mode of circulation: those regions with a relatively thick uCW layer have a correspondingly thin lCW

layer and vice versa. The similarity between the observed circulation patterns and the bottom depth of each layer suggests that the flow might be approximately represented with a 3.5 layer geostrophic model (three active layers and a quiescent fourth layer; see e.g. section 4.1 in *Xuang*, [2010]). The surface layer would correspond to the layer directly driven by Ekman pumping. The second and third layers would correspond to the uCW and lCW layers and the fourth layer, formed by deeper waters, would be passive. Let us call z_u and z_l the depths where we find the bottom of the uCW and lCW layers. According to this simple geostrophic layered model, the stream function lCW would roughly match with the contours of constant z_l, (Figure 7b and 8b). And similarly, the streamlines for the second layer would follow contours of constant z_{u+} z_l; since the horizontal gradients of z_u are substantially larger than those for z_l , this means that the stream lines in the second layer will approximately follow the contours of constant z_u (Figs. 7a and 8a). Therefore, the circulation patterns in the uCW and lCW layers display opposite directions, as expected for a baroclinic mode of oscillation in a layered ocean.

A complementary explanation for these distinct patterns may come from requirements of conservation of potential vorticity (PV) by water parcels (Figs. 8e and 8f). The predominant widening of the uCW in the naOMZ region limits the transfer of water from the subtropical gyre; In order to preserve the PV, a southward displacement of a water parcel, thus a stretching, should be balanced by an increase in its planetary vorticity, i.e. a northward displacement. This is the principle for the existence of the shadow

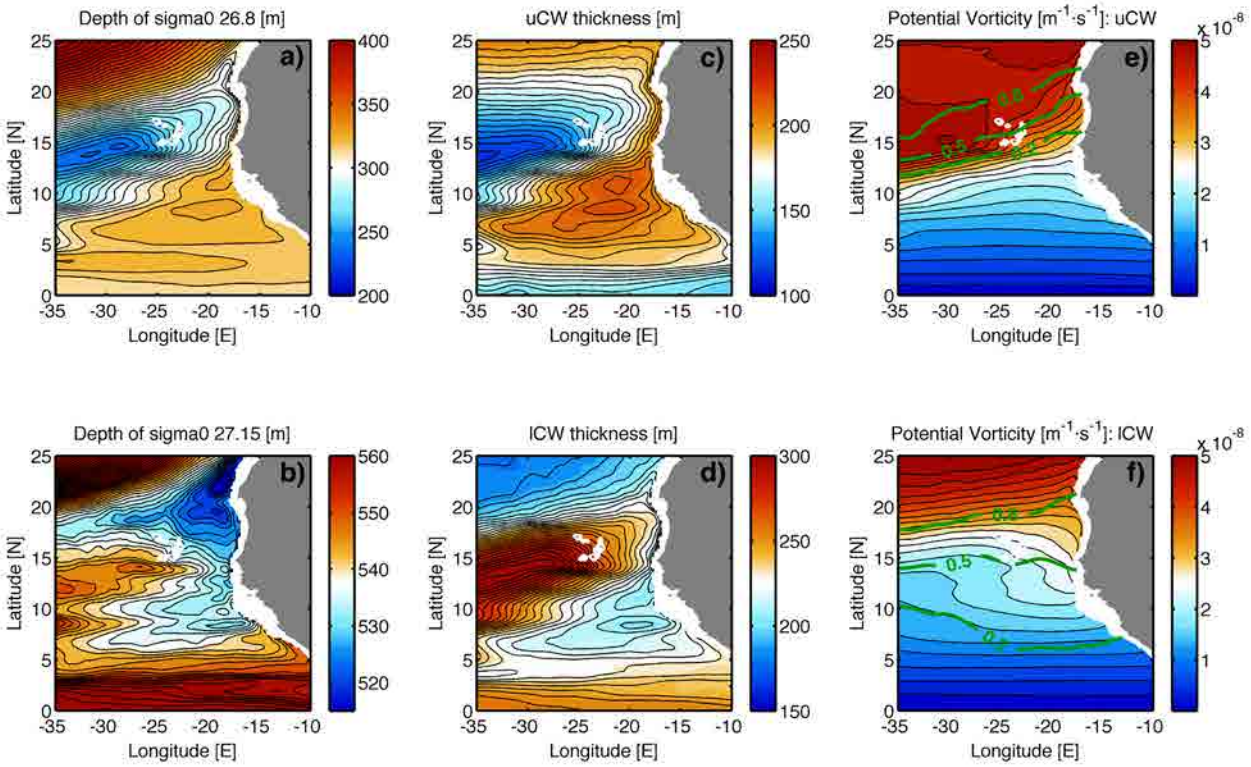

Figure 8. Annual-mean depth of the (a) σ26.8 and (b) σ27.15 density levels, respectively located at the base of the uCW and lCW layers; the contour intervals are 4 m and 2 m for the upper and lower layer. (c and d) Mean thickness for both the uCW and lCW strata, respectively (contours intervals of 5 m). (e and f) Planetary component of the potential vorticity for both the uCW and lCW strata, respectively; green contours represent the average proportion of NACW.

zone in the classical theory of the thermocline ventilation [*Luyten et al.*, 1983]. However, the opposite situation occurs in the lCW; The thinning of this stratum favours the existence of a southward flow, manifested by the southward deformation of the PV contours and revealing a water transfer from the subtropical gyre within the lCW.

3.4.2 The Cape Verde Current System

As mentioned before, most of the water supply to the naOMZ is traditionally attributed to the NEUC and nNECC, both flowing south of 10ºN [*Stramma et al.*, 2005, 2008b; *Brandt et al.*, 2010]. While this is clearly observed in the vertically averaged uCW velocity field (Figure 7a), in the lCW these southern jets appears not directly connected with the naOMZ. Instead, further north of 10ºN, Figure 7b reveals a band of eastward flow extending as north as 18ºN and with a high content of NACW. These flows appear as major contributors in the lCW supply to the naOMZ, which have not been taken into account in previous studies.

We may examine these northern flows in further detail by looking at the ECCO2 velocity field across a meridional section along 25ºW (Fig. 9) and comparing it with previous studies. The most notable of these flows is found at 14ºN, clearly visible down to 800 m (Fig. 9a) and extending from 35ºW to the African continent. In the smoothed annual-mean ECCO2 velocity field this current, with velocities of a few cm s^{-1}, appears as the most pronounced eastward flow north of 5ºN. In agreement with the circulation pattern presented in the previous section, this current at 14ºN is predominantly fed in the uCW from the south with SACW and from the north with a mixture of SACW and NACW in the (Fig. 9b). The reproduction of this modelled current at 14ºN agrees with the averaged velocity field as determined from several observational studies for the Central Water stratum in this area. Acoustic Doppler Current Profiler (ADCP) observations along 23ºW in July 2006 [*Stramma et al.*, 2008b] show an intense eastward current at 14ºN, reaching 20 cm/s in the uCW and 10 cm/s in the lCW. In the same study, the time-averaged zonal velocity field deduced from trajectories of autonomous floats drifting at 200 m depth (i.e. in the uCW) shows peak eastward flow of 5 cm/s again at 14ºN. Furthermore, the average zonal flow computed from several meridional sections, carried out during different seasons between 1999 and 2008 and between 28ºW and 23ºW [*Brandt et al.*, 2010], displays an intense eastward mean flow at 14ºN, exceeding 10 cm/s in the whole CW stratum. Brandt et al. [2010] suggested this current was a recirculation around the Cape Verde Islands but our results show that it flows all the way from the western Atlantic margin to the African continent, although it also includes water recirculating from the south.

ECCO2 also reproduces an eastward current centred at 12ºN but only in the uCW and notably linked to the nNECC flow, thus fed with SACW [Figure 12a]. In this region, between 10ºN and 13ºN, observations [*Stramma et al.*, 2005, 2008b; *Brandt et al.*, 2010; *Hahn et al.*, 2014] suggest more flow variability, yet with preferential westward/eastward paths south/north of 12ºN and similar to the ECCO2 mean field (Figure 9a). North of the Cape Verde Islands, eastward flows are mainly found in the lCW with a

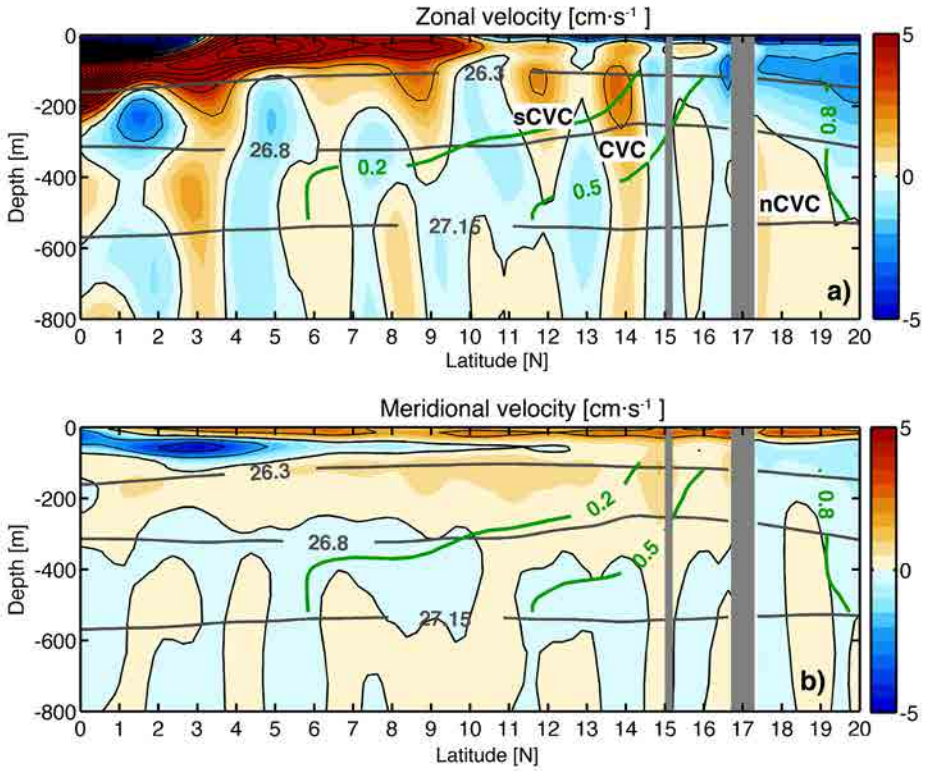

Figure 9. Annual-mean (a) zonal and (b) meridional velocity components along 25ºW as deduced from the ECCO2 model. Positive values denote eastward and northward flow; contours of 0.02 m s-1 are shown with black lines. Thick grey lines represent the density levels that confine the uCW and lCW layers. The observed NACW proportion is denoted with green contours. The grey shade corresponds to one of the Cape Verde Islands.

high contribution of NACW. In this region there are very few velocity observations. A Lowered ADCP (LADCP) section along 28ºW in summer 2003 displayed a dominant mean eastward flow between 12ºN and 18ºN only for the 300-600 m layer (i.e. roughly the lCW stratum) with velocities at 14ºN and 17ºN above 5 cm/s [*Stramma et al.*, 2008b], again in agreement with the ECCO2 results.

The existence of prevailing eastward geostrophic undercurrents far from the equator (north of 10ºN), as calculated using the Argo program *T/S* profiles, has been recently reported for the North Pacific Ocean by *Qiu et al.*, [2013a, 2013b]. These authors mainly found eastward jets below the westward flow of the subtropical gyre located respectively at 9ºN, 13ºN and 18ºN in the western Pacific margin. The vertical extension of these jets may reach down to 1000 m, with the upper limit typically varying between σ26.0 and σ27.0 and shoaling eastwards. These «NEUC jets», as *Qiu et al.*, [2013a, 2013b] dubbed them, seem to be good candidates for the eastward currents observed north of 10ºN in the Atlantic ECCO2 field, though with several significant differences. They almost surface south of the Cape Verde Islands likely due to the northern location of the Trade Wind Convergence Zone in the eastern Atlantic, as compared with the eastern Pacific. On the other hand, several current cores with small meridional separation are found in the eastern Atlantic (25ºW), probably related to the presence of the Cape Verde Islands. Since the NEUC is traditionally used in the Atlantic to refer to the undercurrent at 4ºN [*Stramma and Schott*, 1999], we will refer to all these eastward jets north of 10ºN as the Cape Verde Current (CVC) system and comprised of three defined branches; southern (sCVC) at 12ºN, central (CVC) at 14ºN and northern (nCVC) at 18ºN.

South of 10ºN, the nNECC is also realistically reproduced in the model, located between 8ºN and 10ºN and covering most of the thermocline. However, further south, important discrepancies with observations appear. The most notable is the absence of the Equatorial Intermediate Current within the lCW. The NEUC is reproduced slightly further south than observed, connecting at 2ºN with the North Intermediate CounterCurrent, that does not seem to occur in the real ocean [*Brandt et al.*, 2010]. These issues are likely due to the limited horizontal resolution of ECCO2, as high resolution appears necessary to properly model the intermediate depth equatorial circulation [*Duteil et al.*, 2014]. Nevertheless, Figure 7 and 8 show that the lCW of the naOMZ is weakly linked to this equatorial region so we expect that the significance of these differences to be likely small.

3.5. Discussion and conclusions

The analysis of a comprehensive *T/S* dataset confirms the existence of a permanent abrupt thermohaline transition at σ26.8 (about 300 m depth) in the eastern tropical North Atlantic Ocean. A water mass analysis reveals the predominance of SACW in the uCW (σ26.8 to σ26.3) and an abrupt increase in the contribution of NACW when entering the lCW (σ26.8 to σ27.15). The maximum proportion of NACW (50%) is reached at the core of the naOMZ (at σ27.1), where minimal oxygen content is found. Such a markedly different water mass composition suggests that distinct circulation patterns rule the uCW and lCW, with a potentially important role of previously unreported water transfer from the well-ventilated northern subtropical gyre into the naOMZ core.

The vertically averaged velocity field of ECCO2 in the eastern margin of the Tropical Atlantic is in broad agreement with the distributions of SACW and NACW. The circulation in the uCW appears embedded within a broad cyclonic pattern, with the eastward NEUC-nNECC flowing as the southern limb and the westward NEC as the northern arm of the gyre (Figure 10a), assuring the direct supply of SACW to the naOMZ. Previous studies have always related this scheme to the local and shallow wind-driven Guinea Dome [*Stramma et al.*, 2005, 2008b; *Brandt et al.*, 2010]. However, the relatively deep (reaching 300 m) vertical extension of the prevailing cyclonic circulation in the uCW, together with the horizontal distribution of the ECCO2 vertical velocities, suggest that the water supply in this layer is driven by the large-scale subtropical cell [*Zhang et al.*, 2003; *Schott et al.*, 2004].

The circulation in the lCW is markedly different from that of the uCW (Figure 10b). On the one hand, the lCW presents predominant eastward flows around the Cape Verde Islands and westward currents further south. This pattern sketches a broad anticyclonic circulation in the naOMZ, in agreement with the predominance of an inner well-mixed water mass variety (SACWcv) [*Peña-Izquierdo et al*., 2012] and two distinguishable frontal zones in the southern (SACW-SACWcv) and northern boundaries (SACWcv-NACW) (Fig. 4d). On the other hand, the horizontal distributions in vertical velocities and layer thickness

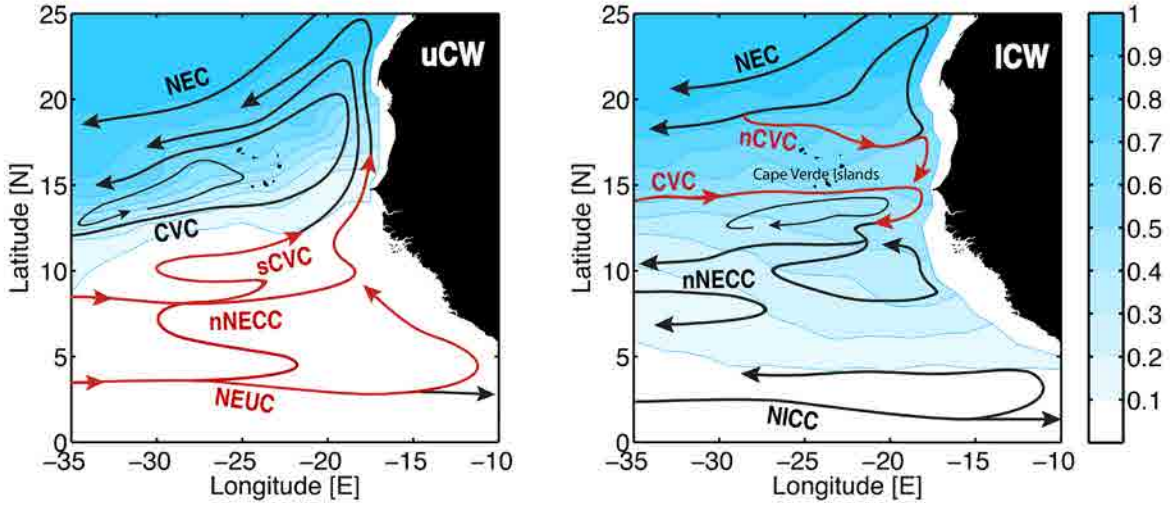

Figure 10. Scheme of the average circulation in the northeastern tropical Atlantic in the uCW (left) and lCW (right) layers. The distribution of the observed proportion of NACW is shown with blue-contours. Major pathways to the naOMZ are highlighted in red.

are also approximately antisymmetric in both layers. All these features have led us to hypothesize the existence of a lower subtropical cell within the lCW, with an inverse but weaker circulation scheme compared to the uCW, analogous to the equatorial stacked tropical cells proposed by *Wang* [2005]. We suggest that both CW strata may interact through a normal baroclinic mode of circulation that leads to opposite circulation patterns.

One of the key features in the ECCO2 circulation system is the existence of a band of subsurface eastward flows between 10ºN and 18ºN. These currents, here referred as the Cape Verde Current system, should also play an important yet unreported role in the water supply to the naOMZ, especially in the supply of NACW. The existence of such subsurface eastward jets, north of 10ºN and below the westward flow of the subtropical gyre, have also been recently pointed out for the North Pacific Ocean [*Qiu et al.*, 2013a] and can be identified in earlier velocity observations [*Brandt*, 2014].

The existence of the proposed inverted cells emerges as a suggestive approach for the study of world OMZs. The substantial interannual and decadal variability of these cells [*Schott et al.*, 2008] emerges as one of the major causes of the observed oxygen anomalies during the last decades in the world OMZs [*Deutsch et al.*, 2014, *Ridder and England*, 2014].

Chapter IV

A Lagrangian point of view

This chapter is the second part of the work Peña-Izquierdo J., E. van Sebille, J.L. Pelegrí, J. Sprintall, E. Mason, P.J. Llanillo and F. Machín. Water mass pathways to the North Atlantic OMZ. Under review, JGR

Abstract

Chapter III has highlighted the existence of a previously unreported subtropical advective pathway in the eastern tropical North Atlantic Ocean, from the well-ventilated northern subtropical gyre to the North Atlantic Oxygen Minimum Zone (naOMZ). However, advection is only part of the story: recent studies have shown the major role that mesoscale eddy and diapycnal diffusion play a very important role in the ventilation of a stagnant naOMZ. In this study we perform numerical Lagrangian simulations to include both the advective and diffusive components as part of a comprehensive description of water mass renewal in the naOMZ. A purely isopycnal simulation shows that marked different pathways within the upper and lower Central Water (CW) layers lead to the abrupt water mass vertical transition observed within the naOMZ. The along-trajectory diapycnal diffusion greatly smoothes this transition through a prevailing upward/downward vertical flux of particles within the faster/slower upper/lower layer, leading to a maximum 20% decrease/increase in the water supply rate within each layer. Mesoscale eddy diffusion further increases the mass exchange across the frontal zone between the tropical and subtropical gyres, enhancing the water renewal rate of the naOMZ by up to 25%. The joint effect of all these three elements (isopycnal advection, diapycnal and eddy mesoscale diffusion) accurately reproduces the observed vertical changes in water mass composition within the naOMZ. In the upper CW, the supply of water mainly comes from the south (56%) via the North Equatorial UnderCurrent (NEUC) and the northern North Equatorial CounterCurrent (nNECC) with an 85% contribution of southern origin particles. In the lower CW, this tropical pathway is drastically weakened in favor of a subtropical pathway - more than two thirds of the total supply takes place north of 10ºN in this layer, mainly via both the Cape Verde Current (along 14ºN, 30%) and flows recirculated from the northern subtropical gyre (30%).

4.1. Introduction

The observed expansion of the world OMZs [*Stramma et al.*, 2008a; *Brandt et al.*, 2010] and the remarkable impact it may have on the marine ecosystem [*Stramma et al.*, 2010, 2011; *Wright et al.*, 2012] has led to a growing interest in the study of the circulation within the ocean shadow zones, aiming at a deeper understanding of the OMZs dynamics. A case of special interest is the North Atlantic OMZ (naOMZ), being the smallest in extension and highest in oxygen content among all OMZs [*Karstensen et al.*, 2008] but, in contrast, having a deoxygenation rate at least twice larger than in the others regions. Chapter III has presented a rather novel description of the naOMZ circulation with two markedly distinct vertical dynamic domains: the upper and the lower Central Water (uCW and lCW respectively). The uCW (between density levels σ_θ=26.3 kg m^{-3} and σ_θ=26.8 kg m^{-3}) exhibits a strong connection with the tropical system of jets south of 10ºN and thus a predominant contribution of SACW. The lCW (between density levels σ_θ=26.8 kg m^{-3} and σ_θ=27.15 kg m^{-3}) displays a more diffuse circulation pattern and shows that the core of the naOMZ is made up with a 50% mixture of SACW and NACW; this result implies a transfer of mass from the northern subtropical gyre and thus a previously unaccounted supply of oxygen to the core of the naOMZ [Figure 1].

The large-scale circulation based on Eulerian time-averaged fields, as presented in Chapter III, is a principal factor settling the development of the naOMZ. Nevertheless, it does not take into account the

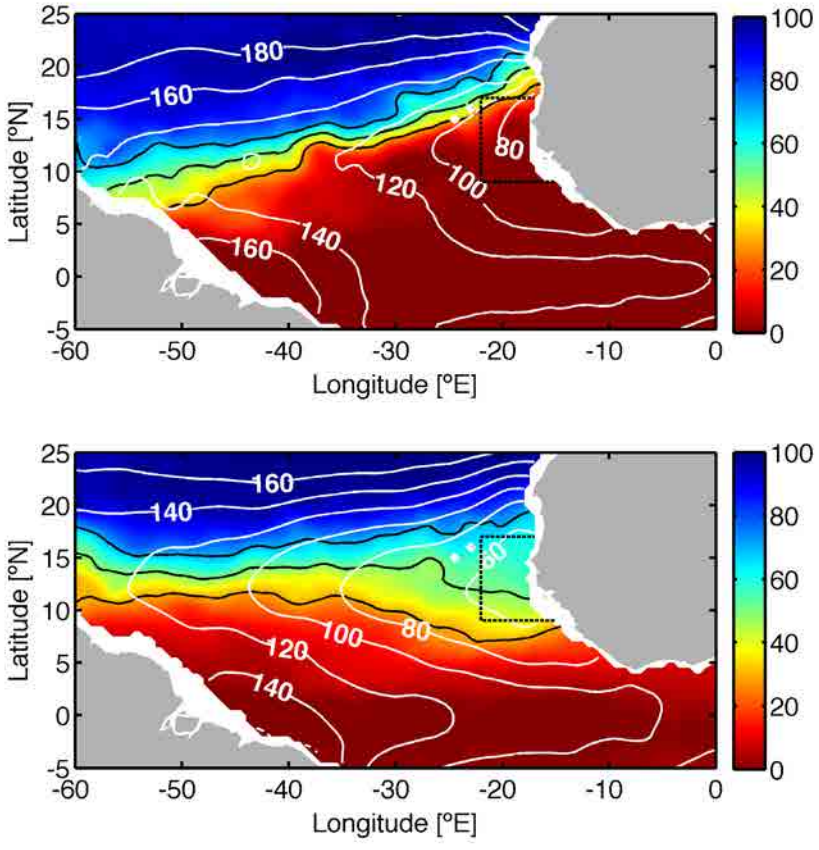

Figure 1. Observational distribution of the NACW content (percentage, in color) obtained from the water mass analysis performed in chapter III at σ26.5 (upper) and σ27.1 (bottom). This levels present the lowest oxygen content of the naOMZ within the uCW and the lCW respectively. Contours of 30%, 50% and 80% are shown with black lines. Climatological oxygen content [umol kg^{-1}] from the annual WOCE atlas [*Gouretski, V. and Koltermann*, 2004] is shown in white contours. The naOMZ box where particle are released is represented with a dotted black box.

role played by mesoscale eddies and diapycnal diffusion in the local renewal of the naOMZ thermocline. By applying the Osborn–Cox model to a set of repeated observations along meridional sections crossing the naOMZ, *Hahn et al.* [2014] obtained that the eddy-driven meridional oxygen supply contributes more than 50% of the total oxygen demand, and *Fischer et al.* [2013] found that diapycnal fluxes supply at least one third of the oxygen consumed at the core of the naOMZ. Hence, the complete description of the oxygen supply to the naOMZ should include a complex three-dimensional pathway of large-scale circulation and local mixing [*Brandt et al.*, 2014; *Duteil et al.*, 2014].

In this work we extend the description in Chapter III by using a Lagrangian approach that includes, in addition to the mean flow, the seasonal variability, the mesoscale eddy field and the diapycnal diffusion; the advantage of the Lagrangian perspective is that provides for the joint effect of these different processes, which have only been considered separately in earlier Eulerian studies [*Elmoussaoui et al.*, 2005; *Stramma et al.*, 2005; *Brandt et al.*, 2010; *Fischer et al.*, 2013; *Hahn et al.*, 2014]. We actually perform several numerical Lagrangian simulations of increased complexity with the purpose of isolating the contribution of each of these different processes (turbulent and diapycnal diffusion) to the water renewal in the naOMZ. Moreover, the comparison with the water mass distribution obtained in Chapter III, and the water mass composition as deduced from the Lagrangian pathways, shall provide a consistent validation of the results.

4.2. Data and methods

4.2.1 The velocity field

The numerical velocity field to run the Lagrangian experiment is the ECCO2 assimilative product already used in Chapter III. The horizontal resolution of the simulation is a 1/4 of degree, with 50 vertical levels, spanning 20 years from 1992 to 2011 with a temporal resolution of 3 days. Two different velocity fields will be used to describe the processes that lead to the thermohaline transition at σ_θ=26.8 kg m^{-3} (σ26.8). On a first and simplified case, we will use a fully isopycnal two-dimensional (2D) field computed by vertically averaging the original ECCO2 horizontal velocities over 0.05 kg m^{-3} density layers. The Lagrangian advection within this 2D field will always follow isopycnal surfaces and the vertical velocity is therefore solely related to the isopycnals' slope. Second, we will use the original three-dimensional (3D) ECCO2 velocity field. The comparison between outcomes from both velocity fields allows distinction between the isopycnal and diapycnal components in the ECCO2 product.

The isopycnal/diapycnal analysis will be used to obtain an order-of-magnitude estimate for the diapycnal fluxes in OMZs, as it has been argued that they may account for up to one-third of the total oxygen supply in these regions [*Fischer et al.*, 2013]. Nonetheless, we will take special caution when interpreting these results because the vertical velocity in ECCO2 is computed as a residual from the mass conservation

condition in the horizontal plane. ECCO2, as a depth-coordinate model, may have a preferential advection along z-constant surfaces. Hence, in regions where the isopycnals are notably tilted, these models may lead to an artificial diapycnal flux [*Griffies et al.*, 2000].

On the other hand, the eddy-permitting, but not fully-resolving, ECCO2 velocity field may underestimate the strength of the tropical system of jets and the horizontal turbulent diffusion. *Duteil et al.* [2014] have shown that the model horizontal resolution, i.e. the model ability to resolve mesocale structures, plays a major role in reproducing the thermocline oxygen content of the tropical Atlantic. Although we focus on the water mass distribution rather than oxygen content, in order to compensate for this underestimation of small-scale dispersion, sub-grid diffusion will be artificially added in the computation of the Lagrangian trajectories as proposed by *Döös et al.* [2011] and briefly summarized below.

4.2.2 The Lagrangian experiment

Lagrangian trajectories are computed using the Connectivity Modeling System version 1.1 (CMS) [*Paris et al.*, 2013] that tracks virtual particles within a numerical circulation model. An advantage of the CMS package is that it allows adding of artificial eddy diffusivity to simulate dynamics with a smaller spatial scale than the model grid resolution. This artificial turbulence is here parameterized by adding a stochastic impulse (*I*) each time-step particles are advected. As in *Döös et al.* [2011], this impulse consists of an extra horizontal velocity parameterized according to , where *K* is the horizontal eddy diffusivity coefficient, *dt* is the time step, and *r* is a random number between -1 and 1 from a Gaussian distribution. In our case, with a 1/4º horizontal resolution model, we tested 0, 50, 100 and 1000 $m^2 s^{-1}$, and the best fit to observations (section 4.3.1) corresponded to $m^2 s^{-1}$ for the original 3D velocity field. This value is in agreement with *Döös et al.*, [2011] who obtained $m^2 s^{-1}$ as the best fit between the dispersion of real ocean surface drifters and virtual particles within a 1/4º resolution model. The focus on subsurface levels in our study likely explains the smaller values we use for *K*.

In order to discern the role that diapycnal mixing and the horizontal subgrid-scale diffusion play in the water mass renewal of the naOMZ, we will use four different Lagrangian simulations of increased complexity, corresponding to the 2D and 3D velocity fields with and without a subgrid scale diffusion of $m^2 s^{-1}$. Specifically, we will compare the outcomes from the following four simulations: 2D isopycnal velocity field without subgrid-scale diffusion (ISO-K0); 2D isopycnal velocity field adding subgrid-scale diffusion (ISO-K100); original ECCO2 3D velocity field with no diffusion (3D-K0); and the 3D velocity field with added subgrid-scale diffusion (3D-K100). In particular, the contribution of the diapycnal fluxes to the water supply will be assessed by comparing the ISO-K100 and 3D-K100 simulations.

As we are interested in the source of the naOMZ waters, we release particles within the naOMZ and advect them backwards in time for up to 100 years. This means that we are computing all trajectories that end up in the naOMZ in a realistic forward time simulation. In order to attain a time series 100 years long,

the available 20-year numerical simulation is therefore looped in the same way as in *van Sebille et al.* [2012, 2013]. The release region for the virtual particles, hereafter defined as the naOMZ box, is located between 9ºN and 17ºN and east of 22ºW (Figure 1). This box roughly comprises the region where most of the lowest oxygen values have been recently located [*Fischer et al*., 2013] at the core of the naOMZ. The area of study spans the entire North Atlantic tropical Ocean (from 60ºW to 0º) and from the southern hemisphere to beyond the southern edge of the North Atlantic Subtropical Gyre (from 5ºS to 30ºN). In each experiment, a total of 170,000 virtual particles are randomly seeded every 15 days during the first 5 years of the simulation. For simplicity, although the Lagrangian simulation is computed backwards in time from the naOMZ box, in the manuscript we will always describe particles trajectories in a realistic forward time, always ending in the naOMZ.

4.3. Lagrangian simulations

The contribution of the different water masses that make up certain regions of the ocean can also be inferred from the trajectories of the water parcels, or Lagrangian particles, that end up in that region. Specifically, the analysis of the origin of all particles ending in the naOMZ should be comparable with the observational water mass analysis carried out in chapter III. Both analyses should independently lead to similar water mass contributions to the naOMZ. Therefore, a good agreement among them should be considered as a consistent validation of the modelled Lagrangian trajectories and the numerical ocean model velocity fields from which they are derived.

4.3.1 Lagrangian stream function

One way to reveal the average pattern of a set of trajectories is to compute a Lagrangian stream function (LSF). Analogous to the standard (Eulerian) stream function, which accounts for the flux between neighbouring points at any given time, the LSF accounts for the net number of particles (or trajectories) that flow between two grid points throughout the entire simulation. However, it is important to note that the LSF does not show the average circulation within a region, as the Eulerian stream function does. Instead, it represents the average pathways followed by a selected set of particles, in what can be referred to as conditional pathways. Thus, the LSF only shows a subset of the circulation, in our case, the pathways to the naOMZ.

To compute a stream function, the flow should always be non-divergent. In the case of a LSF, this means that trajectories should start and end out of the domain. The summation of the latitudinally flowing particles is carried out along parallels, moving east from the western boundary and considering as positive (negative) counts those particles that move north (south), i.e. particles always flow with larger LSF values to the right. We have also taken the zero LSF reference value at the south-western grid point of the domain. These definitions means that the sign of the LSF is related to the origin of the trajectories;

positive (negative) values are related with southern (northern) origin particles. Finally, the LSF values are normalized by the total number of particles, so they represent the proportion of particles that follow a specific pathway. For further details about the LSF computation, the reader is referred to *Blanke et al.*, [1999] or *Döös et al.*, [2008].

In chapter III we have shown that the thermohaline transition observed at σ26.8 is a permanent feature of the northeastern Tropical Atlantic. Such a marked and persistent hydrographic footprint requires a continuous generating mechanism. We suggest that the uCW and lCW should be governed by different dynamics leading to a continuous supply of distinct water masses in each layer. However, diffusive processes, especially diapycnal mixing, should counteract this differentiation. To distinguish between developing and erasing processes, we use three of the Lagrangian simulations: isopycnal velocity field and no added subgrid-scale diffusion (ISO-K0), 3D velocities but no added subgrid-scale diffusion (3D-K0), and 3D velocities together added subgrid-diffusion (3D-K100) (see section 4.2.2).

Figure 2 compares, for all three simulations, the mean vertical profile of the observed proportion of NACW within the naOMZ (black line) with the proportion of particles having a northern origin (coloured lines). Note that in order to show the Lagrangian pathways within the tropical Atlantic, the LSF is computed between 5ºS and 30ºN. This implies that particles of southern and northern origin respectively come from south of 5ºS and north of 30ºN. This criterion is potentially too restrictive, as SACW/NACW presents a contribution above 80% south/north of 6ºN/20ºN (Fig. 4 in chapter III). Therefore, we could alternatively assign a SACW/NACW fingerprint to those particles arriving to the naOMZ from south/north of 6ºN/20ºN. Hereafter, we will distinguish between particles arriving from south/north of 6ºN/20ºN and the more restrictive definition of particles of southern/northern (5ºS/30ºN) origin. Notice that, with the less restrictive definition (6ºN/20ºN), a trajectory starting south of 5ºS but flowing between 20ºN and 3º0N within the northern subtropical gyre before entering into the naOMZ will be considered as a 20ºN particle despite its southern origin. For comparison, Figure 2 shows the profiles following both criteria in each simulation. The two profiles agree in general although, as expected, the 6ºN/20ºN is closer to the observations for all simulations.

4.3.2 Water mass pathways: ISO-K0

A marked depth increase in the contribution of northern particles is evident near σ26.8 for all simulations, in agreement with observations. However, the transition in the vertical profile is especially abrupt in the isopycnal simulation (ISO-K0, Fig.2a), with a roughly constant 10% contribution of 20ºN particles all above σ26.8 but a marked increase just below, reaching 63% at σ27.1. This unrealistic abrupt transition between the uCW and lCW is likely due to the neglect of diapycnal fluxes. Nevertheless this also points to the markedly distinct dynamics that rule the isopycnal circulation in each layer.

The LSF clearly shows different patterns between the uCW and lCW for the ISO-K0 case (Figure 3a

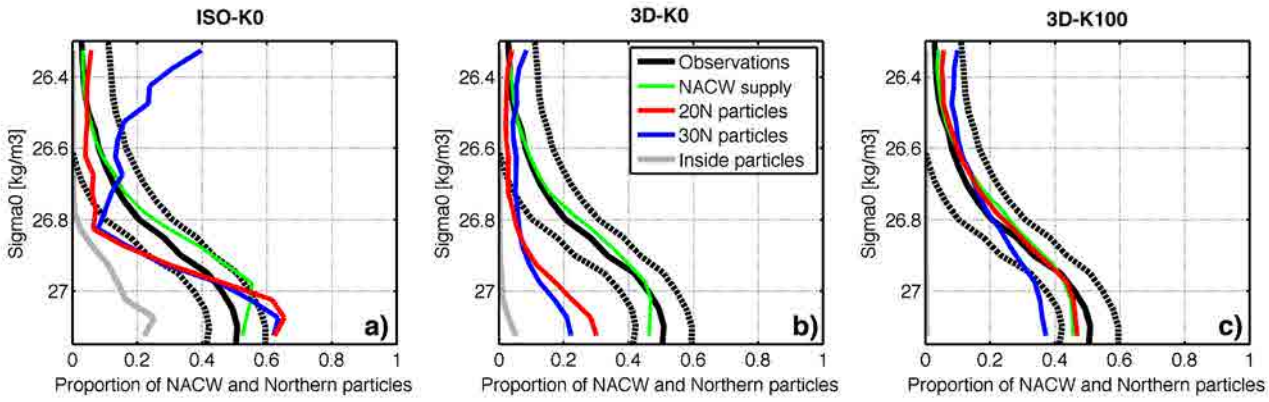

Figure 2. Comparison between the mean observed vertical profile of NACW within the naOMZ box (black line) with the one deduced from the number of particles entering the naOMZ with different origins (red/blue line, particles arriving from north of 20N/30N). The green line is calculated as the contribution of NACW particles that cross into the naOMZ box. The dashed line shows one standard deviation from the mean. Grey line denotes the fraction of particles that do not leave the domain during the whole 100 year simulation.

and b). For the uCW, the major (above 80%) contribution of southern origin particles (red contours) is displayed via a continuous and successive northward branching from the tropical system of jets toward the naOMZ and throughout the whole zonal basin extension. Most of these particles cross the equator along the American continent via the North Brazil Current and then retroflect east to feed the EUC at 0ºN and the NEUC at 4ºN. East of 40ºW, northward branching of these jets joins the nNECC flow at 8ºN. In the same manner, the nNECC also branches successively northward to enter into the naOMZ mostly within a broad latitudinal band between 10ºN and the Cape Verde Islands, the Cape Verde current system (see chapter III). Northern origin particles (blue contours) within this layer enter the tropics mostly in the western margin, retroflecting east from the southwestward subtropical gyre flow, in agreement with observational studies [*Kirchner et al.*, 2009]. Note however that the contribution of northern origin particles is overestimated in this simulation (Figure 2a) likely due to the inability of the isopycnal simulation to reproduce the enhanced vertical mixing of the upper levels near their outcropping region, north of 20N.

For the lCW, the LSF computed from the ISO-K0 simulation (Fig 3b) displays three main differences in comparison with the uCW. The first one, as previously shown in Figure 2a, is the notable contribution of northern origin particles. They retroflect eastwards south of 20ºN in to the north branch of the Cape Verde Current (nCVC), just north of the Cape Verde Islands, from the main southwestward flow of the eastern boundary current and eventually reach the naOMZ, directly from this zonal current or after recirculating southward along the continental slope. The second difference is the pathways followed by southern origin particles. They enter into the tropical North Atlantic also via the NBC and retroflect to directly feed the nNECC at about 8ºN. Virtually all southern origin particles leave the nNECC before 30ºW, branching north into a progressively narrowing band of eastward flow. This occurs just south of 15ºN in what appears to be the main conduit of southern origin particles to the naOMZ in this lower layer, the Cape Verde Current (CVC). The simulation reveals that, within the lCW and in contrast with the uCW,

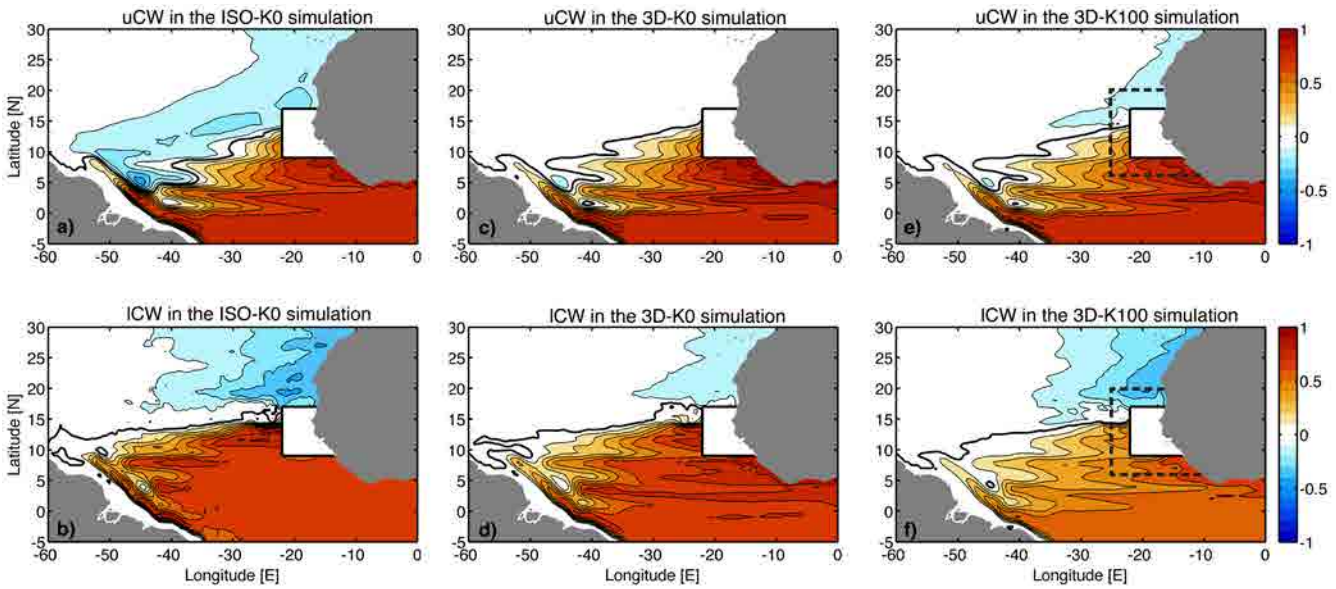

Figure 3. Lagrangian pathways to the naOMZ for the three experiments within the uCW (top panel) and the lCW (bottom panel). Simulations are from the ISO-K0 (left panels), 3D-K0 (middle panels) and 3D-K100 (right panels) runs. The LSF is normalized by the total number of particles per layer, i.e. increments between contours refer to the proportion of particles that flow in between, with LSF values increasing to the right of the flow. The zero reference LSF is selected in the south-western corner of the domain, so positive (negative) values of the LSF are related to southern (northern) origin pathways. The control section used in Figure 5 is displayed with a black dashed line.

there is essentially no pathway from the tropics to the naOMZ east of 30ºW and south of 10ºN.

Finally, the third difference between the uCW and lCW pathways relates to their time scales. Figure 4a,b (blue lines) display the average time required by particles to reach the naOMZ box from any point of the domain. For example, we can compare the regions where southern and northern origin particles enter in to the tropical North Atlantic, via the NBC across the equator and via the southwestward flow of the NEC between 20ºN and 25ºN respectively. No matter the origin, the times are similar within a layer: between 10 and 15 years for the uCW and between 40 and 50 years for the lCW. The isopycnal simulation suggests that the time scales is 3-4 times longer in the lCW than in the uCW. The advection times show a notable disconnection within the lCW, between the naOMZ and the region lying just south, with transit times over 50 years for a distance shorter than 3º of latitude (Fig. 4b).

4.3.3 Water mass pathways: 3D-K0

When Lagrangian particles are allowed to change their density level along their trajectory (3D-K0), the abrupt vertical transition between the uCW and the lCW is greatly smoothed (Fig. 2b). The exchange of particles from different density levels leads to a homogenization in the water mass supply of the naOMZ. Part of the particles originally in less dense levels, thus with a predominant southern origin, will finally end within the naOMZ at more dense levels, explaining the reduction of northern influenced particles in the lCW. This feature is also noticeable in the LSF of the lCW layer (Fig. 3d): the pathways followed by

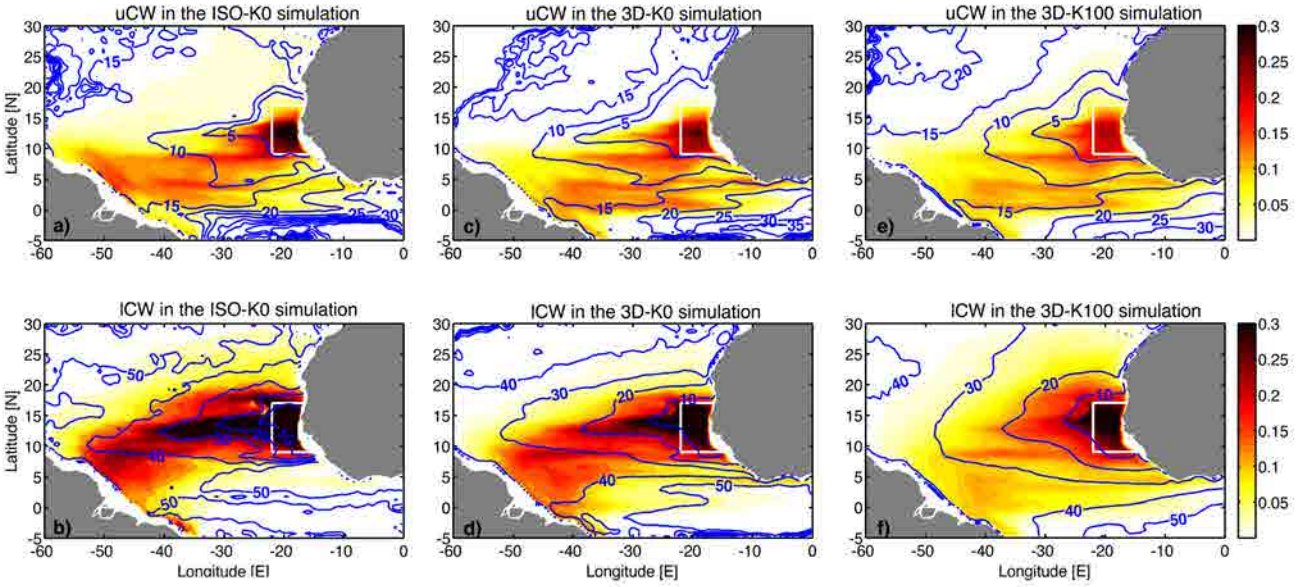

Figure 4. Density of particles (in color) found within 0.5º×0.5º horizontal bins during the whole duration of each simulation for the uCW (top panel) and the lCW (bottom panel) strata. Simulations are from the ISO-K0 (left panels), 3D-K0 (middle panels) and 3D-K100 (right panels) runs. The advection times to the naOMZ box (white-edged box) are displayed with blue contours. For each bin, the advection time is estimated as the median value of the travelling-time distribution for particles at that location to reach their seeding location.

the particles ending in the lCW of the naOMZ now resemble those followed by the uCW particles. In this simulation roughly 30% of all lCW particles reach the naOMZ directly from the nNECC (south of 10ºN) or from even further south, in comparison with the isopycnal simulation (Fig. 3b) where this pathway is totally absent. Also, the advection times within the lCW are reduced by about 25% (Fig. 4d). In contrast, the contribution to the uCW of northern particles is still minimal, i.e. no transfer from deeper levels is observed. Consistently, the general scheme of the LSF and the advection times for uCW are only slightly modified with respect to the ISO-K0 simulation. This asymmetry in the vertical transfer of particles between the two layers will be described in detail in section 4.3.5.

On the other hand, the diapycnal diffusion in the 3D-K0 simulation underestimates the contribution of northern particles, especially in the lCW. This suggests there may be other processes playing an important role in the water mass renewal of the naOMZ. The next section addresses this question.

4.3.4 Water mass pathways: 3D-K100

Mesoscale dynamics may play a major role in the renewal of the OMZ thermocline [*Duteil et al.*, 2014; *Hahn et al.*, 2014]. Since the eddy-permitting ECCO2 model does not fully resolve those processes responsible for the generation of mesoscale eddies, the ventilation of the naOMZ may be underestimated (Fig. 2b). For this reason, in our Lagrangian approach, the effect of the unresolved eddies is simulated by adding horizontal subgrid-scale diffusion to the model trajectories (3D-K100 simulation, see Methods).

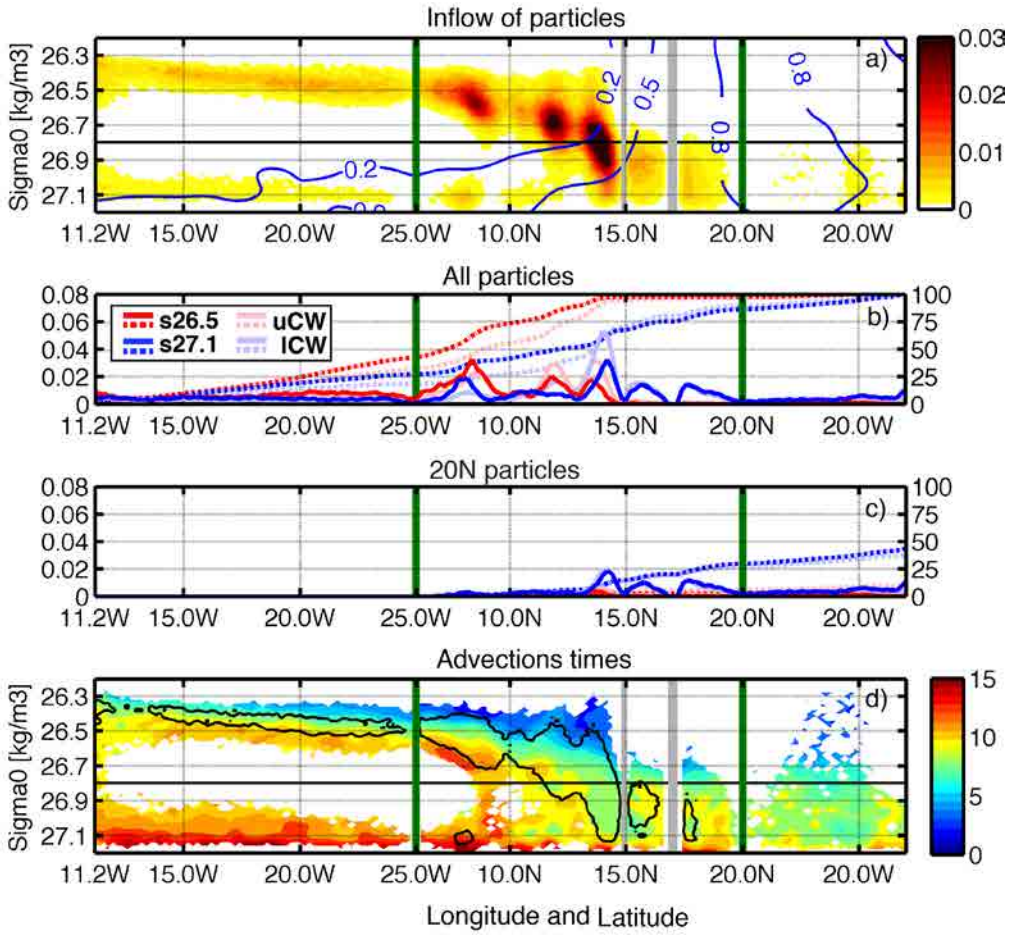

Figure 5. Water supply across the naOMZ control section in the 3D-K100 simulation. (a) The normalized density of inwards particles (colored) is compared to the along-section proportion of observed NACW (blue contours). (b) The normalized local (solid lines) and along-section cumulative (dashed lines) inflow of all particles is represented in different color for different levels and layers (see inset legend); similarly (c) for 30N particles. (d) Average advection times (in years) between the time particles cross the naOMZ control section and the time they reach their seeding location; for comparison, the contour of 0.05 units of the density of inwards particles (displayed in a) is shown with black line. The control section is displayed in Figure 3.

The added diffusion enhances the proportion of northern particles, and is remarkably similar to the observational profile (Fig. 2c). The added horizontal diffusion has two main effects. First, it leads to a substantial increase in the water transfer from the northern subtropical gyre across the frontal zone, particularly in the lCW where the main flow is sluggish. The added diffusion increases the number of northern origin particles leaving the subtropical gyre and entering the naOMZ via the eastward flow of the nCVC just south of 20ºN (Fig. 3f), as also seen in the ISO-K0 simulation. The second effect is to

Table 1. Contribution (%) of the different flows to the water mass supply (WM) of upper Central Water (uCW) and lower Central Water (lCW) to the naOMZ across the control section* (see section 4.4)

		NEUC/ NICC	nNECC	12ºN	14ºN	16ºN	18ºN	20ºN
WM	uCW	**32 (43)**	24 (31)	22 (16)	17 (18)	01 (00)	01 (00)	03 (02)
	lCW	18 (**27**)	09 (14)	14 (10)	**29** (16)	10 (08)	09 (11)	11 (14)
nWM	uCW	00 (00)	00 (00)	01 (01)	**03 (02)**	00 (00)	00 (00)	**03 (02)**
	lCW	00 (00)	01 (02)	03 (04)	10 (09)	05 (05)	08 (09)	**11 (14)**

* Respective contributions within the uCW and lCW (the values in parenthesis correspond to the σ26.5 and σ27.1 levels). nWM refers to the proportion of the total flow formed by northern origin particles (Fig. 5c). Bold numbers emphasize those flows with the highest contributions.

strengthen the northward transfer from the NEUC and nNECC, contrary to that of the ISO-K0 case. As a consequence, the advection times (Figs. 4e and 4f) from the subtropical gyre and the north equatorial jets into the naOMZ are reduced (20-30%) compared with the two previous simulations. This is especially relevant for the supply of oxygen, as it implies an enhanced connection from these more oxygenated regions (Fig. 1) and thus a more efficient ventilation of the naOMZ.

A more detailed vertical description on how the water supply to the naOMZ takes place is presented in Figure 5. It shows, for the 3D-K100 simulation, the inflow of particles across a control section located 3º outside the naOMZ box, where particles were released; this allows distinction of the preferential pathways entering the naOMZ. Since particles may cross this control section several times, we only show where and when they cross it for the last time before reaching the naOMZ box. The results of the 3D-K100 simulation may also be used to calculate the fraction of NACW that enters the naOMZ box at different levels. This supply is calculated as the observational proportion of NACW at the location where each particle enters the box, and then summing these contributions from all arriving particles. The profile of this NACW supply (green line in Fig. 2) fits the observations remarkably well in all simulations, although becomes progressively better as we introduce diapycnal motions and added diffusion. The goodness of this agreement, which depends on both the particle pathways and the NACW content at the location where the particles enter the box, permits further confidence in the model velocity field, i.e. if the entry pathways were incorrect then the NACW supply would differ from the proportion of NACW observed within the naOMZ box.

Several inflows are clearly distinguished in Figure 5a and their contribution to the total supply is summarized in Table 1. Within the uCW, the shallow northward branch from the NEUC and the direct inflow of the nNECC are the major contributors (56%), with only a minor inflow arriving north of the Cape Verde Islands (5%). For the lCW, the water supply is more northerly: the combined contribution of the NEUC and nNECC is halved (28%), a pronounced maximum inflow occurs via the CVC at 14ºN (29%), and the inflow north of the Cape Verde Islands (30%) mainly via the nCVC. At the core of the naOMZ (σ27.1), a major contributor (27%) is the northward flow arriving from south of 6ºN; since the ISO-K0 simulation shows a negligible inflow south of 6ºN, the conclusion is that this inflow is primarily driven by diapycnal fluxes and enhanced eddy diffusion. Nevertheless, the zonal flow north of the Islands contributes one third of the total supply, in remarkable contrast with the importance traditionally assigned to the southern pathways (NICC and nNECC) in the water mass renewal of the naOMZ. Morover, notice that the contribution of 20ºN particles reaches up to a 45% at σ27.1 (Fig.2c), in comparison with the 50% observed fraction of NACW (Fig.6 in chapter III), thus the supply from the northern subtropical gyre is still underestimated in this simulation at this level. Additionally, the mean advection times for arrival from the control section to the naOMZ box (Fig. 5d) are much shorter for the northern pathways than for the southern ones.

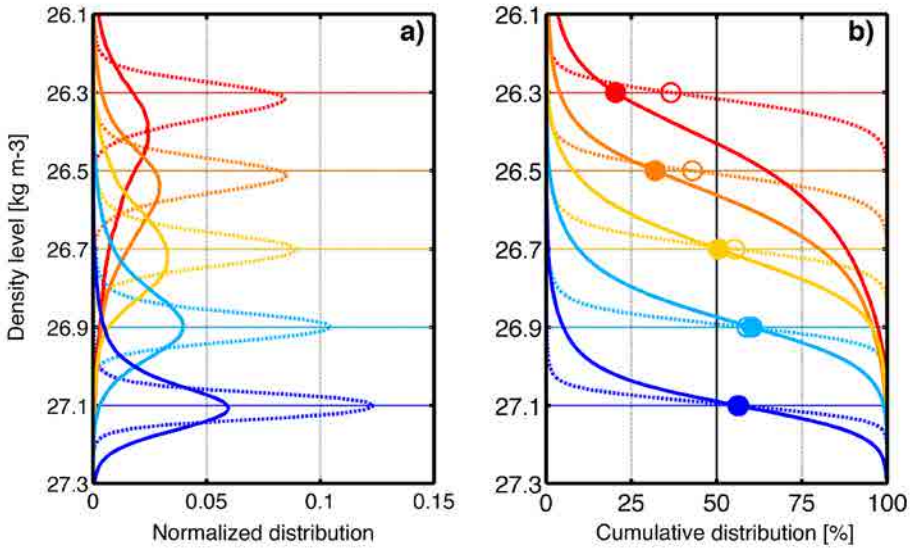

Figure 6. (a) Potential density distribution for five sets of particles (each set corresponds to a different color) as observed 1 and 10 years (dashed and solid lines, respectively) before they reached the naOMZ. Particles within each set end their trajectory in the one selected density level (σ26.3, σ26.5, σ26.7, σ26.9 and σ27.1). (b) Cumulative distributions with circles highlighting the proportion of particles with densities smaller than the final density level. Note that more (less) than 50% of the particles ending at a specific density levels above (below) σ26.7 present initially larger (smaller) densities.

4.3.5 Diapycnal component

The changes in the pathways for the ISO-K0 and 3D-K0 simulations indicate a remarkable role of the diapycnal motions in the renewal and vertical redistribution of the naOMZ water mass, especially within the lCW. To understand why this occurs, we look at the evolution of the density distribution of particles ending at several density levels within the naOMZ (Fig. 6). As expected, the density distributions are Gaussian-like, approximately centered around the ending density level. For some destination levels, however, there are significant net upward or downward deformations (Fig. 6a). Particles ending in the upper levels of the naOMZ, above σ26.7, come mainly from higher densities thus pointing to upward diapycnal velocities (Fig. 6b). And conversely, below σ26.7, particles mostly have a lighter density origin, i.e. downward diapycnal velocities. This contrasting behaviour within the uCW and lCW is added to the distinct horizontal patterns already shown in the previous sections for the two layers.

However, these results should be taken with caution since, as noted earlier in section 2, z-coordinate models as ECCO2 may induce spurious diapycnal mixing especially in those levels where the isopycnals are more vertically slanted, such as in the upper levels. In order to verify if the diapycnal processes leading to the distributions are within realistic values, we estimate the mean diapycnal velocity as the change in time of the average density of a subset of particles that end in a specific density level (Fig. 6b). We may assign this average density to the median of the density distribution at a given time. The mean diapycnal velocities calculated in this way range between $+4.1\times10^{-10}$ kg m^{-3} s^{-1} in the upper levels and -1.8×10^{-10} kg m^{-3} s^{-1} in the lower levels. These values may be compared with the average diapycnal velocity as obtained from the GUTRE tracer experiment [Banyte et al., 2012] carried out in this same region; the velocity at σ26.9 was determined to be $+1.5\pm2.7\times10^{-10}$ kg m^{-3} s^{-1}, slightly smaller but of the same order of magnitude as our estimates. This result suggests that the net diapycnal supply deduced from the Lagrangian simulation is not grossly biased by spurious diapycnal mixing. Therefore, this diapycnal flux

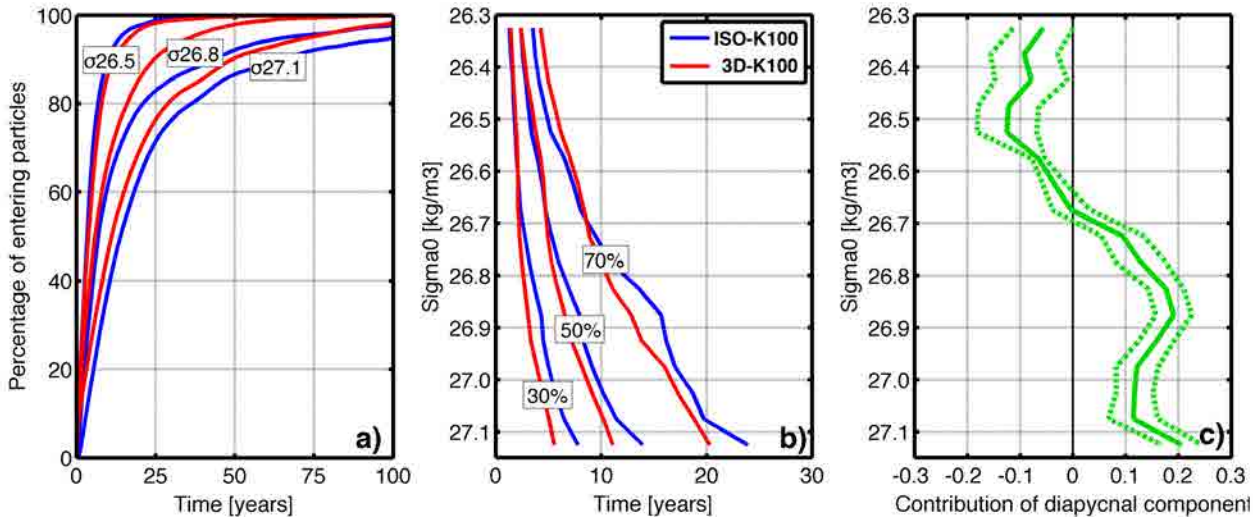

Figure 7. Results from the ISO-K100 and 3D-K100 simulations (blue and red lines, respectively). (a) Temporal increase in the proportion of particles as they fill the naOMZ control section (shown in Figure 6) for three different final density levels; when the proportion of particles reaches 100% the naOMZ is assumed to be completely renewed. (b) Number of years required to fill the control section at the 30, 50 and 70% levels, as a function of the final density level. (c) Mean vertical profile (solid line) of the diapycnal flux contribution to the renewal of the naOMZ (fdia, see text); positive/negative values represent enhanced/reduced diapycnal water supply. fdia is computed for different times of the simulation. One standard deviation from the mean is plotted with dashed lines.

can be attributed to a real large-scale process that is reasonably well reproduced in the ECCO2 model.

The exchange of particles between distinct density levels (Fig. 6) points out that diapycnal fluxes should have an impact on the naOMZ renewal times, as different levels have different advection times (Fig.4). We can quantify the contribution of this diapycnal component in the renewal of the naOMZ water mass by comparing the Lagrangian simulations with and without diapycnal fluxes (3D-K100 and ISO-K100). The only difference between the two outcomes will respond to the diapycnal fluxes. A first step is computing the function, *n(t)*, that counts the amount of particles within naOMZ as a function of time, thereby identifying the time scales of water mass renewal (Fig. 7a). When this function reaches 100%, the naOMZ is completely renewed, full of particles; this moment corresponds to the beginning of the backward simulation. From this function, inferring the renewal times, i.e. the required time to renew a certain percentage of the whole naOMZ water mass, is straightforward (Fig. 7b). Renewal times in the uCW are typically two to three times shorter thant in the lCW (blue lines in Figure 7b).

The inflow of particles towards the naOMZ is given by the change of *n(t)* in time, $F(t)=dn/dt$. We may then compute the purely isopycnal inflow, $F_{iso}(t)$, obtained from the ISO-K100 simulation and the isopycnal+diapycnal inflow, $F_{3D}(t)$, from the 3D-K100 experiment. The effect of diapycnal fluxes in the water mass renewal of the naOMZ is quantified as $f_{dia}= F_{dia}/F_{3D}= (F_{3D}-F_{iso})/F_{3D}$.

Figure 7c shows the average vertical profile of f_{dia}. Below σ26.7, f_{dia} is positive because a large proportion of particles ending in these levels come originally from lighter and swifter levels (Fig. 6b). As

a consequence of this prevailing downwelling, the water supply to the naOMZ is enhanced about 10-20% within the lCW. On the other hand and within most of the uCW, the predominant upwelling leads to a 10% weakening of the water mass renewal.

4.4. Discussion and conclusions

The water mass supply to the naOMZ has been studied through four Lagrangian numerical simulations. The simulations reveal distinct dynamics and pathways in the upper and lower CW layers. The uCW presents stronger ventilation than the lCW with renewal times two to three times smaller. This is attained through the more efficient water supply ascribed to the Subtropical Cell [*Schott et al.*, 2004] and thus mainly (56%) carried out by the nNECC and the northward branching of the NEUC, with a predominant contribution of southern origin particles. However, within the lCW these jets markedly reduce their contribution in accordance with an enhancement in the supply of jets located further north, simultaneous with an abrupt increase in the proportion of northern origin particles. In fact, more than two thirds of the total water supply within this layer occurs north of 10ºN through the Cape Verde Current system, the main contributions being the CVC at 14ºN (29%) and the further north flows related with the nCVC fed with waters recirculating from the northern subtropical gyre (30%).

In contrast with previous Eulerian studies, the Lagrangian description simultaneously incorporates the seasonal variability, the diapycnal exchange, and the mesoscale eddy-field. Thus, the comparison of different Lagrangian simulations of increased complexity allows isolating the contribution of the isopycnal/diapycnal fluxes and the model subgrid-scale eddy diffusion to the water supply. While the markedly distinct isopycnal circulation patterns of the uCW and lCW lead to the abrupt thermohaline transition at σ26.8, the diapycnal fluxes smooth this transition through the interlayer exchange of particles. Furthermore, the Lagrangian simulations reveal prevailing diapycnal velocities of opposite sign within each layer. This fact is especially relevant within the sluggish lCW, where downwelling (from shallower and faster to deeper and slower density levels) prevails along the trajectories, enhancing the water supply by up to 20%. This result points to the significant role that diapycnal fluxes play in the water renewal of the naOMZ, in agreement with the results of *Fischer et al.* [2013].

Another remarkable element in the water supply to the naOMZ is the relevance of meridional eddy stirring, as recently shown by *Hahn et al.* [2014] through the analysis of the latitudinal variability in the oxygen field. In our case, the non-fully eddy resolving ECCO2 field is unable to correctly reproduce the water mass composition of the naOMZ. Nevertheless, the addition of parameterized subgrid-scale diffusion in the computation of trajectories leads to the accurate simulation of the observational hydrographic profiles. A major consequence of this added diffusion is the reduction of the water renewal times (by 25%) due to an enhanced water transfer from the meridional boundaries of the naOMZ, i.e. the NEUC/nNECC region at the south and the subtropical gyre at the north.

Our results imply that the traditionally constraint for the OMZ ventilation from the subtropical gyre [*Luyten et al.*, 1983] is limited, at least in the North Atlantic, to those layers above σ26.8, i.e. in the uCW stratum. In contrast, within the lCW a weak but significant southward pathway exists from the subtropical North Atlantic to its shadow zone, with major implications for the oxygen supply to the naOMZ.

Chapter V

General conclusions

In this dissertation we have presented a consistent and comprehensive description of the circulation in the North Atlantic shadow zone through the analysis of both hydrographic and velocity data from observations and numerical models. The present results provide a valuable contribution to better understand the role of circulation and diffusion in the ventilation of the naOMZ.

Chapter II provides novel estimates of the transport associated with the continental slope current system off NW Africa during the fall season, as deduced from direct observations taken during the CANOA 2008 cruise. The description characterizes the circulation in the slope region of the shadow zone at a time when the northward flow is maximum and, thus, the ventilation of the naOMZ is more intense, occurring through the seasonal development of the Mauritanian Current and the Poleward UnderCurrent. This dynamical description is complemented with a water mass analysis within the Central Water stratum in order to discern the exchange between the tropical and subtropical regimes.

In chapter III, the picture presented in the previous chapter is extended to the annual climatological mean for the whole naOMZ. This is attained, firstly, through the generation of a new dataset with historic temperature and salinity observations within the tropical North Atlantic. The temperature-salinity dataset is used to compute the content of NACW and SACW through the implementation of a water mass analysis. Secondly, a numerical model is used to unveil the circulation pattern that leads to this water masses distribution. A good agreement is observed between both the observational and numerical velocity fields provided in chapters II and III.

The water mass pathways to the naOMZ are computed in chapter IV through several Lagrangian simulations that include the long spatio-temporal scales dynamics described in the previous chapters. Four distinct simulations of distinct complexity are performed in order to describe and quantify the role played by diapycnal and eddy diffusion, in addition to isopycnal advection, in the water mass renewal of the naOMZ. The simulated Lagrangian pathways provide an alternative way of validating the ECCO2 velocity field through the comparison between the observational and the trajectory-inferred water mass composition of the naOMZ.

The main scientific contributions arising from this dissertation follow:

* The origin of the remarkable vertical thermohaline transition at sigma0 26.85 (roughly 300 m depth) is confirmed with direct velocity observations: A predominant northward flow of SACW is observed above sigma0 26.85 while a southward current transporting NACW influenced waters is detected below this density level.

* The northward flow above sigma26.85 is comprised by the Mauritanian Current (MC) at the surface layer (sigma<26.46) and the Poleward UnderCurrent (PUC) at subsurface (26.46<sigma<26.85). Direct velocity (ADCP) measurements give a maximum total transport of 2.7 Sv for the MC+PUC system (1.7 Sv + 1 Sv) south of the Cape Verde Frontal Zone off Cape Blanc. A northward flow of 1.7 Sv (1 Sv + 0.7 Sv) is still observed at 24ºN, well beyond the frontal zone, highlighting the role of the MC and the PUC in the large-scale return flow of the Meridional Overturning Circulation.

* In contrast, a southward transport of 0.8 Sv is observed below sigma 26.85 south of Cape Blanc with an important signal of NACW. Although a southward flow of 0.5 Sv is still observed at 24ºN, this current does not appear to continuously extend along the continental slope directly linking the subtropical gyre with the tropical gyre. Instead, it appears to be fed mostly from the ocean interior in some basin-wide anticyclonic gyre.

* A regional water mass variety is proposed for the naOMZ thermocline. This is the Cape Verde SACW (SACWcv), a mixture of SACW and NACW but with oxygen exhausted after the long residence time characteristic of the naOMZ.

* The analysis of the historic temperature-salinity dataset shows that the vertical thermohaline transition extends over the whole North Atlantic shadow zone, pointing to different water dynamics above and below sigma 26.8.

* The water mass analysis for the eastern tropical North Atlantic shows that the frontal zone between SACW and NACW is well-defined and northward tilted in the uCW (26.3<sigma26.8<26.8) while it is

tilted southward in the lCW (26.8<sigma0<27.15), unfolding into two branches associated with the encountering of pure SACW with SACWcv at 10ºN and of pure NACW with SACWcv at 20ºN.

* The shadow zone thermocline is completely made up of SACW within the uCW while there is a 50% contribution of NACW within the lCW, at the core of the naOMZ (at sigma 27.1), where minimal oxygen content is observed. This result implies a remarkable link between the subtropical gyre and the shadow zone at the lCW and thus a relevant, previously unaccounted, supply of oxygen to the naOMZ.

* The annual mean velocity fields deduced from the ECCO2 numerical circulation model show a markedly different circulation for the uCW and the lCW of the shadow zone. The flow within the uCW is governed by the broad cyclonic circulation of the subtropical cell (STC) that includes substantial along-path upwelling. Below sigma0 26.8, the modelled velocity field suggests the existence of a lower subtropical cell within the lCW with an inverse but weaker circulation as compared to the uCW, i.e. an anticyclonic flow pattern and predominant downwelling. This contrasted scheme of circulation ensures the supply of pure SACW to the uCW while an increased contribution of NACW in the lCW, in agreement with the previously presented observational velocity fields and water mass distributions.

* The essential role played by the upper and lower STCs in the circulation of the shadow zone, together with their substantial interannual and interdecadal variability [*Schott et al*., 2007, *Deutsch et al.,* 2014], highlights the importance of our results for an improved understanding of the temporal evolution of the naOMZ.

* One key element in this model-inferred shadow zone circulation is the existence of a broad band of eastward flows located between 10ºN and 20ºN, at latitudes just below the westward flowing NEC, as also reported in the Pacific Ocean from observational studies (*Qiu et al.* 2013a, 2013b). These flows, here referred as the Cape Verde Current system, appear to be the major water supplier to the shadow zone.

* The accurate numerical reproduction of the water mass composition within the naOMZ thermocline, as directly deduced from particle-track Lagrangian simulations, supports the goodness of the ECCO2 velocity field.

* The Lagrangian simulations also allow computing the exact contribution of each pathway to the naOMZ. In the uCW, most of the water supply (56%) occurs south of 10ºN, directly linked to the northward branching of the NEUC and to the nNECC, with a predominant contribution of southern origin particles. In contrast, in the lCW, more than two thirds of the total water supply takes place north of 10ºN, mainly via the Cape Verde Current at 14ºN (29%) and via the direct recirculation of waters from the subtropical gyre, north of the Cape Verde Islands (30%).

* Both the observational data and the numerical model confirm the transfer of mass from the subtropical

gyre to the shadow zone, emerging as an essential component of the ventilation of the naOMZ.

* In addition to the very different ventilation pathways for the uCW and lCW strata, the renewal times within the shadow zone are two to three times smaller in the upper layer.

* Due to the typical long residence times within the shadow zone, diapycnal diffusion appears to play a notable role in the thermocline ventilation. The predominant upwelling within the uCW stratum leads to a 10% weakening of water supply to the naOMZ; in contrast, the prevailing downwelling within the lCW stratum leads to a 20% strengthening of water input to the naOMZ.

* Eddy diffusion remarkably enhances the water supply to the stagnant shadow zone. The contribution of the subgrid-scale eddies has been estimated through along-pathway parameterization. The sole contribution of these smaller eddies (less than 25 km) leads to a 25% reduction in the renewal times, particularly enhancing the transfer of mass across the boundaries of the shadow zone – the southward transfer from the subtropical gyre and the northward flux from the equatorial region.

Appendix

Omptimum Multiparameter analisis

The Optimum Miltiparameter analysis (OMP) used in *Pastor et al.* [2012] aims to solve the following

$$\sum_i x_i \theta_i = \theta_{obs} + R_\theta$$

$$\sum_i x_i S_i = S_{obs} + R_S$$

$$\sum_i x_i (PO_4)_i = (PO_4)_{obs} + R_{PO_4}$$

$$\sum_i x_i (SiO_4)_i = (SiO_4)_{obs} + R_{SiO_4}$$

$$\sum_i x_i (O_2)_i = (O_2)_{obs} + R_{O_2}$$

$$\sum_i x_i = 1$$

linear system of mixing equations for each water sample:

where θ_i, S_i, $(PO4)_i$, $(SiO4)_i$, and $(O_2)_i$ are the values for each source water mass and θ_{obs}, S_{obs}, $(PO_4)_{obs}$, $(SiO4)_{obs}$, and $(O_2)_{obs}$ are the observed values, the last equation being for mass conservation.

Before resolving the system, the water type matrix is normalized to commensurate the different variables,

$$W_j = \frac{\sigma_j^2}{\delta_{j\max}}$$

and different weights are applied to each variable. The weights (W_j) are calculated following *Tomczak and Large* [1989]:

where σ is the standard deviation of the water type matrix for variable *j*, a measure for the ability of variable *j* to resolve differences in water mass content; and $\delta_{j\max}$ is a measure of the environmental variability of the variable *j* that characterizes the water type, here estimated as the largest variance in variable *j* for the definition of any water type. Weights are then normalized to temperature, i.e., a weight of one is given to temperature and values less than one to the other variables, and a weight of 10 is assigned to equation 6 in order to emphasize mass conservation.

An essential component of OMP is the definition of the water type matrix. We follow the approach of defining values in the vicinity of the study region rather than in the remote areas of water mass formation. The values used are given in table 1. Subsurface inorganic nutrients may be affected by the sinking and remineralization of organic matter (e.g. *Llanillo et al.* [2012]); however, by using the local water types we expect to minimize these remineralization effects. We will nevertheless have to check *a posteriori* the implicit underlying assumption behind the OMP classic analysis; i.e., that phosphates, silicates, and oxygen are approximately independent and conservative.

Six source water masses may be discerned in the study area. The upper part of the water column, down to $\sigma_\theta = 27.14$, is dominated by the central water masses of northern (NACW) and southern origin (SACW). Here we have used the θ-S characteristics that Tomczak (1981) defined using hydrographic data from the region 20 to 26ºN. Due to their formation process, the θ-S relationship for central waters is defined by a straight line (Mamayev 1975). Therefore, in order to characterize a central water mass in the σ_θ range 26.46–27.14, we require two source water types; i.e., for each water mass we need upper (U) and lower

	θ (ºC)	S	PO_4 (μmol L^{-1})	SiO_4 (μmol L^{-1})	O_2 (mL L^{-1})
$NACW_U$	18.65	36.76	0.25	0.36	4.60
$NACW_L$	11.00	35.47	1.05	5.65	3.66
$SACW_U$	15.25	35.70	1.41	6.92	1.08
$SACW_L$	9.70	35.18	1.94	14.08	1.20
SACW*	12.08	35.27	1.62	9.31	1.44
AAIW	6.50	34.90	2.02	22.55	2.21
MW	11.74	36.50	0.67	7.20	4.42
NADW	2.50	34.94	1.40	34.80	5.71
Weight	1.00	0.86	0.21	0.14	0.15

Table 1. Source water mass values used in the optimum multiparameter analysis for potential temperature (θ), salinity (S), phosphate (PO4), silicate (SiO4), and dissolved oxygen (O2). NACW: North Atlantic Coastal Water; SACW: South Atlantic Central Water; SACW*: South Atlantic Central Water of tropical origin; AAIW: Antarctic Intermediate Water; MW: Mediterranean Water; The upper (U) and lower (L) end members are indicated

(L) end members ($NACW_U$, $NACW_L$, $SACW_U$, $SACW_L$).

An additional water type of southern origin is detected in the southernmost part of the study region, at stations along the continental slope above 200 m depth, in waters having a relative salinity and temperature minimum and oxygen maximum. This variety, here named SACW*, has been previously identified as a regional SACW variety from the tropical region [*Fraga F.*, 1974; *Voituriez and Chuchla*, 1978]. The θ-S characteristics for SACW* have been defined using those southern stations that display a salinity minimum in the central water mass layer.

Two water masses are found at intermediate layers: MW and AAIW. The θ-S values for MW have been derived from the World Ocean Circulation Experiment (WOCE) Hydrographic Climatology [*Gouretski, V. and Koltermann*, 2004], by searching the temperature and salinity values that correspond to the salinity maximum in an intermediate layer within a region bounded by latitudes 12 and 49ºN and from the coast to 1500 km offshore. For the AAIW we used a modified type defined by *Fraga et al.* [1985] at about 20ºN, a variety that was also employed by *Perez et al.* [2001] to study the regional water masses.

Having assigned the θ-S characteristics of the source water types, we determined their nutrient and dissolved oxygen characteristics using stations in our data set that closely match each source water type θ-S definition. The same data from the WOCE climatology has been used for the MW.

Hence, seven source water types are identified in the study domain: $NACW_U$, $NACW_L$, $SACW_U$, $SACW_L$, SACW*, MW, AAIW. However, from the available variables a maximum of six source water types may be resolved as contributing to any observed water mixture. Therefore, we have followed a procedure where the data set has been divided into two groups, north or south of 21ºN, so that at any location only six water types contribute to the water mixture (table 2).

This grouping is not arbitrary. The central and intermediate layers were analyzed considering only $NACW_U$, $NACW_L$, $SACW_U$, $SACW_L$, SACW*, and MW, to conclude that the 21ºN latitude sets a clear boundary between SACW* and MW in the upper part of the water column; i.e., neither MW is found south of this latitude nor SACW* north of it.

	Group 1		Group 2	
Latitudes	>21° N		<21° N	
σ_θ	26.46–27.32		26.46–27.32	
Water types	$NACW_U$	$NACW_L$	$NACW_U$	$NACW_L$
	$SACW_U$	$SACW_L$	$SACW_U$	$SACW_L$
	AAIW	MW	SACW*	AAIW

Table 2. Bounding latitudes and densities, and water types used to group the data in three subsets for the optimum multiparameter analysis.

References

Arhan, M., H. Mercier, B. Bourle, and Y. Gouriou (1998), Hydrographic sections across the Atlantic at 7°30N and 4°30S, *Deep Sea Res. Part I Oceanogr. Res. Pap.*, *45*, 829–872.

Arístegui, J., E. D. Barton, X. a. Álvarez-Salgado, a. M. P. Santos, F. G. Figueiras, S. Kifani, S. Hernández-León, E. Mason, E. Machú, and H. Demarcq (2009), Sub-regional ecosystem variability in the Canary Current upwelling, *Prog. Oceanogr.*, *83*(1-4), 33–48, doi:10.1016/j.pocean.2009.07.031.

Banyte, D., T. Tanhua, M. Visbeck, D. W. R. Wallace, J. Karstensen, G. Krahmann, A. Schneider, L. Stramma, and M. Dengler (2012), Diapycnal diffusivity at the upper boundary of the tropical North Atlantic oxygen minimum zone, *J. Geophys. Res. Ocean.*, *117*(C9), doi:10.1029/2011JC007762.

Barton, E. E. (1987), Meanders , eddies and intrusions in the thermohaline front offNorthwest Africa, *Oceanol. Acta*, *10*(3), 267–283.

Barton, E. (1989), The Poleward undercurrent on the eastern boundary of the subtropical north atlantic, in *Coastal and Estuarine Studies*, edited by C. N. K. M. S.Neshyba, R.L., Smith, pp. 82–95, Springer-Verlag.

Benazzouz, A., J. L. Pelegrí, H. Demarcq, F. Machín, E. Mason, A. Orbi, J. Peña-Izquierdo, and M. Soumia (2014), Journal of Geophysical Research : Oceans, *J. Geophys. Res. Ocean.*, *119*, 1–25, doi:10.1002/2013JC009559.

Blanke, B., M. Arhan, G. Madec, and S. Roche (1999), Warm Water Paths in the Equatorial Atlantic as Diagnosed with a General Circulation Model, *J. Phys. Oceanogr.*, *29*(11), 2753–2768.

Bopp, L., C. Le Quéré, M. Heimann, A. C. Manning, and P. Monfray (2002), Climate-induced oceanic oxygen fluxes : Implications for the contemporary carbon budget, *Global Biogeochem. Cycles*, *16*(2).

Bozec, A., M. S. Lozier, E. P. Chassignet, and G. R. Halliwell (2011), On the variability of the Mediterranean Outflow Water in the North Atlantic from 1948 to 2006, *J. Geophys. Res.*, *116*(C9), C09033, doi:10.1029/2011JC007191.

Brandt, P., V. Hormann, B. Bourlès, J. Fischer, F. a. Schott, L. Stramma, and M. Dengler (2008), Oxygen tongues and zonal currents in the equatorial Atlantic, *J. Geophys. Res.*, *113*(C4), C04012, doi:10.1029/2007JC004435.

Brandt, P., V. Hormann, A. Körtzinger, M. Visbeck, G. Krahmann, L. Stramma, R. Lumpkin, and C. Schmid (2010), Changes in the Ventilation of the Oxygen Minimum Zone of the Tropical North Atlantic, *J. Phys. Oceanogr.*, *40*(8), 1784–1801, doi:10.1175/2010JPO4301.1.

Brandt, P. et al. (2014), On the role of circulation and mixing in the ventilation of oxygen minimum zones with a focus on the eastern tropical North Atlantic, *Biogeosciences Discuss.*, *11*(8), 12069–12136,

doi:10.5194/bgd-11-12069-2014.

Brandt, P., A. Funk, A. Tantet, W. E. Johns, and J. Fischer (2014), The Equatorial Undercurrent in the central Atlantic and its relation to tropical Atlantic variability, *Clim. Dyn.*, *43*(11), 2985–2997, doi:10.1007/s00382-014-2061-4.

Broecker, W. S. (1991), The Great Conveyor Belt, *Oceanography*, *4*, 79–89.

Burkholder, K. C., and M. S. Lozier (2011), Mid-depth Lagrangian pathways in the North Atlantic and their impact on the salinity of the eastern subpolar gyre, *Deep Sea Res. Part I Oceanogr. Res. Pap.*, *58*(12), 1196–1204, doi:10.1016/j.dsr.2011.08.007.

van Camp, L., L. Nykjaer, E. Mittelstaedt, and P. Schlittenhardt (1991), Upwelling and boundary circulation off Northwest Africa as depicted by infrared and visible satellite observations, *Prog. Oceanogr.*, *26*, 357–402.

Döös, K., J. Nycander, and a. C. Coward (2008), Lagrangian decomposition of the Deacon Cell, *J. Geophys. Res.*, *113*(C7), C07028, doi:10.1029/2007JC004351.

Döös, K., V. Rupolo, and L. Brodeau (2011), Dispersion of surface drifters and model-simulated trajectories, *Ocean Model.*, *39*(3-4), 301–310, doi:10.1016/j.ocemod.2011.05.005.

Duteil, O., F. U. Schwarzkopf, C. W. Böning, and A. Oschlies (2014), Major role of the equatorial current system in setting oxygen levels in the eastern tropical Atlantic Ocean: A high-resolution model study, *Geophys. Res. Lett.*, *41*(6), 2033–2040, doi:10.1002/2013GL058888.

Csanady, G. T. (1977), Intermittent “Full” Upwelling in Lake Ontario, *J. Geophys. Res.*, *82*(3), 397–419.

Deutsch, C., H. Brix, T. Ito, H. Frenzel, and L. Thompson (2011), Climate-forced variability of ocean hypoxia., *Science*, *333*(6040), 336–9, doi:10.1126/science.1202422.

Elmoussaoui, a., M. Arhan, and a. M. Treguier (2005), Model-inferred upper ocean circulation in the eastern tropics of the North Atlantic, *Deep Sea Res. Part I Oceanogr. Res. Pap.*, *52*(7), 1093–1120, doi:10.1016/j.dsr.2005.01.010.

Fischer, T., D. Banyte, P. Brandt, M. Dengler, G. Krahmann, T. Tanhua, and M. Visbeck (2013), Diapycnal oxygen supply to the tropical North Atlantic oxygen minimum zone, *Biogeosciences*, *10*(7), 5079–5093, doi:10.5194/bg-10-5079-2013.

Fraga F. (1974), Distribution des masses d’eau dans l’upwelling de mauritanie, *Tethysethys*, *6*, 5–10.

Fraga, F., E. D. Barton, and O. Llinás (1985), The concentration of nutrients salts in “pure” North and South Atlantic Central Waters, in *International Symposium on the Most Important Upwelling Areas of*

Western Africa, Inst. Inv. Pesq., Barcelona, 1: 25–36., vol. 2, pp. 25–36.

Fratantoni, D. M., W. E. Johns, T. L. Townsend, and H. E. Hurlburt (2000), Low-Latitude Circulation and Mass Transport Pathways in a Model of the Tropical Atlantic Ocean *, *J. Phys. Oceanogr.*, *30*, 1944–1966.

Fu, L.-L. (2009), Pattern and velocity of propagation of the global ocean eddy variability, *J. Geophys. Res.*, *114*(C11), C11017, doi:10.1029/2009JC005349.

Gabric, A. J., L. Garcia, L. Van Camp, L. Nykjaer, W. Eifler, and W. Schrimpf (1993), Offshore Export of Shelf Production in the Cape Blanc (Mauritania) Giant Filament as Derived From Coastal Zone Color Scanner Imagery, *J. Geophys. Res. Ocean.*, *98*, 4697–4712.

Garcia, H., A. Cruzado, L. Gordon, and J. Escanez (1998), Decadal-scale chemical variability in the subtropical North Atlantic deduced from nutrient and oxygen data, *J. Geophys. Res.*, *103*(C2), 2817, doi:10.1029/97JC03037.

Garzoli, S. L., A. Ffield, E. Johns, and Q. Yao (2004), North Brazil Current retroflection and transports, *J. Geophys. Res.*, *109*(C1), C01013, doi:10.1029/2003JC001775.

Gasser M., J.L. Pelegrí, J. Nash, H. Peters, J. García-Lafuente (2011), Topographic steering of the early plunging Mediterranean outflow. Geo-Marine Letters, 31, 301-314.

Gnanadesikan, A., J. L. Russell, F. Zeng, and G. Fluid (2007), How does ocean ventilation change under global warming ?, *Ocean Sci.*, 43–53.

Gouretski, V. and Koltermann, P. (2004), *WOCE Global Hydrographic Climatology—A Technical Report. Berichte des Bundesamtes fur Seeschifffahrt und Hydrographie*.

Griffies, S. M., R. C. Pacanowski, and R. W. Hallberg (2000), Spurious Diapycnal Mixing Associated with Advection in a z -Coordinate Ocean Model, *Mon. Weather Rev.*, *128*, 538–564.

Hagen, E. (2000), Northwest African upwelling scenario, *Oceanol. Acta*, *24*(Supplement), s113–s128.

Hahn, J., P. Brandt, R. J. Greatbatch, G. Krahmann, and a. Körtzinger (2014), Oxygen variance and meridional oxygen supply in the Tropical North East Atlantic oxygen minimum zone, *Clim. Dyn.*, doi:10.1007/s00382-014-2065-0.

Hazeleger, W., and S. Drijfhout (2006), Subtropical cells and meridional overturning circulation pathways in the tropical Atlantic, *J. Geophys. Res.*, *111*(C3), C03013, doi:10.1029/2005JC002942.

Helm, K. P., N. L. Bindoff, and J. a. Church (2011), Observed decreases in oxygen content of the global ocean, *Geophys. Res. Lett.*, *38*(23), n/a–n/a, doi:10.1029/2011GL049513.

Hughes, P., and E. D. Barton (1974), Stratification and water m a s s structure in the upwelling area off northwest Africa in April / May 1969, *Deep Sea Res. Part I Oceanogr. Res. Pap.*, *21*, 611–628.

Iselin, C.O. (1939). The influence of vertical and lateral turbulence on the characteristics of the waters at mid-depths. Transactions, American Geophysical Union 20: doi: 10.1029/TR020i003p00414. issn: 0002-8606.

Johns, W. E., T. N. LEE, R. C. Beardsley, J. Candela, R. Limeburner, and B. Castro (1998), Annual Cycle and Variability of the North Brazil Current, *J. Phys. Oceanogr.*, *28*, 103–128.

Johnson, G. C., and D. Zhang (2003), Structure of the Atlantic Ocean Equatorial Deep Jets *, *J. o*, 600–609.

Joos, F., G.-K. Plattner, T. F. Stocker, A. Körtzinger, and D. W. R. Wallace (2003), Trends in marine dissolved oxygen: Implications for ocean circulation changes and the carbon budget, *Eos, Trans. Am. Geophys. Union*, *84*(21), 197, doi:10.1029/2003EO210001.

Karstensen, J., L. Stramma, and M. Visbeck (2008), Oxygen minimum zones in the eastern tropical Atlantic and Pacific oceans, *Prog. Oceanogr.*, *77*(4), 331–350, doi:10.1016/j.pocean.2007.05.009.

Kawase, M., J. L. Sarmiento, and F. D. Prowlram (1985), Nutrients in the Atlantic Thermocline, *J. Geophys. Res. Ocean.*, *90*(5), 8961–8979.

Keeling, R. F., K. Arne, and N. Gruber (2010), Ocean Deoxygenation in a Warming World, , doi:10.1146/annurev.marine.010908.163855.

Kirchner, K., M. Rhein, S. Hüttl-Kabus, and C. W. Böning (2009), On the spreading of South Atlantic Water into the Northern Hemisphere, *J. Geophys. Res.*, *114*(C5), C05019, doi:10.1029/2008JC005165.

Klein, B., and M. Tomczak (1994), Identification of diapycnal mixing through optimum multiparameter analysis: 2. Evidence for unidirectional diapycnal mixing in the front between North and South Atlantic Central Water, *J. Geophys. Res.*, *99*(C12), 25275, doi:10.1029/94JC01948.

Lam, P., and M. M. M. Kuypers (2011), Microbial Nitrogen Cycling Processes in Oxygen Minimum Zones, *Ann. Rev. Mar. Sci.*, *3*(1), 317–345, doi:10.1146/annurev-marine-120709-142814.

Lankhorst, M., D. Fratantoni, M. Ollitrault, P. Richardson, U. Send, and W. Zenk (2009), The mid-depth circulation of the northwestern tropical Atlantic observed by floats, *Deep Sea Res. Part I Oceanogr. Res. Pap.*, *56*(10), 1615–1632, doi:10.1016/j.dsr.2009.06.002.

Lázaro, C., M. J. Fernandes, a. M. P. Santos, and P. Oliveira (2005), Seasonal and interannual variability of surface circulation in the Cape Verde region from 8 years of merged T/P and ERS-2 altimeter data,

Remote Sens. Environ., *98*(1), 45–62, doi:10.1016/j.rse.2005.06.005.

Liu, Z., and S. G. H. Philander (1994), A GCM Study of Tropical-Subtropical Upper-Ocean Water Exchange, *J. Phys. Oceanogr.*, *24*, 2606–2623.

Llanillo, P., J. Pelegrí, C. Duarte, M. Emelianov, M. Gasser, J. Gourrion, and A. Rodríguez-Santana (2012), Meridional and zonal changes in water properties along the continental slope off central and northern Chile, *Ciencias Mar.*, *38*(1B), 307–332.

Lu, P., J. P. McCreary, and B. A. Klinger (1998), Meridional Circulation Cells and the Source Waters of the Pacific Equatorial Undercurrent, *J. Phys. Oceanogr.*, *28*, 62–84.

Luyten, J. R., J. Pedlosky, and H. Stommel (1983), The Ventilated Thermocline, *J Phys. Ocean.*, *13*, 292–309.

Machín, F., a. Hernández-Guerra, and J. L. Pelegrí (2006), Mass fluxes in the Canary Basin, *Prog. Oceanogr.*, *70*(2-4), 416–447, doi:10.1016/j.pocean.2006.03.019.

Machín, F., and J. L. Pelegrí (2009), Northward Penetration of Antarctic Intermediate Water off Northwest Africa, *J. Phys. Oceanogr.*, *39*(3), 512–535, doi:10.1175/2008JPO3825.1.

Machín, F., J. L. Pelegrí, E. Fraile-Nuez, P. Vélez-Belchí, F. López-Laatzen, and a. Hernández-Guerra (2010), Seasonal Flow Reversals of Intermediate Waters in the Canary Current System East of the Canary Islands, *J. Phys. Oceanogr.*, *40*(8), 1902–1909, doi:10.1175/2010JPO4320.1.

Mackas, D. L., K. L. Denman, and A. F. Bennett (1987), Least squares multiple tracer analysis of water mass composition, *J. Geophys. Res.*, *92*(C3), 2907, doi:10.1029/JC092iC03p02907.

Marshall, J., A. Adcroft, C. Hill, L. Perelman, and C. Heisey (1997), A finite-volume, incompressible Navier Stokes model for studies of the ocean on parallel computers, *J. Geophys. Res.*, *102*(C3), 5753, doi:10.1029/96JC02775.

Mason, E., F. Colas, J. Molemaker, A. F. Shchepetkin, C. Troupin, J. C. McWilliams, and P. Sangrà (2011), Seasonal variability of the Canary Current: A numerical study, *J. Geophys. Res.*, *116*(C6), 1–20.

Matear, R. J., and a. C. Hirst (2003), Long-term changes in dissolved oxygen concentrations in the ocean caused by protracted global warming, *Global Biogeochem. Cycles*, *17*(4), n/a–n/a, doi:10.1029/2002GB001997.

Mittelstaedt, E. (1983), The upwelling area off Northwest Africa—A description of phenomena related to coastal upwelling, *Prog. Oceanogr.*, *12*(3), 307–331.

Mittelstaedt, E. (1991), The ocean boundary along the northwest African coast: Circulation and oceano-

graphic properties at the sea surface, *Prog. Oceanogr.*, *26*(4), 307–355.

Nykjaer, L., and L. van Camp (1994), Seasonal and interannual variability of coastal upwelling along northwest Africa and Portugal from 1981 to 1991, *J. Geophys. Res. Ocean.*, *99*(7), 197–207.

Oschlies, A., K. G. Schulz, U. Riebesell, and A. Schmittner (2008), Simulated 21st century's increase in oceanic suboxia by CO 2 -enhanced biotic carbon export, *Global Biogeochem. Cycles*, *22*(4), n/a–n/a, doi:10.1029/2007GB003147.

Paris, C. B., J. Helgers, E. van Sebille, and A. Srinivasan (2013), Connectivity Modeling System: A probabilistic modeling tool for the multi-scale tracking of biotic and abiotic variability in the ocean, *Environ. Model. Softw.*, *42*, 47–54, doi:10.1016/j.envsoft.2012.12.006.

Pastor, M. V., J. Peña-Izquierdo, J. L. Pelegrí, and Á. Marrero-Díaz (2012), Meridional changes in water mass distributions off NW Africa during November 2007/2008, *Ciencias Mar.*, *38*, 223–244.

Paulmier, a., D. Ruiz-Pino, and V. Garçon (2011), CO_2 maximum in the oxygen minimum zone (OMZ), *Biogeosciences*, *8*(2), 239–252, doi:10.5194/bg-8-239-2011.

Pelegrí, J. L., J. Arístegui, L. Cana, M. González-Dávila, a. Hernández-Guerra, S. Hernández-León, a. Marrero-Díaz, M. F. Montero, P. Sangrà, and M. Santana-Casiano (2005), Coupling between the open ocean and the coastal upwelling region off northwest Africa: water recirculation and offshore pumping of organic matter, *J. Mar. Syst.*, *54*(1-4), 3–37, doi:10.1016/j.jmarsys.2004.07.003.

Pelegrí, J. L., a. Marrero-Díaz, and a. W. Ratsimandresy (2006), Nutrient irrigation of the North Atlantic, *Prog. Oceanogr.*, *70*(2-4), 366–406, doi:10.1016/j.pocean.2006.03.018.

Peña-Izquierdo, J., J. L. Pelegrí, M. V. Pastor, P. Castellanos, M. Emelianov, M. Gasser, J. Salvador, and E. Vázquez-Domínguez (2012), The continental slope current system between Cape Verde and the Canary Islands, *Sci. Mar.*, *76*(S1), 65–78, doi:10.3989/scimar.03607.18C.

Perez, F. F., C. G. Castro, M. Alvarez, A. Kortzinger, M. Santana-casiano, M. J. Rueda, and A. F. Rıos (2001), Mixing analysis of nutrients, oxygen and inorganic carbon in the Canary Islands region, *J. Mar. Syst.*, *28*(3-4), 183–201.

Poole, R., and M. Tomczak (1999), Optimum multiparameter analysis of the water mass structure in the Atlantic Ocean thermocline, *Deep Sea Res. Part I Oceanogr. Res. Pap.*, *46*(11), 1895–1921, doi:10.1016/S0967-0637(99)00025-4.

Qiu, B., D. L. Rudnick, S. Chen, and Y. Kashino (2013a), Quasi-stationary North Equatorial Undercurrent jets across the tropical North Pacific Ocean, *Geophys. Res. Lett.*, *40*(10), 2183–2187, doi:10.1002/grl.50394.

Qiu, B., S. Chen, and H. Sasaki (2013b), Generation of the North Equatorial Undercurrent Jets by Triad Baroclinic Rossby Wave Interactions, *J. Phys. Oceanogr.*, *43*(12), 2682–2698, doi:10.1175/JPO-D-13-099.1.

Reid, J. L. (1994), On the total geostrophic circulation of the North Atlantic Ocean: Flow patterns, tracers, and transports, *Prog. Oceanogr.*, *33*(1), 1–92, doi:10.1016/0079-6611(94)90014-0.

Rhein, M., K. Kirchner, C. Mertens, R. Steinfeldt, M. Walter, and U. Fleischmann-Wischnath (2005), Transport of South Atlantic water through the passages south of Guadeloupe and across 16°N, 2000–2004, *Deep Sea Res. Part I Oceanogr. Res. Pap.*, *52*(12), 2234–2249, doi:10.1016/j.dsr.2005.08.003.

Rhines, P. B., and W. R. Young (1982), Homogenization of potential vorticity in planetary gyres, *J. Fluid Mech.*, *122*, 347–367.

Ridder, N. N., and M. H. England (2014), Sensitivity of ocean oxygenation to variations in tropical zonal wind stress magnitude, *Global Biogeochem. Cycles*, n/a–n/a, doi:10.1002/2013GB004708.

Rodríguez-Marroyo, R., Á. Viúdez, and S. Ruiz (2011), Vortex Merger in Oceanic Tripoles, *J. Phys. Oceanogr.*, *41*(6), 1239–1251, doi:10.1175/2011JPO4582.1.

Rosell-Fieschi, M., J. L. Pelegrí, and J. Gourrion (2015), Zonal jets in the equatorial Atlantic Ocean, *Prog. Oceanogr.*, *130*, 1–18, doi:10.1016/j.pocean.2014.08.008.

Sarmiento, J. L., C. G. H. Rooth, and W. Roether (1982), The North Atlantic Tritium distribution in 1972, *J. Geophys. Res. Ocean.*, *87*(C10), 8047–8056.

Sarmiento, J. L., T. M. C. Hughes, R. J. Stouffer, and S. Manabe (1998), Simulated response of the ocean carbon cycle to anthropogenic climate warming, *Nature*, *393*, 246–249.

Schott, F. A., and C. W. Böning (1991), The WOCE Model in the Western Equatorial Atlantic: Upper Layer Circulation, *J. Geophys. Res. Ocean.*, *96*(C4), 6993–7004.

Schott, F. A., J. P. Mccreary, and G. C. Johnson (2004), Shallow Overturning Circulations of the Tropical-Subtropical Oceans tropical subduction regions of both hemispheres to the eastern , equatorial upwelling, in *Earth Climate: The Ocean-Atmosphere Interaction, Geophys. Monogr. Ser*, edited by S. Wang, P. . Xie, and J. A. Carton, pp. 261–304, AGU, Washington D.C.

Schott, F. a., L. Stramma, W. Wang, B. S. Giese, and R. Zantopp (2008), Pacific Subtropical Cell variability in the SODA 2.0.2/3 assimilation, *Geophys. Res. Lett.*, *35*(10), L10607, doi:10.1029/2008GL033757.

van Sebille, E., W. E. Johns, and L. M. Beal (2012), Does the vorticity flux from Agulhas rings control the zonal pathway of NADW across the South Atlantic?, *J. Geophys. Res.*, *117*(C5), C05037,

doi:10.1029/2011JC007684.

van Sebille, E., P. Spence, M. R. Mazloff, M. H. England, S. R. Rintoul, and O. a. Saenko (2013), Abyssal connections of Antarctic Bottom Water in a Southern Ocean State Estimate, *Geophys. Res. Lett.*, *40*(10), 2177–2182, doi:10.1002/grl.50483.

Siedler, G., N. Zangenberg, and R. Onken (1992), Seasonal Changes in the Tropical Atlantic Circulation: Observation and Simulation of the Guinea Dome, *J. Geophys. Res. Ocean.*, *97*, 703–715.

Stark, J. D., C. J. Donlon, M. J. Martin, and M. E. Mcculloch (2007), OSTIA : An operational, high resolution, real time, global sea surface temperature analysis system, in *Proc. Oceans '07, Marine Challenges: Coastline to Deep Sea, Aberdeen, Scotland, IEEE/ OES*, pp. 1–4.

Stommel, H. (1979), Determination of water mass properties of water pumped down from the Ekman layer to the geostrophic flow below., *Proc. Natl. Acad. Sci. U. S. A.*, *76*(7), 3051–5.

Stramma, L., and F. Schott (1999), The mean flow field of the tropical Atlantic Ocean, *Deep Sea Res. Part II Top. Stud. Oceanogr.*, *46*(1-2), 279–303, doi:10.1016/S0967-0645(98)00109-X.

Stramma, L., S. Hüttl, and J. Schafstall (2005), Water masses and currents in the upper tropical northeast Atlantic off southwest Africa, *J. Geophys. Res. Ocean.*, *110*(C12), C12006.

Stramma, L., G. C. Johnson, J. Sprintall, and V. Mohrholz (2008a), Expanding oxygen-minimum zones in the tropical oceans., *Science*, *320*(5876), 655–8, doi:10.1126/science.1153847.

Stramma, L., P. Brandt, J. Schafstall, F. Schott, J. Fischer, and A. Körtzinger (2008b), Oxygen minimum zone in the North Atlantic south and east of the Cape Verde Islands, *J. Geophys. Res.*, *113*(C4), C04014, doi:10.1029/2007JC004369.

Stramma, L., M. Visbeck, P. Brandt, T. Tanhua, and D. Wallace (2009), Deoxygenation in the oxygen minimum zone of the eastern tropical North Atlantic, *Geophys. Res. Lett.*, *36*(20), L20607, doi:10.1029/2009GL039593.

Stramma, L., S. Schmidtko, L. a. Levin, and G. C. Johnson (2010), Ocean oxygen minima expansions and their biological impacts, *Deep Sea Res. Part I Oceanogr. Res. Pap.*, *57*(4), 587–595, doi:10.1016/j.dsr.2010.01.005.

Stramma, L., E. D. Prince, S. Schmidtko, J. Luo, J. P. Hoolihan, M. Visbeck, D. W. R. Wallace, P. Brandt, and A. Körtzinger (2011), Expansion of oxygen minimum zones may reduce available habitat for tropical pelagic fishes, *Nat. Clim. Chang.*, *2*(1), 33–37, doi:10.1038/nclimate1304.

Suga, T., and L. D. Talley (1995), Antarctic Intermediate Water circulation in the tropical and subtropical

South Atlantic Toshio Suga • and Lynne, *J. Geophys. Res. Ocean.*, *100*(C7), 13,441–13,453.

Sverdrup, H. (1947), Wind-Driven currents in a baroclinic ocean; with application to the equatorial currents of the eastern Pacific, *Proc. Natl. Acad. Sci.*, *33*(11), 318–326.

Talley, L. D., Pickard, G. L., Emery, W. J., and Swift, J. H. (2011) in Descriptive Physical Oceanography, an introduction, 6th edition, Elsevier.

Tomczak, M. (1972), Problems of Physical Oceanography in Coastal Upwelling Investigations, *Geoforum*, *11*, 23–34.

Tomczak, M. (1981), An analysis of mixing in the frontal zone of South and North Atlantic Central Water off North - West Africa, *Prog. Oceanogr.*, *10*, 173–192.

Tomczak, M., and D. G. B. Large (1989), Multiparameter Analysis of Mixing in the Thermocline represent of the Eastern Indian Ocean, *J. Geophys. Res. Ocean.*, *94*(Cll), 16,141–16,149.

Tomczak, M. (1999), Some historical , theoretical and applied aspects of, , 275–303.

Tomczak, M., and J. S. Godfrey (1994), *Regional oceanography: An introduction*, Elsevier, New York.

Vaquer-Sunyer, R., and C. Duarte (2008), Thresholds of hypoxia for marine biodiversity, *Proc. Natl. Acad. Sci. U. S. A.*, *105*(40), 15452–15457.

Voituriez, B., and R. Chuchla (1978), Influence of the Southern Atlantic Central Water on the distribution of salinity and oxygen in the northeast tropical Atlantic Ocean, *Deep. Res*, *25*, 107–117.

Wang, C. (2005), Subthermocline tropical cells and equatorial subsurface countercurrents, *Deep Sea Res. Part I Oceanogr. Res. Pap.*, *52*(1), 123–135, doi:10.1016/j.dsr.2004.08.009.

Warren, B. a. (1983), Why is no deep water formed in the North Pacific?, *J. Mar. Res.*, *41*(2), 327–347, doi:10.1357/002224083788520207.

Whitney, F. A., H. J. Freeland, and M. Robert (2007), Progress in Oceanography Persistently declining oxygen levels in the interior waters of the eastern subarctic Pacific, , *75*, 179–199, doi:10.1016/j.pocean.2007.08.007.

Xuang, R. X. (2010), *Ocean Circulation, Wind-Driven and Thermohaline Processes*, Cambridge University Press, New York.

Zenk, W., B. Klein, and M. Schröder (1991), Cape Verde Frontal Zone, *Deep Sea Res. Part I Oceanogr. Res. Pap.*, *38*(Suppl. 1), S505–S530.

Zhang, D., M. J. McPhaden, and W. E. Johns (2003), Observational Evidence for Flow between the Subtropical and Tropical Atlantic : The Atlantic Subtropical Cells *, *J. Phys. Oceanogr.*, *33*, 1783–1797.